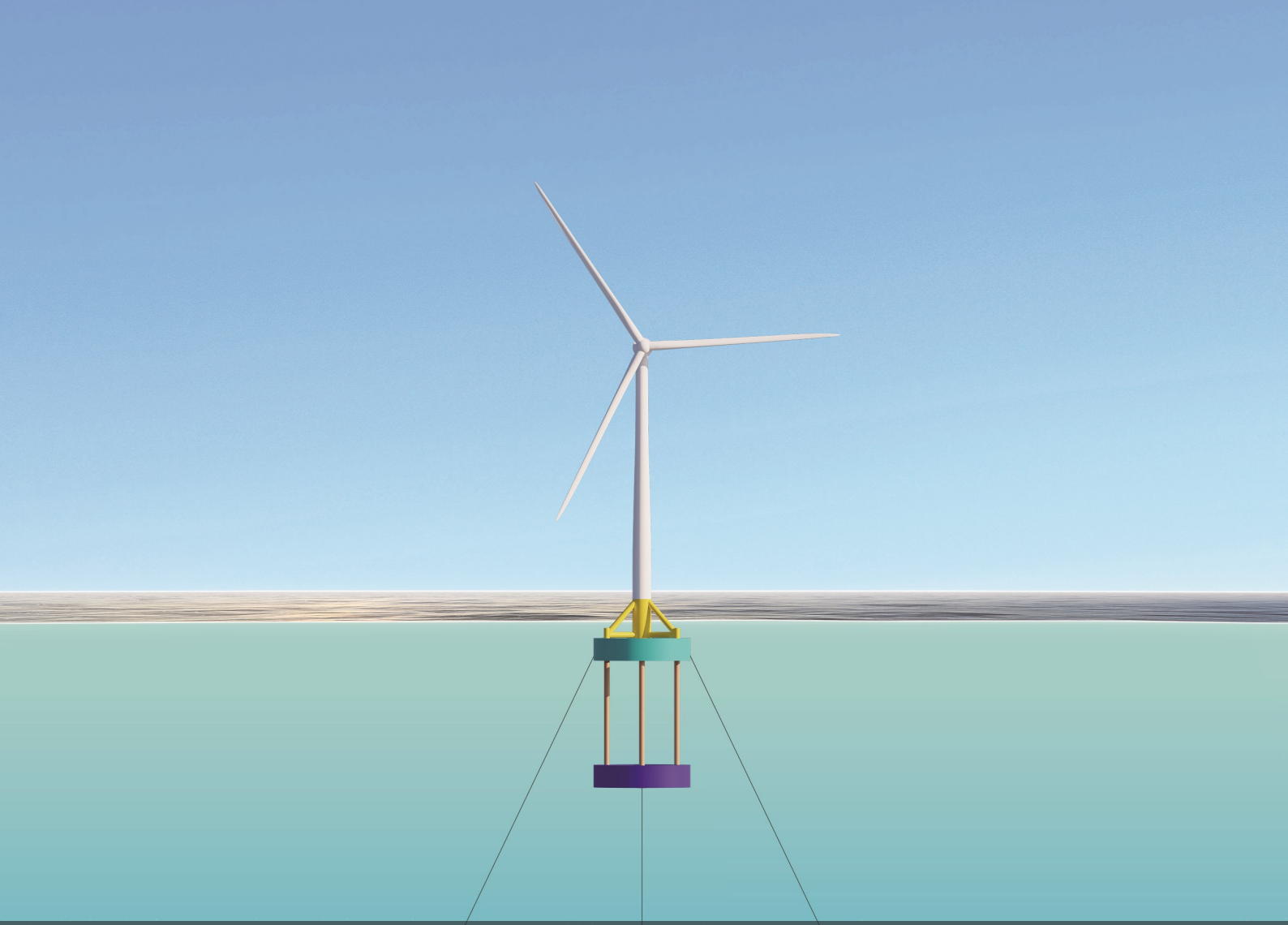

Numerical Model Development for a Deep-Water Floating Wind Turbine

A mooring-line dynamic amplification assessment for the Elevator concept near Curaçao

MSc Offshore and Dredging Engineering

E.P.J. (Eleanore) Cammeraat

TU Delft

Allseas

Numerical Model Development for a Deep-Water Floating Wind Turbine

A mooring-line dynamic amplification assessment for the Elevator concept near Curaçao

by

E.P.J. (Eleanore) Cammeraat

in partial fulfilment of the requirements for the degree of
Master of Science
in Offshore and Dredging Engineering
at Delft University of Technology

Graduation committee:

Chair and TU Delft supervisor:	Dr. ir. J.S. Hoving	TU Delft
Examiner:	Prof. dr. A.V. Metrikine	TU Delft
Company supervisor:	Ir. A.L.J. Steenhuis	Allseas
Company supervisor:	Ir. V.C. Terlouw	Allseas

Project duration:	November 2025 to July 2026
Faculty:	Mechanical Engineering

TU Delft

Allseas

“Not all those who wander are lost.”

—J.R.R. Tolkien

Preface and acknowledgements

Dear reader,

This thesis marks the final step of my MSc in Offshore and Dredging Engineering at Delft University of Technology. The research was carried out in collaboration with Allseas Engineering B.V. and focuses on the numerical model development of the Elevator concept and a mooring-line dynamic amplification assessment for a floating wind concept near Curaçao.

My interest in the maritime environment grew even further by spending many hours on the water during sailing and rowing. This project allowed me to combine that interest with floating wind, mooring-system behaviour, hydrodynamic modelling, and numerical simulation. I especially appreciated learning new software tools, including Rhino, OrcaWave, and OrcaFlex, and building a numerical model step by step. I am grateful that this thesis also became the start of my next step at Allseas.

I would like to thank my TU Delft supervisor, Jeroen, for his guidance, useful insights, and pleasant meetings throughout the project. His questions and suggestions helped me to structure the thesis and to improve the interpretation of the results. His careful attention to terminology and physical interpretation was greatly appreciated.

I would also like to thank Andrei for his role as examiner and for his perspective on the interpretation of this work.

I am grateful to André and Vera from Allseas for their guidance during the weekly meetings with the other graduates. Their technical support, practical insights, and regular discussions helped me to improve both the thesis and the modelling route that led to the final results. I would also like to thank them for their kindness, support, and good humour, which made my time at Allseas both valuable and enjoyable.

Finally, I would like to thank my parents, family, friends, and fellow students for their support throughout the project. I am especially grateful to Stijn for his patience, encouragement, and support during the final months of this thesis. I would also like to thank the fellow graduates in the Oval Office, and especially Philip and Ewoud, for making me feel welcome from the start. The shared lunch walks, coffee and tea breaks, good conversations, and many laughs made the graduation period much more enjoyable.

During the preparation of this work and the development of the simulation workflow, generative AI tools were used for text editing, formatting alignment, and debugging software errors. All suggestions were reviewed and verified by the author.

I hope you enjoy reading my thesis!

E.P.J. (Eleanore) Cammeraat
Delft, June 2026

Summary

Curaçao has a strong offshore wind resource, but the water depth increases rapidly and reaches about $800\ \mathrm{m}$ within a few kilometres from shore. This makes floating support structures and their mooring systems a relevant design challenge. The case considered in this thesis is the 15 MW Elevator concept, a hybrid floating wind concept with hull- and ballast-based stability and three inclined taut HMPE mooring lines. The mooring lines provide station-keeping and horizontal restoring.

This thesis develops a numerical model of the Elevator concept and uses it to assess whether a dynamic (DYN) mooring-line model changes the predicted maximum horizontal platform offset and governing fairlead effective tension compared with a quasi-static (QS) mooring-line model. This modelling question is relevant because a QS mooring model is attractive for early design and screening: it is simpler, less computationally demanding, and requires fewer dynamic line inputs than a DYN model. However, for long, tensioned mooring lines in deep water, it is not always clear whether the omitted line-dynamic effects remain negligible.

Before the QS-DYN mooring comparison, the Elevator concept was translated from design inputs into a numerical Rhino-OrcaWave-OrcaFlex model through several modelling iterations. Early simplified models were used to check the modelling workflow, while later OrcaWave models were used to select a feasible diffraction-body representation. The numerical Elevator model developed in this thesis consists of a common floater representation, an OrcaWave hydrodynamic database, and an OrcaFlex time-domain setup. The implemented model was checked through hydrostatic consistency, still-water equilibrium, target pretension, local restoring behaviour, and free-vibration periods.

The QS-DYN mooring-line comparison is performed in OrcaFlex for selected first-order, wave-only irregular-wave cases in $800\ \mathrm{m}$ water depth near Curaçao. The two models use the same floater representation, hydrodynamic database, mooring geometry, target pretension, unstretched line length, sea states, wave headings, wave seed, simulation settings, and post-processing method. The only intended difference is the mooring-line representation. The QS model uses instantaneous static line equilibrium, while the DYN model represents the mooring lines as finite-element lines with distributed inertia, hydrodynamic drag, added mass, and time-dependent line motion.

For the selected cases, the QS and DYN models give almost identical predictions of maximum horizontal platform offset and governing fairlead effective tension. The largest horizontal offset occurs in SS2, the long-period swell case with $H_s = 1.30\ \mathrm{m}$ and $T_p = 18.07\ \mathrm{s}$, and is approximately $1.15\ \mathrm{m}$. The largest governing-line maximum effective tension occurs in LC2a, the 0° heading case of SS2, with $963.5\ \mathrm{kN}$ in the QS model and $963.2\ \mathrm{kN}$ in the DYN model. The corresponding tension range above the mean is approximately $63\ \mathrm{kN}$, or about 7% of the mean effective tension. The case-specific offset DAF ranges from 0.997 to 1.002, while the tension-range DAF ranges from 0.975 to 0.997.

The small QS-DYN differences can be explained by the limited fairlead excitation in the selected first-order wave-only cases. The dominant wave periods remain below the estimated global moored-system response periods in surge, heave and pitch. As a result, the platform moves only a small distance in the horizontal plane, with the largest offset below approximately $1.2\ \mathrm{m}$. For a taut line with a mean effective tension close to $900\ \mathrm{kN}$, these motions produce only limited changes in axial extension and line geometry. The dynamic line terms in the DYN model are therefore weakly excited for the evaluated ULS quantities. A separate line-eigenfrequency check shows a small response near the first transverse line-mode frequency in SS3, but this response does not increase the governing fairlead effective tension. An axial line-frequency hand check places the lowest axial estimate well above the selected first-order wave-frequency range, so direct axial tension resonance is not expected in these cases.

The sensitivity analyses show that this conclusion is linked to the selected pretension, mooring geometry, and load types. Changing the unstretched line length strongly affects the static pretension level. The HMPE plausibility check shows that the $900\ \mathrm{kN}$ pretension state corresponds to about 22% of the minimum breaking load and about 1.4% axial strain. The steady-thrust sensitivity shows that a mean aerodynamic load can cause a large mean offset and a significant redistribution of the line tensions. Together, these sensitivities show that the mooring input parameters and the included load types must be reconsidered before applying the same conclusion to broader wind-wave-current cases.

A first VIV screening further shows that current-induced line vibration cannot be excluded for current-

loaded cases. This does not affect the selected wave-only QS-DYN results, but it confirms that current and VIV require separate assessment before the conclusion is extended to wind-wave-current design cases.

The results indicate that, within the selected first-order wave-only comparison, the DYN mooring-line model does not noticeably change the predicted maximum horizontal platform offset or governing fairlead effective tension relative to the QS model. This conclusion applies only to the selected comparison setup and should not be generalised to cases with stronger low-frequency fairlead motion, including second-order wave-drift loading, current-induced line vibration, VIV, or wind thrust and turbine-control effects from an operating turbine. The main contribution of this thesis is therefore twofold: the development of a numerical Rhino-OrcaWave-OrcaFlex implementation of the Elevator concept, and a QS-DYN mooring-line comparison that explains why dynamic mooring-line effects are small under the selected first-order wave-only conditions.

Contents

List of figures

List of tables

Abbreviations

Abbreviation	Definition
DAF	Dynamic amplification factor
DNV	Det Norske Veritas
DOF	Degree of freedom
DYN	Dynamic
ERA5	ECMWF Reanalysis v5
FOWT	Floating offshore wind turbine
HMPE	High-modulus polyethylene
JONSWAP	Joint North Sea Wave Project
LC	Load case
MBL	Minimum breaking load
NREL	National Renewable Energy Laboratory
QS	Quasi-static
QTF	Quadratic transfer function
RAO	Response amplitude operator
RNA	Rotor-nacelle assembly
SS	Sea state
SWL	Still water level
TLP	Tension-leg platform
ULS	Ultimate limit state
VIV	Vortex-induced vibration
WL	Waterline

Symbols

Symbol	Definition	Unit
A_{wp}	Waterplane area	m^2
C_d	Drag coefficient	$-$
C_m	Morison inertia coefficient	$-$
D	Diameter	m
EA_{eff}	Effective axial stiffness	N
f_n	Natural frequency	Hz
f_s	Vortex-shedding frequency	Hz
H_s	Significant wave height	m
h	Water depth	m
I	Mass moment of inertia	$\mathrm{kg\ m}^2$
L_0	Unstretched line length	m
m'	Structural line mass per unit length	$\mathrm{kg/m}$
$r(t)$	Horizontal platform offset time history	m
r_{max}	Maximum horizontal platform offset	m
Re	Reynolds number	$-$
St	Strouhal number	$-$
T_p	Peak wave period	s
T_{eff}	Effective tension	N
$\bar{T}_{eff}$	Mean effective tension	N
ΔT_{eff}	Tension range above the mean effective tension	N
U_n	Relative-flow component normal to the line	$\mathrm{m/s}$
V_r	Reduced velocity	$-$
β	Mooring-line inclination from vertical	deg
ε	Axial strain	$-$

1 Introduction

This chapter introduces the research problem and the scope of the thesis. Section 1.1 describes the deep-water floating-wind context and the Elevator concept. Section 1.2 defines the modelling gap addressed in this study. The research aim, objectives, research questions, scope, research approach, and thesis structure are then presented in Sections 1.3 to 1.8.

1.1. Background and societal relevance

Floating offshore wind turbines enable offshore wind energy production in locations where bottom-fixed support structures are not feasible. Curaçao is an example of such a location because the water depth increases rapidly and reaches values of the order of 800 m within a few kilometres from shore [1].

These deep-water conditions introduce technical and economic challenges for floating wind support structures and their mooring systems. Conventional catenary systems may require long and heavy mooring lines and a large seabed footprint, while classical tension-leg systems require high tendon pretension and suitable anchors [2, 3]. Mooring-system design is therefore an important part of the feasibility of floating wind concepts in deep water.

This study considers the 15 MW Elevator floating wind concept developed in the Curaçao design study by Belis et al. [1]. The Elevator is a hybrid floating concept in which upright stability is mainly provided by the hull and ballast configuration, while three inclined taut HMPE mooring lines provide station-keeping and horizontal restoring.

In the design study, the mooring system is represented through a local linear restoring stiffness around the static equilibrium. This is suitable for concept-level estimates of mooring-restoring behaviour and natural periods, but it does not describe the time-dependent motion, inertia, drag, or added-mass effects of the mooring lines [1].

This motivates the development of a numerical Elevator model and a mooring-line dynamic amplification assessment. In this assessment, QS and DYN OrcaFlex mooring-line models are used to evaluate whether the DYN mooring-line representation changes the predicted maximum horizontal platform offset and governing fairlead effective tension relative to the QS representation in selected first-order, wave-only ULS cases.

1.2. Problem description and knowledge gap

The main modelling uncertainty addressed in this thesis is whether the DYN mooring-line representation changes the predicted response of the Elevator model relative to the QS representation. In a quasi-static mooring-line model, the mooring force is calculated from the instantaneous fairlead position and the corresponding static line equilibrium. This means that the model updates the line force as the platform moves but assumes that the line itself has no time-dependent motion. It therefore captures the geometric and axial restoring behaviour of the line but does not resolve distributed line inertia, hydrodynamic drag, added mass, or time-dependent line-shape effects [2, 4].

For long, tensioned mooring lines in deep water, these excluded dynamic effects may influence the predicted platform response and line tension. This is relevant for the Elevator concept because its mooring system is not only a station-keeping component but also a main contributor to horizontal restoring. A dynamic mooring-line model represents the line as a moving system so that the predicted tension depends on both instantaneous geometry and time-dependent line motion. Previous floating-wind studies have shown that the choice between quasi-static and dynamic mooring modelling can affect predicted platform motions and mooring loads under certain conditions [5, 6].

This modelling question is relevant for the design cycle of the Elevator concept because early-stage floating-wind studies often rely on simplified mooring representations to support concept-level design decisions [1, 2]. If the quasi-static and dynamic models give similar predictions for the selected response quantities, the quasi-static representation can be used as an approximation for this specific

setup. If the predictions differ, the dynamic model may be needed to avoid misinterpreting extreme offsets or fairlead tensions. Such a misinterpretation would affect the assessment of station-keeping performance, mooring-line utilisation, and the modelling level required for later design stages. In both cases, the comparison improves understanding of the load mechanisms that should be considered in later design stages, including detailed ULS checks, fatigue assessment, and certification-level design assessment.

For the Elevator concept, this dynamic amplification assessment has not yet been performed. The Belis et al. [1] study provides the geometry, hydrostatic properties, mass properties, target mooring tension, linearised restoring targets, and screening-level natural periods. However, it does not provide a numerical model of the Elevator or a time-domain comparison between QS and DYN mooring-line representations under the same irregular-wave input.

The knowledge gap addressed in this thesis is therefore case-specific. The Belis et al. [1] study defines the Elevator concept and its linearised mooring-restoring behaviour, but it does not show how the same floater responds when the mooring lines are represented with time-dependent line dynamics. It is therefore unknown whether the line-dynamic terms included in a DYN model alter the predicted platform offset and fairlead effective-tension response in the selected first-order, wave-only cases.

1.3. Research aim

The aim of this study is to develop and verify a numerical Rhino-OrcaWave-OrcaFlex model of the Elevator concept and to use this model to quantify mooring-line dynamic amplification through a QS-DYN OrcaFlex comparison.

The comparison is performed with two OrcaFlex models that use the same floater representation, hydrodynamic input, mooring geometry, target pretension, unstretched line length, environmental input, simulation settings, and post-processing method. One model uses a QS mooring-line representation, while the other uses a DYN mooring-line representation. This setup allows differences in offset and fairlead effective tension to be attributed mainly to the mooring-line representation.

The modelling difference is quantified using dynamic amplification factors for maximum horizontal platform offset, total maximum fairlead effective tension, and the fairlead-tension range above the mean.

1.4. Research objectives

To achieve the research aim, the following objectives are defined.

1. **Literature and design basis**
   Identify the relevant response quantities, load mechanisms, and modelling assumptions for taut synthetic mooring systems in deep water.
2. **Reference system definition**
   Define the Elevator reference model and the quantities required to develop and check the numerical model.
3. **Hydrodynamic model setup and consistency checks**
   Develop the OrcaWave hydrodynamic model for the Elevator representation and check whether the resulting hydrostatic and hydrodynamic quantities are physically plausible.
4. **OrcaFlex model development and static verification**
   Develop the OrcaFlex implementation of the Elevator model with two mooring-line representations: one quasi-static and one dynamic. Verify that both representations reproduce the intended still-water equilibrium, fairlead effective tension, target pretension, and local restoring behaviour.
5. **Dynamic amplification assessment**
   Assess dynamic amplification by comparing quasi-static and dynamic mooring-line representations in OrcaFlex under the same selected first-order irregular-wave cases. The assessment focuses on maximum horizontal platform offset, governing fairlead effective tension, the fairlead-tension range above the mean, and selected platform motions.
6. **Response interpretation and sensitivities**
   Assess how selected modelling sensitivities affect the interpretation of the dynamic amplifica-

tion results, with emphasis on target pretension, unstretched line length, the resulting static line-tension state, and a simplified steady-thrust load.

7. **Limitations and recommendations**
   Identify the additional analyses required before extending the conclusions to broader wind-wave-current and certification-level mooring assessment.

1.5. Research questions

The research aim is addressed through the following research questions.

- **RQ1:** What response quantities, load mechanisms, and modelling assumptions are relevant for comparing QS and DYN mooring-line models of a taut synthetic mooring system in deep water?
- **RQ2:** How can a numerical Rhino-OrcaWave-OrcaFlex model of the Elevator concept be developed and verified for the mooring-line dynamic amplification assessment?
- **RQ3:** How do QS and DYN mooring-line representations compare under the selected first-order irregular-wave ULS cases in terms of maximum horizontal platform offset, governing fairlead effective tension, fairlead-tension range above the mean, and selected platform motions?
- **RQ4:** How can the QS-DYN differences be expressed using case-specific dynamic amplification factors for the selected response quantities?
- **RQ5:** How do pretension, unstretched line length, and simplified steady-thrust loading affect the dynamic amplification results and their interpretation?

Together, these research questions structure the thesis from the theoretical and numerical model basis to the QS-DYN response comparison, sensitivity analysis, and recommendations.

1.6. Scope and assumptions

This study assesses mooring-line dynamic amplification for the developed Elevator model within a defined wave-only comparison setup. The following scope and assumptions apply.

- The comparison focuses on maximum horizontal platform offset, governing fairlead effective tension, and fairlead-tension range above the mean. The selected sea states are ERA5-based cases and are not formal 50-year certification design load cases.
- The QS-DYN comparison is limited to first-order irregular-wave excitation. Second-order mean and difference-frequency wave-drift forces are not included, although they may be important for low-frequency platform motion and mooring-line tension.
- Current and turbulent wind loading are not included in the QS-DYN load cases. A simplified steady-thrust sensitivity is included separately to assess the effect of a mean horizontal thrust load on mean offset and line-tension redistribution.
- Current-induced line response is not simulated. A first VIV screening is included only to identify whether current-induced line vibration requires further study. It is not a prediction of VIV response, fatigue damage, or lock-in behaviour.
- Fatigue limit state, accidental limit state, line-failure cases, anchor design, installation analysis, and certification-level mooring design are outside the scope.
- The HMPE mooring lines are modelled with a constant effective axial stiffness based on the secant stiffness at the pretension level. Creep, fatigue degradation, marine growth, and nonlinear load-history effects are not modelled.
- The taut HMPE mooring layout is adopted from Belis et al. [1]. Alternative catenary, semi-taut, hybrid, or re-optimised mooring layouts are not assessed.
- The floater is represented by the developed diffraction-body model. The horizontal tripod members and end-can connectors are excluded from the diffraction body, while the global mass, buoyancy, centre of gravity, and inertia properties are recalculated for the retained geometry.
- The results should be interpreted as a model-level dynamic amplification assessment for the selected first-order, wave-only cases. They should not be interpreted as a full certification-level mooring design check.

1.7. Research approach

The research approach is summarised in Figure 1.1. The workflow starts from the Elevator design inputs, [1], and translates them into a numerical Rhino-OrcaWave-OrcaFlex model. The developed model is then used for QS and DYN OrcaFlex simulations with the same floater representation, hydrodynamic input, sea states, wave seeds, simulation settings, and post-processing method. The resulting platform-offset and fairlead-tension responses are compared using absolute response quantities and case-specific DAFs. The interpretation is supported by restoring and free-vibration checks, line-frequency checks, VIV screening, and selected sensitivity analyses.

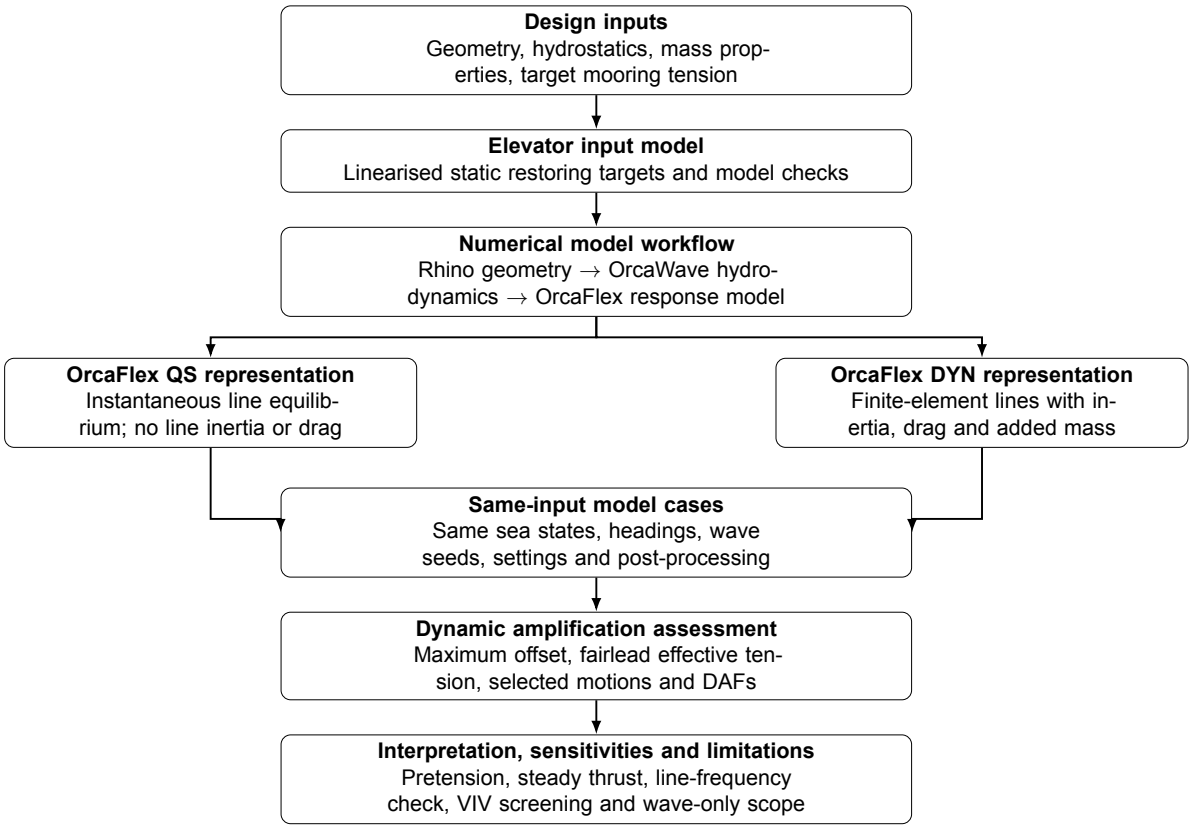

Figure 1.1: Research workflow used to develop the numerical Elevator model and assess dynamic amplification between quasi-static and dynamic mooring-line representations.

1.8. Thesis structure

The thesis is structured as follows. Chapter 2 presents the literature review and theoretical basis for the dynamic amplification assessment. Chapter 3 defines the Elevator design case and the input quantities used for the numerical model. Chapter 4 describes the Rhino-OrcaWave-OrcaFlex model setup and the verification checks. Chapter 5 presents the QS-DYN response comparison, including the DAF results, line-frequency checks, VIV screening, and physical interpretation. Chapter 6 presents the sensitivity analyses for unstretched line length, pretension, and simplified steady-thrust loading. Chapter 7 gives the conclusions and recommendations. The appendices A, B, C, D provide supporting reference values, derived quantities, hydrodynamic checks, and additional response statistics.

2

Literature review and theoretical basis for the dynamic amplification assessment

This chapter presents the literature review and theoretical basis for the mooring-line dynamic amplification assessment. Section 2.1 first describes the literature search strategy. Sections 2.2 to 2.7 then introduce the floater concepts, hydrodynamic loading, mooring-line mechanics, and dynamic-response mechanisms relevant to the Elevator model. Sections 2.8 and 2.9 discuss the response quantities and modelling levels used later in the thesis. This chapter is deliberately focused on mechanisms that affect platform offset and fairlead effective tension in a deep-water taut mooring system. Particular attention is given to floater-mooring interaction, local line-dynamic effects, and consistency between subsystem models. The chapter closes by linking the reviewed literature to the case-specific research gap addressed in this thesis.

2.1. Literature search strategy

A targeted literature review was carried out to identify the physical mechanisms, modelling assumptions, and design requirements relevant to the mooring-line dynamic amplification assessment. The search focused on sources that support the QS-DYN mooring-line comparison and the interpretation of the floater response.

The main sources were Scopus, Google Scholar, the TU Delft repository and library, NREL and IEA Wind reports, DNV and ABS guidance documents, and Orcina documentation. Peer-reviewed journal papers were used where possible for floating-wind dynamics, mooring dynamics, hydrodynamic modelling, and synthetic mooring-line behaviour. Technical reports, standards, and software documentation were used when they provided design-basis information, modelling guidance, or implementation details.

Sources were selected when they were relevant to floating-wind system dynamics, deep-water mooring layouts, taut or synthetic mooring systems, QS and DYN mooring modelling, hydrodynamic modelling, ULS response quantities, or OrcaFlex implementation. The reviewed literature supports the modelling approach, but it does not directly validate the Elevator model. The reviewed studies use different floaters, mooring layouts, water depths, and loading assumptions. They therefore motivate the case-specific numerical model development and dynamic amplification assessment carried out in this thesis.

2.2. Floating offshore wind turbine concepts

Floating offshore wind turbines (FOWTs) are used at sites where bottom-fixed support structures become impractical or uneconomical. In deep water, the support structure and mooring system must be considered together. Water depth affects mooring layout, line length, anchor spacing, dynamic cable configuration, and turbine spacing [2, 7]. These design choices also influence the project cost and layout feasibility [2].

A FOWT consists of a wind turbine mounted on a floating support structure that is kept on station by a mooring system. In dynamic analysis, the floater and moorings are coupled. Platform motion changes mooring line geometry and tension, while the mooring forces contribute to the global restoring behaviour of the floater [2, 4].

This section positions the Elevator concept relative to the main platform categories and explains why floater-mooring interaction is relevant to the mooring-line dynamic amplification assessment.

2.2.1. Classification of floating platform concepts

Floating offshore wind platforms are commonly grouped into four main categories: spar-buoy platforms, semi-submersible platforms, tension-leg platforms (TLPs), and barge-type platforms (see Figure 2.1). This classification is widely used in floating-wind literature and design studies [2, 4, 8]. The categories mainly differ in static stability mechanism, wave-induced motion behaviour, draft requirement, and the

role of the mooring system in global restoring.

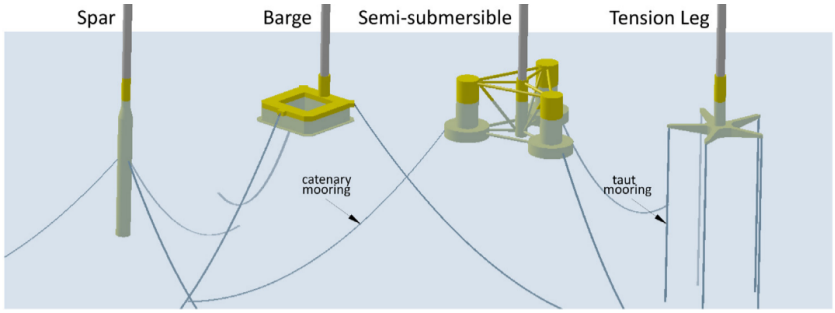

Figure 2.1: Main floating-platform categories used for offshore wind turbines. Reproduced from Edwards et al. [8].

Spar platforms obtain stability mainly from deep draft, ballast, and a low centre of gravity. Semi-submersibles rely mainly on waterplane area, distributed buoyancy, and the spacing between buoyant columns. TLPs use excess buoyancy and highly tensioned tendons, which provide strong restraint in heave, roll, and pitch. Barge-type platforms also rely on waterplane area and buoyancy distribution, but are generally more sensitive to wave-induced motions than the other categories [2, 4, 8].

2.2.2. Comparison of floating platform concepts

The practical differences between floating-platform families are mainly reflected in draft, motion behaviour, and mooring requirements. Spars usually have deep draft and relatively low wave-frequency motions, but this can complicate fabrication, port logistics, and installation. Semi-submersibles have a shallower draft and are generally more favourable for tow-out and assembly, but often require larger hull footprints and can be more sensitive to wave loading. TLPs can strongly reduce heave and pitch response, but depend on continuous tendon tension and therefore place high demands on tendon design, pretensioning, and installation. Barges are geometrically simple, but their wave-induced motions are usually less favourable for offshore wind applications [2, 8, 9].

Table 2.1 summarises the main differences between the four platform families and shows why the role of the mooring system differs between concepts.

Table 2.1: Comparison of floating platform concepts for offshore wind turbines, based on Nielsen [4] and Edwards et al. [8]

Characteristic	Spar	Semi-submersible	TLP	Barge
Main stability mechanism	Deep draft / ballast	Waterplane area / column spacing	Excess buoyancy / tendon restraint	Waterplane area
Typical draft	Deep	Moderate	Shallow to moderate	Shallow
Heave response	Low	Moderate	Very low	Relatively high
Mooring concept	Usually catenary	Catenary or (semi-)taut	Taut, high-tension tendons	Usually catenary
Main limitation	Port / draft constraints	Larger footprint / wave loading	Tendon dependency / installation complexity	Larger motions

For the present thesis, the main relevance of this comparison is that different platform families rely on different stability and restoring mechanisms. For spar and semi-submersible concepts, the mooring system mainly provides station-keeping and horizontal restoring. For a classical TLP, the tendons are part of the primary stiffness mechanism of the platform. The Elevator concept lies between these categories: its upright stability is mainly hull-driven, while horizontal restoring is provided by inclined taut mooring lines. Floater-mooring interaction is therefore directly relevant to the dynamic amplification assessment.

2.2.3. Hybrid floating concepts

Although the four platform categories are useful as a first classification, many recent floating-wind concepts combine features of more than one platform type [1, 8]. This is particularly relevant in deep water, where platform choice is influenced by mooring cost, anchor demand, footprint, installation constraints, and motion behaviour [2, 7].

Hybrid concepts aim to combine favourable properties from different floater classifications. This may involve combining hull-based upright stability with stronger horizontal restoring from taut moorings, or combining deep-water motion performance with installation-friendly geometry. The Elevator concept considered in this thesis is treated as such a hybrid concept. Its upright stability is mainly provided by the hull and ballast configuration, while the inclined taut HMPE mooring lines provide station-keeping and horizontal restoring, as shown in Figure 2.2.

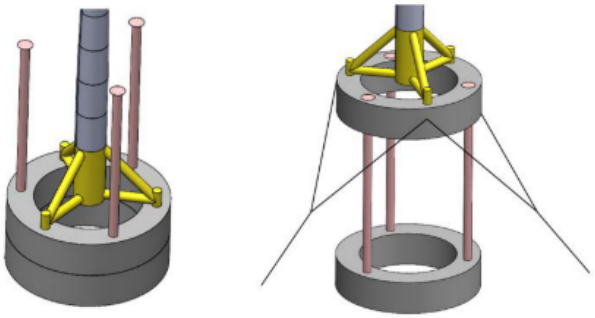

Figure 2.2: Elevator concept before and after installation, illustrating counterweight deployment. Reproduced from Belis et al. [1].

For this thesis, the implication is that the mooring system is not only a station-keeping component but also an important contributor to the horizontal restoring behaviour. The mooring-line representation can therefore influence the predicted platform offset and fairlead effective tension. This is why floater-mooring interaction is central to the mooring-line dynamic amplification assessment. The reference quantities used to define the Elevator case are introduced in Chapter 3, while the numerical model setup is described in Chapter 4.

2.3. Global response modelling of floating wind turbines

The dynamic behaviour of a floating offshore wind turbine is governed by the interaction between aerodynamic loading, hydrodynamic loading, structural inertia, hydrostatic restoring, mooring forces, and turbine control. Floating wind turbines are therefore commonly analysed as coupled aero-hydro-servo-elastic systems [10, 11].

This study uses this coupled-system framework as physical background, but it does not model the full aero-servo-elastic turbine response. The main comparison is limited to the floater and mooring response under first-order irregular wave excitation. This scope is chosen to assess the effect of the mooring line representation, QS or DYN, while keeping the other main modelling inputs as consistent as possible.

2.3.1. Linearised equation of motion

A floating wind turbine is commonly modelled at a global-response level as a rigid body with six degrees of freedom (6-DOF): surge, sway, and heave, roll, pitch, and yaw [4]. The displacement vector $\boldsymbol{\eta}$ is defined as

$$\boldsymbol{\eta} = \begin{bmatrix} x & y & z & \phi & \theta & \psi \end{bmatrix}^T, \tag{2.1}$$

where x, y, and z are the translational motions surge, sway, and heave, and ϕ, θ, and ψ are roll, pitch, and yaw.

A linearised global equation of motion can be written as

$$(\mathbf{M} + \mathbf{A})\,\ddot{\boldsymbol{\eta}} + (\mathbf{B}_v + \mathbf{B}_r)\,\dot{\boldsymbol{\eta}} + (\mathbf{C}_{moor} + \mathbf{C}_h)\,\boldsymbol{\eta} = \mathbf{F}_{wave} + \mathbf{F}_{wind} + \mathbf{F}_{current} + \mathbf{F}_{turbine} \tag{2.2}$$

Here $\mathbf{M}$ is the dry-mass matrix, $\mathbf{A}$ is the hydrodynamic added mass matrix, $\mathbf{B}_r$ is radiation damping, $\mathbf{B}_v$ represents other linearised damping contributions, $\mathbf{C}_h$ is the hydrostatic restoring matrix, and $\mathbf{C}_{moor}$ is the linearised mooring restoring matrix. The right-hand side contains external excitation from wave loading, wind loading on the structure, current loading, and turbine-related loading [4]. In this context, linearised means that the matrices are evaluated around a static equilibrium and describe small motions about that equilibrium.

Equation 2.2 is useful for this study, because it shows how the mooring system is incorporated in a linearised global floater model. Around the static equilibrium position, the mooring lines are represented by the restoring matrix $\mathbf{C}_{moor}$. This relates small platform displacements to restoring forces and moments. This representation captures local mooring stiffness, but it does not resolve distributed line inertia, hydrodynamic drag, or time-dependent line-shape effects along the mooring lines [4].

2.3.2. Frequency-domain form

For linear steady-state response, the equation of motion can be written in the frequency domain as

$$\{-\omega^2 [\mathbf{M} + \mathbf{A}(\omega)] + i\omega\mathbf{B}(\omega) + \mathbf{C}\}\boldsymbol{\eta}(\omega) = \mathbf{F}(\omega) \tag{2.3}$$

Here ω is the angular frequency, $\mathbf{A}(\omega)$ is the frequency-dependent added mass matrix and $\mathbf{C} = \mathbf{C}_h + \mathbf{C}_{moor}$ is the linearised restoring matrix [4].

This formulation is useful for interpreting natural periods, response amplitude operators, and first-order wave-frequency response trends [4]. However, it remains a linear description around a static equilibrium position. It therefore cannot describe the full time history of the mooring lines or the velocity-dependent forces acting along them.

Time-domain analysis is generally required when the response depends on motion history, line velocity, or large changes in mooring geometry [4, 6, 11]. This thesis applies this argument in a limited way. It does not perform a complete aero-servo-elastic simulation of the turbine, controller, floater, and mooring system. Instead, it compares QS and DYN mooring-line models in OrcaFlex under the same first-order wave loading.

2.3.3. Mass, damping, and restoring terms

The inertia terms are represented by the dry structural mass matrix M and the hydrodynamic added-mass matrix A. Added mass represents the inertia of the surrounding water that is accelerated together with the floating body [4].

The damping terms are represented by the damping matrices B_r and B_v. These may include radiation damping, viscous damping, aerodynamic damping, controller-related damping, and mooring-line damping. Radiation damping is associated with wave energy carried away by body motion, while viscous damping is associated with flow separation and drag effects [4]. In the simulations of this study, aerodynamic damping and turbine-control effects are not modelled explicitly, because the comparison is focused on the mooring-line representation.

The restoring terms are represented by the hydrostatic restoring matrix C_h and the mooring-restoring matrix C_{moor}. Hydrostatic restoring follows from the geometry of the floating body and the distribution of buoyancy. Mooring restoring follows from the force-displacement behaviour of the station-keeping system [4]. This distinction is important for the Elevator concept because upright stability is mainly hull-driven, while horizontal restoring is mainly provided by the inclined taut mooring lines.

2.3.4. Natural frequencies and coupled modes

Natural frequencies follow from the balance between effective inertia and restoring stiffness. Using K as the total linearised stiffness matrix, the undamped eigenvalue problem may be written as follows:

$$\left(\mathbf{K} - \omega_0^2 \mathbf{M}_{\text{eff}}\right) \boldsymbol{\psi} = \mathbf{0} \tag{2.4}$$

Here $\boldsymbol{\psi}$ is the mode-shape vector, ω_0 is the natural circular frequency, and $\mathbf{M}_{\text{eff}}$ is the effective inertia matrix [4]. For a floating body, $\mathbf{M}_{\text{eff}}$ may include hydrodynamic added mass, while $\mathbf{K}$ includes hydrostatic and mooring-restoring contributions.

The six rigid-body motions are usually referred to as surge, sway, heave, roll, pitch, and yaw. The actual eigenmodes do not always correspond to pure motions because off-diagonal terms in the mass, added-mass, and restoring matrices can couple the degrees of freedom [4]. This coupling is relevant for floating wind turbines because it can shift natural periods and alter the load transfer between floater motions and mooring tensions.

2.3.5. Quasi-static and dynamic mooring representation

The mooring contribution can first be described by a linearised force-displacement relation around the equilibrium position. For a small displacement $\Delta\boldsymbol{\eta}$, the change in mooring force is

$$\Delta\mathbf{F}_m \approx -\mathbf{C}_{\mathbf{moor}}\Delta\boldsymbol{\eta} \tag{2.5}$$

The minus sign indicates that the mooring force acts as a restoring force, opposing the displacement. This type of linearised mooring contribution is commonly used in global floating-body equations of motion [4].

This representation captures the local stiffness of the mooring system near the static equilibrium. It does not resolve distributed line inertia, hydrodynamic drag, added mass, or time-dependent line-shape effects along the mooring line. For the Elevator model, the specific stiffness terms used to construct $\mathbf{C}_{moor}$ are introduced in Chapter 3.

Three mooring modelling levels are relevant for this thesis. The first is a fixed linearised mooring-restoring matrix around the static equilibrium. The second is a QS mooring-line model, where the static line equilibrium is updated for the instantaneous fairlead position. The third is a DYN mooring-line model, where the line is solved as a time-dependent system with distributed inertia, drag, and added mass.

A QS mooring line model is more general than a fixed linear stiffness matrix because it updates the static line equilibrium for the instantaneous fairlead position. However, it still does not resolve distributed line inertia, hydrodynamic drag, or added mass. A DYN mooring line model resolves the line as a time-dependent system so that the predicted tension depends on both instantaneous geometry and line motion [4, 12].

The QS approximation can become incomplete when fairlead motion changes the line shape with time. In that case, hydrodynamic drag acts along the line, and line inertia and added mass may also affect the top-end tension. These effects can make the DYN line tension differ from the QS prediction, especially when fairlead velocity, low-frequency motion, or long line length becomes relevant [4].

Previous floating-wind studies have shown that the choice between QS and DYN mooring modelling can affect predicted platform motions and mooring loads under certain conditions [5, 6]. The question for this study is therefore not whether dynamic mooring effects exist in general but whether they change the selected response quantities for the Elevator model and the considered first-order ULS cases.

2.4. Aerodynamic loading on wind turbines

Aerodynamic loading contributes to the global force and moment balance of a floating offshore wind turbine. For this thesis, the most relevant aerodynamic load is rotor thrust, because it acts near hub height and can influence mean surge offset, pitch response, and mooring line tension.

In detailed floating-wind analysis, aerodynamic loading is coupled to platform motion, structural dynamics, and turbine control [4, 11]. This full coupling is not modelled in this thesis. The purpose of this section is therefore limited to explaining the role of rotor thrust and the simplified steady-thrust sensitivity used later in the numerical model.

2.4.1. Global thrust representation

At global-response level, the aerodynamic action of the rotor can be represented by the rotor thrust force. For a rotor with swept area A, the thrust can be written as

$$T = \frac{1}{2}\rho_{\mathrm{air}} C_T A U_r^2 \tag{2.6}$$

where ρ_{air} is the air density, C_T is the thrust coefficient, and U_r is the relative wind speed at the rotor [4].

This expression captures the dominant horizontal aerodynamic load without resolving blade-level loading. The associated pitch moment about a reference point near the still-water level can be approximated as

$$M_T = T z_{\mathrm{hub}} \tag{2.7}$$

where z_{hub} is the vertical distance between the thrust application point and the chosen moment reference point. This moment arm is important for floating wind turbines because rotor thrust can change both the mean surge offset and the mean pitch angle [11].

The thrust coefficient is not constant during turbine operation. It depends on wind speed, blade pitch, rotor speed, and controller action [4, 11]. For the IEA 15 MW offshore reference turbine, the rotor diameter is $240\ \mathrm{m}$ and the hub height is $150\ \mathrm{m}$ [13]. These values define the scale of the aerodynamic thrust and its moment arm for the Elevator concept.

2.4.2. Effect of platform motion on aerodynamic loading

For floating wind turbines, aerodynamic loading is not independent of floater motion. Surge motion changes the relative wind speed at the rotor, while pitch motion changes the rotor orientation and the effective inflow angle. Both effects can change rotor thrust and power production [4, 11].

This coupling can also introduce aerodynamic damping. Below rated wind speed, platform surge and pitch motion can contribute to aerodynamic damping contributions. Above rated wind speed, the interaction becomes more complex because the controller modifies blade pitch and rotor speed [4]. Detailed studies also show that platform pitch affects rotor loading, aerodynamic response, and power production [14, 15].

2.4.3. Simplified aerodynamic treatment in floating-wind studies

Full aero-servo-elastic modelling is needed when the objective is to predict detailed turbine loads, controller response, power production, or transient fault behaviour. For the present study, the aerodynamic model is used only to test the global effect of a mean rotor-thrust load on a floater equilibrium.

This distinction is important for the QS-DYN comparison. The comparison is performed under first-order wave loading without turbulent wind, turbine control, or unsteady aerodynamic loading. Aerodynamic loading is included only through a simplified steady-thrust sensitivity, where a mean horizontal thrust force and equivalent pitch moment are applied to assess their effect on mean offset and line-tension redistribution.

2.5. Hydrodynamic loading and modelling

Hydrodynamic loading is a main source of floater motion in waves. Waves generate excitation forces on the floating structure, while the surrounding water contributes to added mass and damping [4]. In this thesis, the hydrodynamic model is important because it defines the floater response that drives the mooring system. The same hydrodynamic input is used for the QS and DYN mooring line models so that the comparison focuses on the mooring line representation rather than on changes in wave loading.

2.5.1. Wave-induced loading on floating structures

For a floating body in waves, the hydrodynamic problem includes wave excitation forces, added mass, radiation damping, and viscous effects [4]. Wave excitation represents the external wave load on the body. Added mass and radiation damping describe how the surrounding water changes the effective inertia and damping of the floating system. These quantities are therefore the main hydrodynamic inputs needed to describe the first-order wave-induced motion of the floater.

2.5.2. Morison-type loading for slender members

For slender cylindrical members, wave loading is commonly represented with a Morison-type formulation. In simplified notation, the load per unit length normal to the member can be written as

$$f_M = \rho C_m A \dot{u} + \frac{1}{2}\rho C_d D\, u|u|, \tag{2.8}$$

where ρ is the water density, C_m is the Morison inertia coefficient, C_d is the drag coefficient, $A = \pi D^2/4$ is the displaced area per unit length, D is the member diameter, and u and $\dot{u}$ are the local normal velocity and acceleration of the water particles [4, 16].

This formulation is appropriate when the member diameter is small relative to the incident wavelength so that the member does not strongly disturb the surrounding wave field [4]. Morison-type loading is therefore widely used for slender offshore members such as braces, columns, and line-like components. Its main limitation is that it does not describe diffraction and radiation effects of large-volume bodies.

2.5.3. Diffraction-radiation methods for large-volume bodies

When the body dimensions are no longer small relative to the wavelength, the structure modifies the surrounding wave field. Wave scattering and radiation effects then become important, and a purely local Morison-type representation is no longer sufficient [4].

Linear potential-flow panel methods are commonly used for such large-volume floating bodies. These methods compute first-order wave-excitation loads, added mass, and radiation damping from a panel representation of the wetted geometry [17].

The resulting hydrodynamic coefficients therefore depend on which parts of the structure are included in the panel body and on the quality of the wetted-surface mesh. It gives a qualitative indication of the relative importance of drag, inertia, and diffraction as a function of characteristic dimension, wave height, and wavelength.

This distinction is important because a floating platform may contain both slender and non-slender components. Figure 2.3 gives a qualitative indication of the wave-force regime based on the characteristic structural dimension D, wave height H, and wavelength λ. The horizontal axis indicates the relative size of the structure compared with the wavelength, while the vertical axis indicates the wave height relative to the structural dimension. Large values of $\pi D/\lambda$ indicate that diffraction effects become important, whereas smaller values are associated with Morison-type inertia and drag loading.

The figure supports the distinction made in this thesis between slender-member loading and diffraction-radiation modelling for the larger-volume floater components.

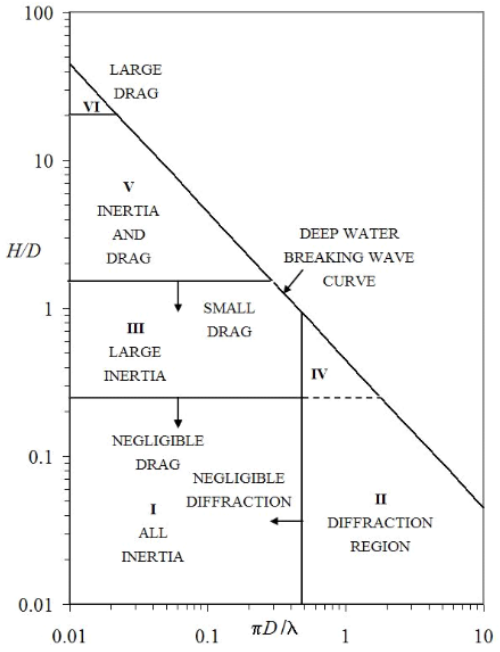

Figure 2.3: Wave-force regimes for offshore structures. Reproduced from DNV [18].

2.5.4. Hydrodynamic implication for the Elevator concept

This modelling issue is directly relevant for the Elevator concept because the structure combines members of different scales. The columns and tripod members are relatively slender, whereas the upper and lower tanks are large-volume components [1]. The Curaçao reference-design study used simplified geometry-based added-mass estimates and surrogate damping values for screening purposes rather than a full diffraction-radiation solution [1].

The literature therefore suggests that the hydrodynamic model for the Elevator should not be treated as uniform across all members. A Morison-type representation may be suitable for the slender structural parts, whereas the larger tanks require a diffraction-radiation treatment. The specific hydrodynamic representation adopted in this thesis is described in Chapter 4.

Mooring systems keep floating offshore wind turbines on station and contribute to the global restoring behaviour of the floater. In floating wind literature, the term tendon is usually associated with highly tensioned TLP elements. The Elevator concept, however, uses inclined taut synthetic mooring lines rather than classical vertical steel TLP tendons [1, 9]. The focus of this section is therefore on the mechanics of tensioned mooring lines in deep water. Figure 2.4 shows the common mooring configurations used for floating offshore structures and the seabed area required per configuration.

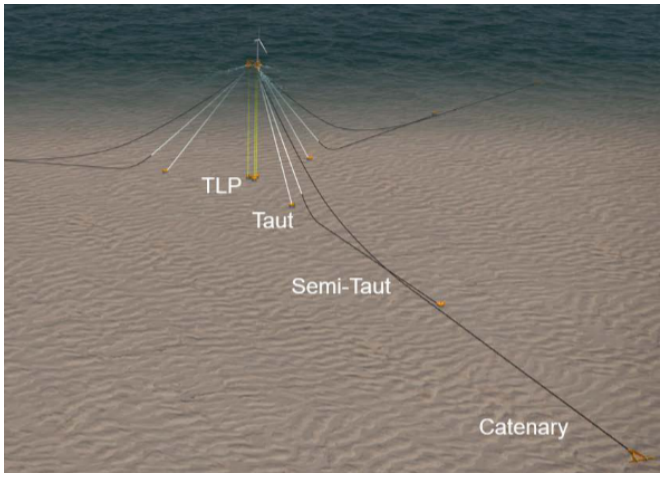

Figure 2.4: Mooring system configurations and seabed area required. Reproduced from Cooperman et al. [7].

2.6. Mooring systems and tensioned line mechanics

2.6.1. Functions and main configuration types

The mooring system of a floating wind turbine has two main functions: it keeps the platform on station and it contributes to restoring under environmental loading [3, 9]. The way in which this restoring is generated depends strongly on the mooring configuration.

In catenary systems, restoring is dominated by line weight, suspended geometry, and seabed interaction. In taut systems, restoring is governed more directly by axial tension, line elongation and line inclination. Tension-leg systems form a special case of highly tensioned moorings with strong vertical restraint [9, 19]. These differences affect platform motions, anchor loads, seabed footprint, and sensitivity to water depth [7, 19].

For deep-water sites, the mooring configuration becomes an important feasibility driver. Increasing water depth increases the required line length, suspended line mass, anchor spacing, and seabed footprint, especially for heavy catenary systems [2, 3]. Taut and semi-taut systems can reduce the footprint and line mass, but they also make the response more dependent on pretension, axial stiffness, and line inclination [9, 19].

2.6.2. Restoring behaviour of taut systems

In a taut mooring system, restoring is generated mainly by changes in line tension and line direction. A displacement of the floater changes the line geometry and axial extension, which changes the fairlead tension and produces a restoring force [9, 19].

The restoring behaviour therefore depends on the mean tension state, the axial stiffness of the line, and the line inclination. Compared with catenary systems, taut systems often provide stronger restoring for a given horizontal displacement, but they also lead to higher fairlead and anchor loads and stronger coupling between floater motion and line tension [3, 19].

For this study, pretension is especially important. The mean line tension defines the state around which the line responds in the irregular-wave simulations. The effective restoring stiffness is therefore not only a material property but also depends on the line geometry and static tension state. This is consistent with the treatment of mooring restoring in linearised floater equations, where the mooring system contributes directly to the restoring matrix of the global system [4].

2.6.3. Synthetic fibre ropes in deep water

Synthetic fibre ropes are attractive for deep-water mooring because of their low submerged weight and high strength-to-weight ratio compared with steel chain or wire. This is especially relevant for floating wind concepts in deep water, where heavy catenary systems can lead to large suspended line mass, large seabed footprint, and high vertical load on the floater [3, 9, 19].

HMPE is particularly relevant for taut deep-water mooring because it combines low line mass with a relatively stiff load-strain response compared with polyester and nylon ropes. Figure 2.5 shows typical stress-strain behaviour for different synthetic fibre families. The figure is used only as material context. It does not represent the specific load-strain curve of the Elevator mooring line.

HMPE fibres have a specific gravity of about 0.97, corresponding to a density of approximately $970\ \mathrm{kg/m^3}$. This is slightly lower than typical seawater density, which is about $1025\ \mathrm{kg/m^3}$. By contrast, steel has a density of about $7850\ \mathrm{kg/m^3}$. The submerged weight of an HMPE rope is therefore much smaller than that of steel, and the rope may be close to neutrally buoyant or positively buoyant depending on rope construction, coating, and terminations [20, 21].

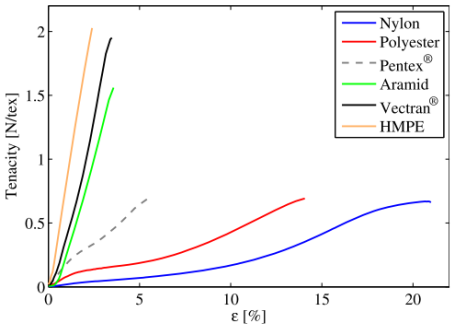

Figure 2.5: Typical stress-strain behaviour of synthetic fibre families. Reproduced from Weller et al. [20].

The stiffness of synthetic fibre ropes is not a single fixed material constant. Experimental work on polyester, aramid, and HMPE ropes under cyclic loading shows nonlinear tension-elongation behaviour, hysteresis, and stiffness evolution with mean load, strain amplitude, and number of cycles [22]. For this reason, HMPE mooring lines are often represented in numerical models using an effective axial stiffness defined for the relevant load range. In this thesis, the HMPE line is therefore modelled with an effective axial stiffness at the selected pretension level. The resulting strain and elastic elongation are checked later to assess whether the adopted pretension state is physically plausible.

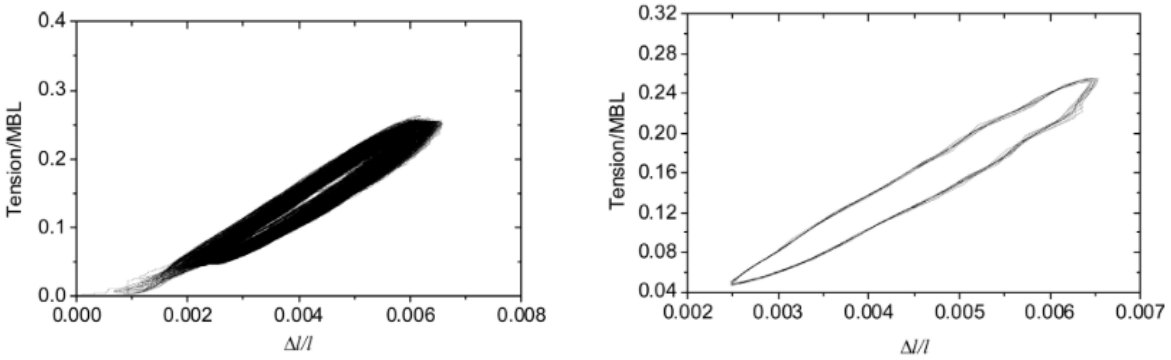

Figure 2.6: Cyclic tension-elongation behaviour of an HMPE rope under cyclic loading. Reproduced from Liu et al. [22]. The figure illustrates nonlinear response and hysteresis and is used only to support the discussion of effective axial stiffness.

2.6.4. Dynamic effects in long tensioned lines

For long tensioned mooring lines, the response is not governed only by the static force-displacement relation. In a quasi-static representation, the line force is obtained from the instantaneous fairlead position and the corresponding static line equilibrium. This neglects distributed line inertia, hydrodynamic drag, added mass, and time-dependent changes in line shape [4].

These omitted terms can become relevant when the fairlead moves with finite velocity, when the line is long, or when the excitation is close to a line or floater response frequency. In that case, the fairlead effective tension may differ from the quasi-static prediction. The difference can result from hydrodynamic resistance to line motion, axial tension propagation, and local line-vibration modes.

Floating-wind studies support this modelling concern. Mooring dynamics can affect the global response of a floating wind turbine, and increasing water depth can change floating-wind dynamics and mooring-system behaviour [5, 6]. Therefore, long tensioned mooring lines in deep water should not automatically be assumed to behave quasi-statically under severe loading.

For the Elevator concept, these dynamic-line effects are relevant because the mooring lines are long, tensioned, and synthetic. This motivates a QS-DYN comparison, while the detailed model setup is introduced later in Chapter 4.

2.6.5. Implication for the mooring layout

The previous sections show that mooring layout selection in deep water is affected by line length, submerged weight, seabed footprint, anchor layout, line stiffness, and line inclination [3, 7, 19]. These factors make the choice of mooring configuration an important design problem in itself.

This thesis does not address that full design problem. Instead, the three-line inclined taut HMPE layout from Belis et al. [1] is adopted as the fixed mooring layout for the Elevator model. Alternative catenary, semi-taut, hybrid, or re-optimised layouts are therefore not compared. Changes in line angle, line length, rope material, and anchor layout are also outside the scope of the main QS-DYN comparison.

For the adopted layout, the relevant modelling quantities are the mean tension state, unstretched line length, effective axial stiffness, line inclination, and possible line-dynamic effects. These quantities determine how fairlead motion is translated into changes in line force. The detailed mooring input values are defined in Chapter 3, and their numerical implementation is described in Chapter 4.

2.7. Dynamic response and resonance

The response of a floating wind turbine depends on the relation between the excitation frequencies and the natural frequencies of the coupled system. This section summarises the response mechanisms that are relevant for interpreting dynamic amplification in the later QS-DYN mooring-line model comparison.

2.7.1. Excitation ranges and response regimes

Floating wind turbines can respond in different frequency ranges. First-order wave excitation acts mainly at wave frequencies. Difference-frequency wave-drift loading can excite low-frequency horizontal motions, while local structural or line modes may occur at higher frequencies [4, 10].

Which response regime is most important depends on the wave spectrum, the system natural frequencies, and the damping level. If the dominant wave periods are far from the relevant natural periods, direct first-order resonance is less likely. However, low-frequency excitation, transient effects, and local mooring-line dynamics can still influence the response [4, 6, 10].

2.7.2. Resonance and dynamic amplification

In a linear system, resonance occurs when the excitation frequency approaches a natural frequency of the system. In that case, the response amplitude can increase compared with a low-frequency or static response. The magnitude of this increase depends strongly on damping [4].

Figure 2.7 illustrates this principle for a simplified heave-response example. At low frequencies the response is mainly governed by restoring, near resonance it is governed by damping, and at high frequencies it is governed by inertia. The figure is used only as a qualitative explanation of frequency-dependent response behaviour.

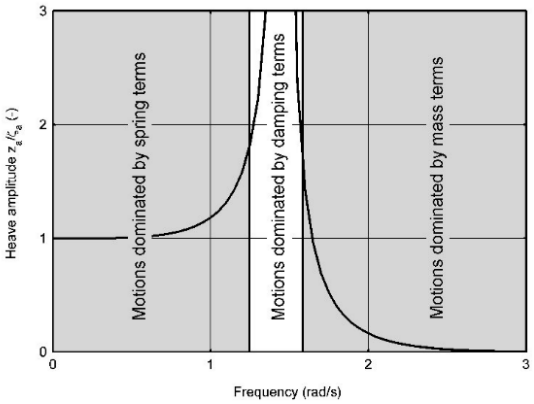

Figure 2.7: Frequency regions for motion response in a simplified heave-response example. Reproduced from Journée and Massie [17].

For floating wind turbines, resonance is more complex than for a simple single-degree-of-freedom oscillator. The relevant modes are coupled rigid-body modes, and their natural periods depend on hydrostatic properties, mass properties, and mooring restoring contributions [4, 10]. Resonance-sensitive behaviour therefore cannot be interpreted from hull properties alone. Changes in mooring stiffness, pretension, and line configuration can shift the relevant response characteristics.

This is relevant for taut systems because the mooring system can contribute strongly to the restoring behaviour. For TLP-type floating wind concepts, recent studies show that unfavourable interaction between structural modes and platform modes should be avoided because resonance-sensitive behaviour can affect the global response [23].

2.7.3. Role of damping and coupled floater–mooring response

Dynamic amplification is not governed by stiffness and inertia alone. Damping also affects the amplitude and phase of the response. For floating wind turbines, damping may arise from wave radiation, viscous effects, aerodynamic effects, control action, and mooring-line behaviour [4]. This means that the same restoring stiffness does not automatically lead to the same predicted response if the damping model changes.

The mooring system can also influence the response through its coupling with the floater. Fairlead motion changes the line geometry and line tension, while the resulting line forces feed back into the platform motion. As discussed in Section 2.6.4, a DYN mooring-line model can include distributed line inertia, drag, added mass, and time-dependent line-shape effects. These terms can change both the magnitude and timing of the line-force response [4, 6].

For response interpretation, the floater and mooring system should therefore be considered as a coupled system. Differences between QS and DYN results should not be interpreted only from restoring stiffness but also from damping, fairlead motion, and line-dynamic effects.

2.7.4. Implication for response interpretation

For the Elevator concept, the response characteristics depend on both hull properties and taut mooring line behaviour [1]. The QS-DYN mooring comparison therefore has to be interpreted together with the restoring behaviour, the main natural periods, and the wave periods in the selected sea states.

This motivates the later use of static restoring checks, free-vibration tests, and response interpretation. These checks do not show that line-dynamic effects are always small. They are used to explain whether the QS and DYN predictions remain close for the selected first-order screening cases.

2.8. Ultimate limit state and design considerations

In floating offshore wind design, the ultimate limit state (ULS) concerns the ability of the system to withstand rare and severe loading without loss of structural or mooring integrity. Floating wind guidance documents distinguish ULS from fatigue and accidental limit states [24, 25].

In this thesis, ULS is used as a ULS-type screening context rather than as a full certification design assessment. The selected cases are used to compare whether the QS and DYN mooring-line models give different predictions for the selected extreme-response quantities: maximum horizontal platform offset and governing fairlead effective tension.

2.8.1. ULS in floating-wind mooring design

For moored floating wind turbines, ULS response is assessed at system level. The floater, mooring system, and environmental loading are coupled, so mooring-line loads cannot be interpreted independently from platform motion [3, 9].

Floating-wind guidance documents therefore consider severe combinations of wind, wave, and current loading, including unfavourable directions and operating conditions [24, 26]. Relevant ULS checks include mooring-line strength, fairlead loads, anchor loads, platform excursions, and global stability.

2.8.2. Governing ULS response quantities

For mooring systems, the most direct ULS response quantity is the maximum line tension. It determines the line load level and affects the demand on connected components such as fairleads and anchors [3, 27]. Platform offset is also important, because large excursions change the mooring geometry and redistribute line loads.

For taut mooring systems, the relation between platform motion and line tension is especially relevant. As discussed in Section 2.6.2, fairlead motion changes line elongation and line inclination. The resulting change in line force depends on the pretension level and axial stiffness [9, 19].

This study therefore focuses on maximum horizontal platform offset, r_{max}, and governing fairlead effective tension, $T_{eff,max}$. The fairlead-tension range above the mean, ΔT_{eff}, is also used as a supporting quantity because it shows how large the wave-induced tension variation is relative to the mean tension level. Platform pitch is treated as a supporting response quantity because it affects the global equilibrium and mooring-line force distribution. These quantities are used for the QS-DYN comparison, not as a complete mooring-capacity or certification check.

2.8.3. Need for coupled analysis in ULS assessment

Simplified mooring models are useful for estimating restoring behaviour, offsets, and first-order response trends. However, a ULS screening result should not be interpreted only from static force balance when dynamic line effects may contribute to the response [3, 6]. This motivates a coupled time-domain comparison in which floater motion and mooring response are solved together.

For the Elevator model, this means that the selected ULS comparison focuses on maximum horizontal platform offset, r_{max}, governing fairlead effective tension, $T_{eff,max}$, and selected supporting platform motions. These quantities are used to assess whether the mooring-line modelling level changes the response.

2.9. Numerical modelling approaches

Floating wind turbines can be modelled with different levels of detail. Linearised and frequency-domain models are useful for identifying the main response characteristics, such as natural periods, response amplitude operators, and first-order wave-frequency response. Time-domain models are used when nonlinear effects, transient behaviour, or motion-history-dependent effects need to be represented [4, 10].

The appropriate modelling approach depends on the response quantity of interest and on the physical effects that must be included. For this thesis, this distinction is important because the floater response is solved dynamically, while the modelling difference concerns the mooring-line representation. The following sections therefore introduce the modelling approaches used for hydrodynamic analysis and coupled floater-mooring time-domain simulation.

2.9.1. Linear frequency-domain models

Linear frequency-domain models are commonly used to interpret the main response behaviour of floating systems. In these models, the system is linearised about a mean equilibrium position, and the response is calculated as a function of frequency. This makes them useful for estimating natural periods, response amplitude operators, and first-order wave-frequency response trends [4, 10].

This modelling level is mainly used for interpretation in this study. It helps identify whether selected wave periods are close to important rigid-body natural periods. However, it does not resolve nonlinear time-domain effects or the motion history of the mooring lines. A time-domain comparison is therefore required for the QS-DYN mooring-line representations.

2.9.2. Time-domain models

Time-domain models calculate the response step by step in time. This allows irregular wave loading, changing mooring geometry, transient effects, and velocity-dependent forces to be represented more directly than in a purely linear frequency-domain model [4, 10].

The required level of coupling depends on the purpose of the analysis and on the response quantities of interest. Full floating-wind design-load simulations may include aerodynamic loading, turbine control, structural dynamics, hydrodynamics, mooring dynamics, and combined wind-wave-current conditions [24, 26]. Such models are needed when the objective is to assess turbine loads, controller response, power production, fatigue, fault cases, or certification-level design loads.

The objective of this thesis is more specific. The time-domain analysis is used to compare two mooring-line representations for the same floater, hydrodynamic input, and first-order irregular-wave loading. This follows from the literature concern that mooring dynamics can influence floating-wind response [4, 6]. The results should therefore be interpreted as a mooring-line modelling comparison, not as a full wind-wave-current design-load assessment.

The QS and DYN mooring-line representations have already been introduced in Section 2.3.5. For the present modelling problem, the key question is whether resolving mooring-line dynamics changes the predicted platform offset and fairlead effective tension relative to a QS mooring-line representation.

2.9.3. Consistency between subsystem models

Adding detail to one part of the model does not automatically improve the overall prediction if the other parts are treated inconsistently. For floating wind turbines, the floater, hydrodynamics, aerodynamics, and moorings interact with each other. The modelling level should therefore be chosen in relation to the research question and the response quantities of interest [9, 10].

This is especially important for hybrid floating concepts, where both hull behaviour and mooring restoring contribute to the response. In such cases, the main modelling question is not how much detail can be included, but which model detail is needed to assess the response quantity of interest. This provides the link to the research gap defined in Section 2.10.

2.10. Research gaps addressed in this study

The previous sections show that floating-wind response depends on the interaction between the floater, hydrodynamic loading, mooring system, and modelling choices. For the present thesis, the relevant gap is not a general lack of knowledge about mooring dynamics, but the case-specific effect of the mooring-line representation on the response of the developed Elevator model.

Deep water is important for this gap. Recent floating-wind reviews identify water depth as a driver for mooring layout, line length, anchor demand, seabed footprint, and mooring-system behaviour [3, 7]. The Elevator concept is considered in a water depth of about $800\ \mathrm{m}$ and uses inclined taut HMPE mooring lines. It is therefore relevant to assess whether a QS mooring-line model gives predictions similar to those from a DYN mooring-line model for the selected response quantities.

Previous studies show that dynamic mooring effects can influence platform motions and mooring loads under certain conditions [5, 6]. These findings cannot be transferred directly to the Elevator concept, because the floater type, water depth, mooring layout, pretension level, and loading assumptions differ. The question for this thesis is therefore not whether dynamic mooring effects exist in general but whether they change the predicted maximum horizontal platform offset, governing fairlead effective tension, and fairlead-tension range above the mean for the developed Elevator model.

A meaningful QS-DYN comparison also requires modelling consistency. The floater representation, hydrodynamic input, mooring geometry, environmental cases, wave seed, simulation settings, and post-processing method must remain the same. Otherwise, differences in offset or fairlead effective tension could be caused by changes in the surrounding model rather than by the mooring-line representation itself.

This thesis addresses this gap by developing a numerical Rhino-OrcaWave-OrcaFlex implementation of the Elevator concept and using it for a same-input QS-DYN mooring-line comparison. The comparison is limited to the selected first-order, wave-only cases defined in this thesis. The resulting conclusions are therefore case-specific and should not be generalised to broader wind-wave-current cases or certification-level design-load conditions.

3

Case definition and model input selection for the Elevator model

This chapter defines the Elevator case and the quantities used to develop the numerical model. The Elevator concept is based on the Curaçao design study by Belis et al. [1]. The purpose of this chapter is to identify which reference quantities are used as model inputs, which quantities are used as verification targets, and how the reference-design values are interpreted before they are implemented in OrcaWave and OrcaFlex.

The Belis et al. [1] report contains both summary values and appendix calculation outputs. Where small inconsistencies occur, the appendix calculation outputs are used as the primary basis because they define the subsequent reference calculations. The full set of reference values is listed in Appendix A, while the main text reports only the quantities needed to understand the selected case definition.

Some implemented quantities differ from the original design values because this thesis uses a simplified diffraction-body representation in OrcaWave. These implementation choices are introduced and verified in Chapter 4. The key requirement for the QS-DYN comparison is that both mooring-line representations use the same numerical Elevator model. This allows later differences in platform offset and fairlead effective tension to be interpreted mainly as the effect of changing the mooring-line representation.

3.1. Case definition and reference design

This thesis uses the 15 MW Elevator floating wind concept from Belis et al. [1] as the case for the QS-DYN mooring-line comparison. The Elevator was selected in that study as a hybrid floating concept for deep-water conditions near Curaçao. It combines an upper buoyant tank, a lower ballast tank, three inter-tank columns, a tripod support structure, and three inclined taut HMPE mooring lines. Figure 3.1 shows the main components of the concept.

The Elevator is treated as a hybrid floater rather than as a conventional TLP, spar, or semi-submersible. Its upright stability is mainly provided by the hull, ballast, and hydrostatic righting behaviour, while the inclined taut mooring lines provide station-keeping and horizontal restoring. This distinction is important because the present thesis focuses on the interaction between floater response and mooring-line representation.

The Belis et al. [1] study is used as the source for the initial geometry, turbine mass data, hydrostatic quantities, target mooring tension, linearised restoring quantities, and screening-level natural periods. In this thesis, these quantities are used as reference inputs and plausibility checks.

The numerical QS and DYN OrcaFlex models are developed in this thesis. They use the same Elevator model and differ only in the mooring-line representation. Some implemented quantities differ from the original reference-design values because the developed OrcaWave-OrcaFlex model uses a reduced diffraction-body representation. These implementation choices are introduced and verified in Chapter 4. The detailed reference design values are provided in Appendix A.

3.2. Coordinate convention and reference quantities

Belis et al. [1] use several vertical reference levels for the Elevator concept. Hydrostatic quantities such as KG, KB, and BM are reported relative to the keel. The appendix calculation outputs use keel-referenced values for KG and KB, while some inertia quantities are reported about a point at still water level. A clear coordinate convention is therefore needed before the reference values can be used in OrcaWave and OrcaFlex.

Unless stated otherwise, the numerical model quantities are expressed relative to a still-water-level (SWL) origin. The positive z-axis points upward. This convention is used to keep the OrcaWave and OrcaFlex inputs consistent.

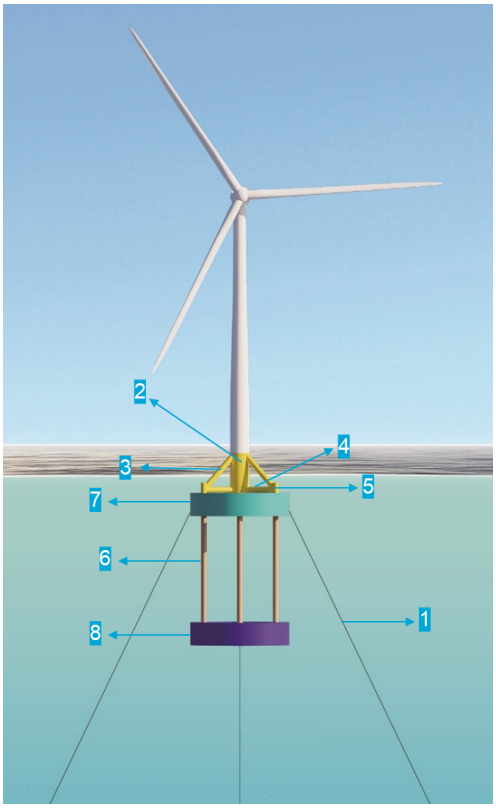

Figure 3.1: Main components of the Elevator concept. Author's illustration based on the Elevator reference concept from Belis et al. [1]. (1) mooring lines; (2) tripod main column; (3) tripod angled members; (4) tripod horizontal members; (5) tripod end-can connectors; (6) inter-tank columns; (7) upper buoyant tank; (8) lower ballast tank.

For a vertical quantity KQ reported as a distance above the keel, the corresponding SWL coordinate is

$$z_Q = KQ - T \tag{3.1}$$

where T is the draft. For the centre of gravity and centre of buoyancy this gives

$$z_G = KG - T, \qquad z_B = KB - T \tag{3.2}$$

Using the rounded reference-design values $KG = 33.35\ \mathrm{m}$, $KB = 41.81\ \mathrm{m}$, and $T = 88\ \mathrm{m}$, this gives

$$z_G \approx -54.65\ \mathrm{m}, \qquad z_B \approx -46.19\ \mathrm{m} \tag{3.3}$$

These values illustrate the coordinate transformation from keel-referenced quantities to SWL quantities. Small differences may occur between rounded summary values and calculation-output values in the reference-design report. For this reason, the implemented mass, inertia, hydrostatic quantities, and reduced-body assumptions are defined and checked separately in Chapter 4.

The main coordinate and reference quantities used to interpret the reference design are summarised in Table 3.1. The detailed source values are listed in Appendix A.

Table 3.1: Reference quantities used for the keel-to-SWL coordinate conversion.

Quantity	Symbol	Reference value	Reference level	SWL value
Draft	T	$88\ \mathrm{m}$	Keel to SWL	–
Centre of gravity	KG	$33.35\ \mathrm{m}$	Above keel	$z_G \approx -54.65\ \mathrm{m}$
Centre of buoyancy	KB	$41.81\ \mathrm{m}$	Above keel	$z_B \approx -46.19\ \mathrm{m}$
Inertia reference point	O'	–	SWL	–

3.3. Linearised mooring-restoring reference formulation

Belis et al. [1] represents the Elevator mooring contribution by a linearised static restoring formulation around the pretensioned equilibrium. This formulation gives the local change in restoring force and moment for small platform displacements about the static equilibrium. It is not a time-domain quasi-static mooring analysis, and it does not represent distributed mooring-line dynamics.

In this thesis, the formulation is used as a static reference estimate. It defines the target pretension and the approximate local restoring level used to check the OrcaFlex models before the QS-DYN response comparison is made. The actual quasi-static and dynamic mooring-line models are developed separately in OrcaFlex in Chapter 4.

The Belis et al. [1] data contain two closely related tension values. The HMPE secant stiffness is based on a working tension of $T_{\mathrm{work}} = 0.90\ \mathrm{MN}$, while the vertical-equilibrium summary reports a static line tension of approximately $T_0 = 0.95\ \mathrm{MN}$. In this study, $T_{\mathrm{work}} = 0.90\ \mathrm{MN}$ is defined as the target pretension for the OrcaFlex mooring calibration, because it is the value used to define the rope strain and secant axial stiffness.

In OrcaFlex, the pretension is obtained through the line geometry and the unstretched line length [28]. The unstretched line length is therefore adjusted such that the static fairlead tension of the implemented model is approximately $900\ \mathrm{kN}$ at the equilibrium position. This calibration defines the still-water mooring state of the OrcaWave-OrcaFlex model. It is not an exact reproduction of all reference-design quantities because a reduced diffraction-body representation is used later in the workflow.

The working load fraction is defined as

$$f = \frac{T_{\mathrm{work}}}{\mathrm{MBL}} \tag{3.4}$$

where T_{work} is the working tension used for the stiffness definition and MBL is the minimum breaking load of one mooring line. The corresponding secant axial stiffness is

$$EA_{\mathrm{sec}} = \frac{T_{\mathrm{work}}}{\varepsilon(T_{\mathrm{work}})} \tag{3.5}$$

where $\varepsilon(T_{\mathrm{work}})$ is the axial strain at the working tension. The secant axial stiffness represents the average tension-strain slope between zero load and the selected working tension. It is therefore tied to the adopted pretension level. It does not describe the full nonlinear load-history-dependent stiffness of an HMPE rope.

For the linear restoring estimate, the axial stiffness must be converted to an axial line stiffness. This gives the force change in one line per unit change in line length. The corresponding linear axial stiffness of one mooring line is

$$k_i = \frac{EA_{\mathrm{sec}}}{L}, \tag{3.6}$$

where L is the straight fairlead-to-anchor distance used in the reference linearised restoring calculation. Dividing EA_{sec} by this length converts the rope axial stiffness to the axial stiffness of one complete mooring line. Within the linear estimate, a small increase in line length then gives a tension increase of approximately $\Delta T_i = k_i \Delta L_i$. Equations 3.7 and 3.8 then express this line-tension change as global surge, sway, and heave-restoring terms.

This reference length is not the OrcaFlex line-length input. In OrcaFlex, the line input is the unstretched line length, L_0, which is adjusted until the static calculation gives the target still-water fairlead tension of approximately $900\ \mathrm{kN}$.

For a symmetric three-line layout, the axial line stiffnesses can be projected into global restoring terms by resolving the line stiffness along the global displacement directions. With β_i defined as the inclination of line i from the vertical, the horizontal mooring-restoring contributions are estimated as

$$c_{11}^{\mathrm{moor}} \approx \sum_{i=1}^{3} k_i \sin^2 \beta_i \cos^2 \psi_i, \qquad c_{22}^{\mathrm{moor}} \approx \sum_{i=1}^{3} k_i \sin^2 \beta_i \sin^2 \psi_i \tag{3.7}$$

and the vertical contribution is estimated as

$$c_{33}^{\mathrm{moor}} \approx \sum_{i=1}^{3} k_i \cos^2 \beta_i \tag{3.8}$$

Here ψ_i is the line azimuth angle in plan view. For three equal lines spaced at 120°, this gives equal surge and sway restoring estimates. These projected coefficients are used only as local reference values around the pretensioned equilibrium [1, 4].

The key quantities used to interpret the reference mooring-restoring formulation are summarised in Table 3.2.

Table 3.2: Key quantities used in the reference mooring-restoring formulation.

Quantity	Symbol	Value	Unit	Role in this thesis
Working tension for secant stiffness	T_{work}	0.90	MN	OrcaFlex pretension target
Reported equilibrium line tension	T_0	0.95	MN	Reference check
Minimum breaking load per line	MBL	4.04	MN	Strength reference and load fraction
Working load fraction	f	0.223	–	Stiffness calculation
Strain at working tension	$\varepsilon(T_{\mathrm{work}})$	1.41×10^{-2}	–	Stiffness calculation
Secant axial stiffness	EA_{sec}	63.66	MN	QS and DYN axial stiffness input
Reference straight-line length	L	976.62	m	Reference linear-restoring calculation
Linear axial stiffness per line	k_i	65.18	kN/m	Restoring projection
Line inclination to vertical	β	35	$^\circ$	Restoring projection

The most relevant projected restoring terms for the present study are the horizontal restoring in surge and sway and the vertical mooring contribution in heave. In the reference calculation, the surge and sway mooring restoring terms are $c_{11}^{\mathrm{moor}} = c_{22}^{\mathrm{moor}} = 32.17\ \mathrm{kN/m}$, while the heave mooring contribution is $c_{33}^{\mathrm{moor}} = 131.2\ \mathrm{kN/m}$. The mooring contribution in heave is small compared with the hydrostatic heave restoring of the floater. This supports the interpretation that vertical restoring is mainly hull-hydrostatics driven, while the taut mooring lines mainly provide station-keeping and horizontal restoring.

The detailed reference line properties, projected restoring coefficients, and full stiffness matrix are listed in Appendix A. In the present chapter, these values are used only to define the target pretension and local restoring reference level. The linearised reference formulation does not include distributed line inertia, hydrodynamic drag, added mass, dynamic tension propagation, or time-dependent line-shape effects. These effects are included only in the dynamic OrcaFlex line model developed later.

3.4. Hydrodynamic quantities from the reference design

Belis et al. [1] uses a linear small-oscillation model for separate rigid-body degrees of freedom. For each degree of freedom, the effective mass or inertia combines the rigid-body term with an estimated added-mass contribution. The restoring term combines hydrostatic restoring and the linearised mooring contribution. The natural period is then estimated from the square root of the ratio between effective inertia and restoring stiffness. The damping treatment is simplified by using a prescribed modal damping ratio rather than frequency-dependent radiation damping from a diffraction-radiation solution.

The wave-screening quantities are evaluated for a wave period of $T_w = 12\ \mathrm{s}$ and a water depth of $h = 800\ \mathrm{m}$. The wave number k is obtained from the finite-depth linear dispersion relation

$$\omega^2 = gk \tanh(kh) \tag{3.9}$$

where $\omega = 2\pi/T_w$ is the angular wave frequency, g is gravitational acceleration, and h is the water depth.

The product kh is dimensionless and is used only as a relative-depth check. For the reported wave number,

$$kh = 0.02795 \cdot 800 = 22.36 \tag{3.10}$$

Because $kh \gg 1$, the $12\ \mathrm{s}$ screening wave is effectively in deep water. The finite-depth dispersion relation is therefore close to the deep-water form,

$$\omega^2 \approx gk \tag{3.11}$$

This check is included only to explain the reference hydrodynamic screening calculation. It is not a separate design criterion.

The main selected dynamic quantities are summarised in Table 3.3. The table includes the effective masses and inertias, the modal damping ratio used in the reference calculation, and the resulting natural periods. The corresponding effective linear damping coefficients are listed in Appendix B.

Table 3.3: Screening-level dynamic quantities from the reference design [1].

Quantity	Symbol	Value	Unit
Evaluation wave period	T_w	12	s
Water depth	h	800	m
Angular frequency	ω	0.524	$\mathrm{rad/s}$
Wave number	k	27.95×10^{-3}	$\mathrm{m^{-1}}$
Relative depth	kh	22.36	–
Effective surge mass	M_1	48.32×10^6	kg
Effective heave mass	M_3	48.32×10^6	kg
Effective roll inertia	M_4	237.9×10^9	$\mathrm{kg \cdot m^2}$
Effective pitch inertia	M_5	237.9×10^9	$\mathrm{kg \cdot m^2}$
Modal damping ratio	ζ_r	0.030	–
Surge natural period	$T_{n,1}$	243.530	s
Heave natural period	$T_{n,3}$	39.502	s
Roll natural period	$T_{n,4}$	59.549	s
Pitch natural period	$T_{n,5}$	59.549	s

The natural periods indicate a very soft horizontal station-keeping mode and substantially shorter vertical and rotational modes. These values are therefore useful for interpreting the expected response regime of the Elevator concept. In particular, they provide reference values for the later free-vibration checks and for comparing the selected first-order wave periods with the main rigid-body natural periods.

The values in Table 3.3 should not be interpreted as a complete hydrodynamic description of the Elevator. They do not include full first-order diffraction excitation, frequency-dependent radiation damping, second-order wave-drift loads, or detailed hydrodynamic coupling between the different floater members. The hydrodynamic representation used in this thesis is developed separately in Chapter 4 using the OrcaWave model.

3.5. Implications for the numerical modelling approach

The reference quantities in this chapter define the Elevator case and the static checks used during model setup. The QS-DYN comparison itself is developed separately in OrcaWave and OrcaFlex, using one common floater model and two mooring-line representations.

For the QS-DYN comparison to be meaningful, the same numerical Elevator model must be used in both OrcaFlex models. The floater representation, hydrostatic properties, mass properties, hydrodynamic input, environmental cases, wave seeds, target pretension, unstretched line length, and post-processing method are kept consistent. This allows differences in horizontal platform offset and fairlead effective tension to be interpreted mainly as the effect of changing the mooring-line representation.

This interpretation remains limited by the modelling assumptions stated in this thesis. The comparison is a same-input assessment for selected first-order, wave-only ULS cases. Chapter 4 describes how the reference quantities are translated into the OrcaWave-OrcaFlex model.

4

Numerical model setup and verification

This chapter describes how the Elevator case defined in Chapter 3 is translated into the numerical Rhino-OrcaWave-OrcaFlex model used for the QS-DYN comparison. The chapter first defines the modelling assumptions and the input setup used to compare the QS and DYN mooring-line representations. It then presents the environmental input, selected sea states, geometry definition, mooring implementation, OrcaWave hydrodynamic database, and OrcaFlex static verification checks.

4.1. Modelling approach and assumptions

The Elevator case and reference inputs were defined in Chapter 3. This section describes how these inputs are implemented in OrcaWave and OrcaFlex before the response comparison is made. All OrcaWave and OrcaFlex calculations were performed using version 11.6.

The numerical workflow follows the modelling logic introduced in Section 1.7. First, the first-order hydrodynamic coefficients and wave-excitation loads of the floater are calculated in OrcaWave. The resulting hydrodynamic database is then imported into OrcaFlex, where the floater response and mooring loads are solved in the time domain. For each load case, two OrcaFlex models are used: one with a quasi-static mooring line representation and one with a dynamic finite-element mooring line representation.

The QS and DYN models use the same floater geometry, dry mass properties, hydrostatic properties, hydrodynamic database, environmental input, wave seed, simulation settings, and post-processing method. The only intended difference between the two models is the mooring line representation.

The global floater response is interpreted using the six-degree-of-freedom equation of motion introduced in Section 2.3. In this study, the mooring force implementation is not defined as a fixed linear stiffness matrix during the time-domain simulations. Instead, OrcaFlex evaluates the mooring reaction from either the quasi-static line model or the dynamic line model. In compact form, the time-domain problem can be written as

$$(\mathbf{M} + \mathbf{A})\,\ddot{\boldsymbol{\eta}} + \mathbf{B}\dot{\boldsymbol{\eta}} + \mathbf{C}_h\boldsymbol{\eta} + \mathbf{F}_m(t) = \mathbf{F}_{\mathrm{wave}}(t), \tag{4.1}$$

where $\mathbf{M}$ is the dry-mass matrix, $\mathbf{A}$ is the hydrodynamic added-mass matrix, $\mathbf{B}$ is the hydrodynamic damping matrix, $\mathbf{C}_h$ is the hydrostatic restoring matrix, $\mathbf{F}_m(t)$ is the mooring force vector, $\mathbf{F}_{\mathrm{wave}}(t)$ is the first-order wave-excitation force vector, and $\boldsymbol{\eta}$ is the six-degree-of-freedom displacement vector.

Equation 4.1 is used as a compact representation of the solved floater-mooring problem. In the OrcaFlex implementation, the hydrodynamic terms are taken from the imported OrcaWave database, and the mooring force is calculated by the selected mooring-line model. Aerodynamic and current load terms are omitted from Eq. 4.1 because they are not included in the main QS-DYN comparison. The simplified steady-thrust case is treated separately as a sensitivity case in Section 6.2.

4.1.1. Model development route

Figure 4.1 summarises the route used to obtain the QS-DYN comparison model. The figure documents the main model-selection and implementation steps. The early OrcaFlex proxy was used only to check the setup logic of the floater-mooring system. A full Elevator panel-body model was then tested in OrcaWave, but this model was not used because of mesh-quality warnings near the still water level. The model used for this thesis therefore uses a reduced diffraction-body representation as the common hydrodynamic basis.

The model development was an iterative part of the thesis work. Several geometry and hydrodynamic representations were tested before the developed diffraction-body representation was selected. The Elevator model in this thesis is therefore a numerical implementation developed, simplified, and verified for the QS-DYN comparison.

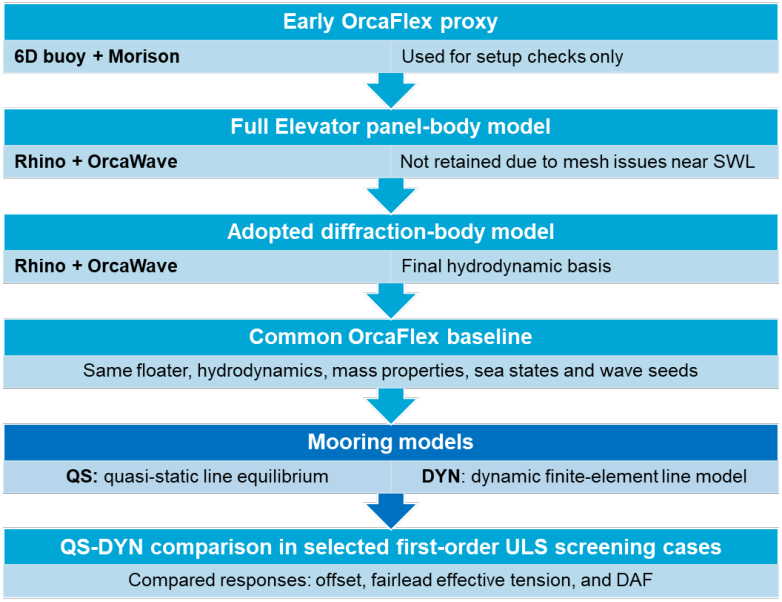

Figure 4.1: Development route towards the OrcaWave-OrcaFlex comparison model. Early models were used to check the modelling workflow and to assess feasible hydrodynamic representations. The QS-DYN comparison is based on one common OrcaFlex model setup, after which only the mooring-line representation is changed.

The retained and omitted geometric components are specified in Section 4.3. The corresponding mass, centre of gravity, buoyancy, and inertia properties are recalculated for the used geometry and are reported in Section 4.4. These properties are then kept identical in the QS and DYN simulations.

4.1.2. Hydrodynamic modelling choice

The initial screening model represented the wetted structural members with Morison elements in OrcaFlex. In such a model, inertia and drag forces are evaluated from the local wave kinematics at each time step. This approach is appropriate when the relevant members are slender relative to the incident wavelength so that the member does not strongly disturb the surrounding wave field [4, 16].

The slenderness check in Section 4.2.6 shows that the inter-tank columns and tripod members can be treated as Morison-type members for the selected sea states. The large annular tanks do not satisfy this slenderness criterion in all selected sea states. A Morison-only floater model was therefore not used as the hydrodynamic representation for the QS-DYN comparison.

The developed model uses an OrcaWave diffraction-radiation calculation for the panel-body representation. This model uses the main wetted components that dominate the global buoyancy, waterplane area, and first-order diffraction-radiation behaviour. The horizontal tripod members (4) and end-can connectors (5) from Figure 3.1 are not included in the used diffraction-body model. Their local hydrodynamic contribution is therefore outside the scope of the present model. The global mass, buoyancy, centre of gravity, and inertia properties are recalculated for the retained geometry, as described in Sections 4.3 and 4.4.

4.1.3. Use of OrcaWave hydrodynamic data in OrcaFlex

OrcaWave is used as the frequency-domain hydrodynamic pre-processor for the diffraction-body representation. The OrcaWave database provides first-order wave-excitation loads, added mass, radiation damping, and hydrostatic quantities. This database is imported into OrcaFlex and is used as the common hydrodynamic input for both the mooring-line models.

In the OrcaFlex simulations, the incident regular or irregular waves are defined in the environment settings. The floater motion is then solved in the time domain from the imported hydrodynamic database, hydrostatic restoring, radiation effects, and mooring forces. The vessel motion is therefore not prescribed from displacement RAOs. This is important because the platform motion must remain a solved response of the coupled floater-mooring system in both the QS and DYN models [29].

The displacement RAOs from OrcaWave are used only as frequency-domain interpretation results. They are used to inspect response trends of the diffraction-body model and to support the later interpretation of the selected wave periods. They are not used to prescribe vessel motions in OrcaFlex and are not used as direct dynamic-amplification results.

4.2. Environmental input and selected sea states

This section defines the environmental input used for the dynamic amplification assessment. The selected cases form a screening matrix for the present modelling study and are not treated as a certification-level metocean design basis or as formal 50-year design load cases.

For a certification-level floating-wind design, the site conditions would normally include site-specific wind, wave, current and water-level descriptions, joint environmental conditions, directional information, return-period estimates, and design load-case combinations [16, 24]. In this thesis, the environmental input is therefore limited to a small set of first-order wave cases selected for a model-level dynamic amplification assessment.

The simulations use long-crested irregular waves without current or steady wind thrust. This keeps the comparison focused on the mooring-line representation. A steady-thrust case is treated separately as a sensitivity case in Chapter 6.2.

4.2.1. Reference metocean location

The environmental data are taken from the ST07 location in Zone H near Curaçao, as used by Belis et al. [1]. Hourly ERA5 reanalysis data from 2015 to 2024 are used to select the sea states [30]. ERA5 is a gridded reanalysis product and is not treated as site measurement data. Table 4.1 lists the station coordinates and ERA5 grid resolution.

Table 4.1: Reference metocean location and ERA5 grid resolution.

Station	**Latitude** (°N)	**Longitude** (°W)	**Wind grid**	**Wave grid**
ST07	12.000	69.250	$0.25°$	$0.5°$

At this latitude, the wind grid corresponds to approximately 28 km and the wave grid to approximately 56 km.

4.2.2. Wave quantities

The ERA5 variables used in this sea-state selection are significant wave height H_s and peak wave period T_p. The associated wind speed U_{10} is used later only to identify the turbine operating region for the steady-thrust sensitivity. To support sea-state selection and the Morison slenderness check, the deep-water wavelength is estimated as

$$\lambda_0 = \frac{gT_p^2}{2\pi}, \tag{4.2}$$

where g is gravitational acceleration. The wave steepness indicator is defined as

$$S = \frac{H_s}{\lambda_0}. \tag{4.3}$$

These quantities are used for case selection and for the Morison slenderness check in Section 4.2.6.

4.2.3. Defined ULS sea states

Three sea states are selected from the 2015 to 2024 hourly ERA5 record at ST07. The selection covers three wave characteristics relevant for first-order floater and mooring response: large wave height, long peak period, and short steep waves. SS1 is selected from the maximum H_s event, SS2 from the maximum T_p event after excluding near-calm conditions, and SS3 from the maximum H_s/λ_0 case within the upper 10% of H_s. Table 4.2 lists the resulting sea-state parameters.

- SS1: maximum H_s, representing the largest wave-height case in the record.
- SS2: maximum T_p with $H_s \geq 0.8$ m, representing long-period swell while excluding near-calm wave conditions.
- SS3: maximum H_s/λ_0 within the upper 10% of H_s, representing a short and steep sea state.

Table 4.2: ERA5-screened sea states at ST07 used to define the irregular-wave load cases.

Sea state	$\mathbf{H_s}$ (m)	$\mathbf{T_p}$ (s)	λ_0 (m)	$\mathbf{H_s}/\lambda_0$ (−)	γ (−)
SS1	2.80	7.76	93.96	0.030	1.52
SS2	1.30	18.07	509.54	0.003	–
SS3	1.83	5.70	50.77	0.036	2.47

The corresponding ERA5 timestamps are SS1: 2020-01-11 07:00 UTC, SS2: 2018-09-30 02:00 UTC, and SS3: 2023-07-05 03:00 UTC. They are used as severe and physically distinct cases for comparing the two mooring-line representations under identical first-order wave input.

4.2.4. Wave headings and spectra

Two wave headings are analysed: $0°$ and $30°$. The $0°$ heading is aligned with one mooring line, while the $30°$ heading lies between two adjacent mooring lines. Because the three mooring lines are spaced at $120°$, these two headings represent the relevant symmetry cases for the present three-line layout. Figure 4.2 shows the mooring-line layout and the two analysed wave headings.

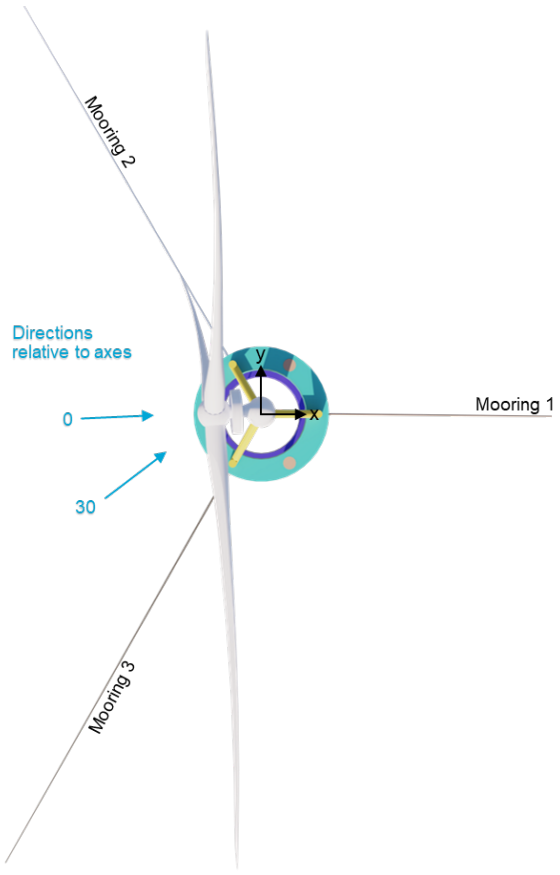

Figure 4.2: Top view of the three-line mooring layout and the two analysed wave headings. Mooring lines are spaced at $120°$.

The wind-sea cases SS1 and SS3 are modelled using a JONSWAP spectrum. The peak-enhancement factor γ is calculated for these cases using the empirical relation from DNV GL [16]:

$$\gamma = \begin{cases} 5, & T_p/\sqrt{H_s} \leq 3.6, \\ \exp\left(5.75 - 1.15 T_p/\sqrt{H_s}\right), & 3.6 < T_p/\sqrt{H_s} < 5, \\ 1, & T_p/\sqrt{H_s} \geq 5. \end{cases} \tag{4.4}$$

The long-period swell case SS2 is represented with a Gaussian swell spectrum. This spectrum is defined by H_s, T_p or f_m, and a spectral width parameter.

The irregular waves are treated as long-crested waves to keep the dynamic amplification assessment focused on the mooring-line representation. Directional spreading is not included, because it would introduce an additional environmental-modelling variable.

4.2.5. Wave-only load-case matrix

The matrix consists of three sea states and two wave headings. Each case is run twice in OrcaFlex. Once with the QS mooring model and once with the DYN mooring model. Table 4.3 lists the six wave-only load cases.

Table 4.3: Selected irregular-wave load cases for the dynamic amplification assessment.

Load case	Sea state	$\mathbf{H_s}$ $(\mathbf{m})$	$\mathbf{T_p}$ $(\mathbf{s})$	Heading $(^\circ)$
LC1a	SS1	2.80	7.76	0
LC1b	SS1	2.80	7.76	30
LC2a	SS2	1.30	18.07	0
LC2b	SS2	1.30	18.07	30
LC3a	SS3	1.83	5.70	0
LC3b	SS3	1.83	5.70	30

The same wave seed is used for both mooring-line representations in each load case. This prevents differences in the irregular-wave realisation from affecting the comparison.

4.2.6. Slenderness check for Morison and diffraction modelling

The hydrodynamic treatment of the floater members is checked using the ratio λ_0/D, where D is the member outer diameter. Table 4.4 gives the resulting ratios for the main Elevator members in the selected sea states. In this thesis, members with $\lambda_0/D \geq 5$ are treated as sufficiently slender for Morison-type loading. Members below this threshold are treated as non-slender for the selected sea state, so diffraction effects may be relevant [4, 16]. Values near or below the limit $\lambda_0/D = 5$ are bold in Table 4.4.

Table 4.4: Slenderness ratios λ_0/D for the main Elevator members in the selected sea states.

Member	$\mathbf{D}$ $(\mathbf{m})$	SS1	SS2	SS3
Mooring line	0.08	1174.5	6369.3	634.6
Tripod main column	10.10	9.30	50.45	**5.03**
Tripod-angled member	3.05	30.81	167.06	16.65
Tripod horizontal member	3.00	31.32	169.85	16.92
Tripod end can	3.05	30.81	167.06	16.65
Inter-tank column	3.00	31.32	169.85	16.92
Ballast tank	52.00	**1.81**	9.80	**0.98**

The ballast tanks are non-slender in SS1 and SS3 and are therefore not suitable for a Morison-only representation. The tripod-angled members, horizontal members, end cans and inter-tank columns satisfy the criterion in all three sea states. The tripod main column is close to the screening limit in SS3, with $\lambda_0/D \approx 5$. It is retained in the diffraction-body representation because it is connected to the main hull system and crosses the SWL.

This check explains why a Morison-only model was not kept. The developed model instead uses an OrcaWave diffraction-body representation for the main wetted components, with the horizontal members and end-can connectors excluded as described in Section 4.3.

4.2.7. Wind thrust and current assumptions

Current is not included in the main wave-only comparison. Current can affect mean offset, mean line tension, line drag, current-induced line response, and VIV, and is normally part of a full floating-wind design-load assessment [24]. It is therefore not assumed negligible. Instead, it is treated as a separate modelling step that should be assessed before extending the present wave-only conclusion to wind-wave-current cases.

A steady horizontal rotor-thrust load introduces an additional mean horizontal force and pitch moment on the floater. This can change the mean offset and redistribute the mooring-line tensions, which would add a different mean-load effect to the wave-only comparison. The steady-thrust case is therefore treated separately as a sensitivity case in Chapter 6.

For the sensitivity case, the SS1 wind speed is used only to identify the turbine operating region. The ERA5 wind speed at $10\ \mathrm{m}$ height for SS1 is $U_{10} = 13.50\ \mathrm{m/s}$. Using the power-law wind-shear relation for the sensitivity check, the SS1 wind speed corresponds to a hub-height wind speed of approximately $16.77\ \mathrm{m/s}$. This is above the rated wind speed of the IEA $15\ \mathrm{MW}$ reference turbine. Because turbine control is not modelled in OrcaFlex, the thrust is not extrapolated with a constant C_T at this wind speed. Instead, a rated-level thrust load is used for the steady-thrust sensitivity [4, 13].

The hub-height wind speed is estimated with

$$U_{\mathrm{hub}} = U_{10} \left(\frac{z_{\mathrm{hub}}}{z_{\mathrm{ref}}} \right)^{\alpha} \tag{4.5}$$

where $z_{\mathrm{ref}} = 10\ \mathrm{m}$, $z_{\mathrm{hub}} = 181.19\ \mathrm{m}$, and $\alpha = 0.075$ for the sensitivity check. This relation is used only to identify the turbine operating region for SS1. The thrust itself is based on the rated-level load rather than on a constant-C_T extrapolation at U_{hub}. Table 4.5 summarises the parameters and load levels used for the steady-thrust sensitivity.

Table 4.5: Parameters and load levels used for the simplified steady-thrust sensitivity.

Quantity	Symbol	Value	Unit
Rated wind speed	U_{rated}	10.59	$\mathrm{m/s}$
Rotor diameter	D	240	m
Rotor area	A_{rotor}	45.2×10^3	$\mathrm{m^2}$
Adopted thrust coefficient	C_T	0.799	–
Air density	ρ_{air}	1.225	$\mathrm{kg/m^3}$
Hub moment arm	h_{hub}	181.2	m
Rated-level thrust force	T_{hub}	2.48	MN
Rated-level pitch moment	M_{trim}	0.450	GNm
Reduced sensitivity force	$0.25T_{\mathrm{hub}}$	621	kN
Reduced sensitivity moment	$0.25M_{\mathrm{trim}}$	112	MNm

The rated-level thrust is calculated using the global thrust expression from Section 2.4. Using the values stated in Table 4.5, this gives $T_{\mathrm{hub}} = 2.48\ \mathrm{MN}$. The corresponding pitch moment about the vessel reference point is $M_{\mathrm{trim}} = T_{\mathrm{hub}} h_{\mathrm{hub}} = 0.450\ \mathrm{GNm}$.

The steady-thrust load is implemented in OrcaFlex as a constant vessel-applied load, not through the wind-load model. This is because the tower, nacelle, and rotor are not included as aerodynamic objects in the model. The applied load consists of a global x-force and an equivalent pitch moment at the vessel reference point [31]. This steady-thrust model is used to test how a simplified global aerodynamic load shifts the equilibrium and redistributes mooring-line tension.

4.3. Geometry, model components and mooring definition

This section defines the geometric representation used for the OrcaWave-OrcaFlex model. It identifies which parts of the Elevator concept are retained in the diffraction-body representation, which parts are omitted, and how the mooring system is implemented for the dynamic amplification assessment.

The full Elevator reference geometry remains the geometric reference for this thesis. The implemented model is a hydrodynamic idealisation derived from that reference geometry. It is not treated as a re-design of the Elevator concept.

4.3.1. Geometric representation

The implemented model keeps the main wetted components that define most of the global buoyancy, waterplane properties, and first-order diffraction-radiation behaviour. These components are the upper buoyant tank, the lower ballast tank, the three inter-tank columns, the tripod main column, and the tripod angled members, see Table 4.6.

A complete Elevator mesh including all structural members was first attempted in Rhino, as shown in Figure 4.4a. This full model included the horizontal tripod members and end-can connectors, but it produced mesh-quality problems around the tripod connections. The complete mesh was therefore not used for the OrcaWave calculations.

The horizontal tripod members and end-can connectors are excluded from the diffraction-body representation, see Figure 4.3. To keep the implemented model internally consistent, the mass, buoyancy, centre of gravity, and inertia properties are recalculated for the retained geometry.

Table 4.6: Components retained and omitted in the Elevator model, see Figure 3.1.

Label	Component	Included in developed model	Treatment
1	Mooring lines	Yes	OrcaFlex line model
2	Tripod main column	Yes	OrcaWave panel body
3	Tripod angled members	Yes	OrcaWave panel body
4	Tripod horizontal members	No	Omitted from panel body
5	End-can connectors	No	Omitted from panel body
6	Inter-tank columns	Yes	OrcaWave panel body
7	Upper buoyant tank	Yes	OrcaWave panel body
8	Lower ballast tank	Yes	OrcaWave panel body
	Tower and RNA	Yes	Dry mass and inertia only, not part of wetted panel body

Table 4.6 refers to the complete numerical model. The mooring lines are not part of the OrcaWave panel body but are included separately in OrcaFlex.

4.3.2. Selected diffraction-body representation

The diffraction-body representation is created in Rhino and imported into OrcaWave as a panel body. The body origin is placed at the still-water-level reference origin defined in Section 3.2. The panel body is used to compute the first-order diffraction-radiation quantities and for the hydrostatic properties associated with the retained geometry.

Three panel meshes were generated to select a feasible mesh for the diffraction-body representation. Table 4.7 summarises the mesh sizes and selection outcome. The medium mesh was rejected because the geometry check indicated self-intersections and because the estimated memory demand was too high for repeated OrcaWave runs. The fine mesh was also rejected because of its high memory demand. The coarse mesh was closed, valid, and computationally feasible. It was therefore selected for the OrcaWave calculations in this thesis.

Table 4.7: Mesh selection for the diffraction-body representation.

Mesh	Vertices	Faces	Status	Reason
Coarse	17 400	19 941	Adopted	Valid and feasible
Medium	38 968	43 087	Rejected	Self-intersections and high memory demand
Fine	69 807	75 873	Rejected	High memory demand

The selected mesh is checked in Section 4.4 using hydrostatic consistency and hydrodynamic coefficient trends. The main checks are displaced volume, centre of buoyancy, waterplane area, added mass, radiation damping, and displacement-response trends.

4.3.3. Omitted members and adjusted model properties

Because the horizontal tripod members and end-can connectors are excluded from the diffraction-body representation, the implemented model is not a full geometric reproduction of the Elevator reference concept. These members are also not reintroduced as Morison elements in the OrcaFlex simulations.

For this reason, the global mass, buoyancy, centre of gravity, and inertia properties are recalculated for the retained geometry. The adjusted total mass, buoyancy, centre of gravity, and inertia properties are reported in Section 4.4. These adjusted properties are then kept fixed for both mooring-line representations.

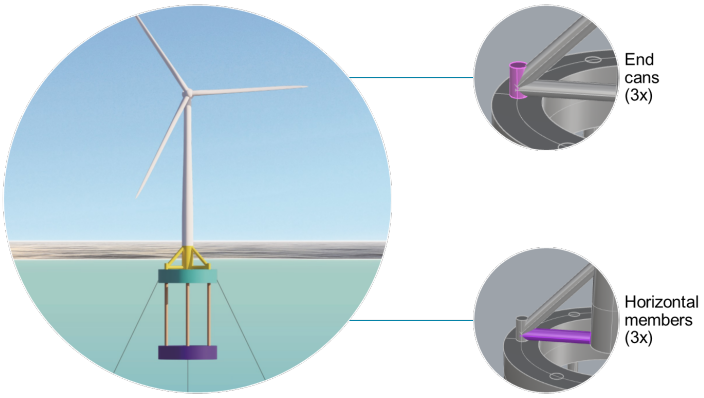

Figure 4.3: Omitted members from the diffraction-body representation. The horizontal tripod members and end-can connectors are excluded from the OrcaWave panel body.

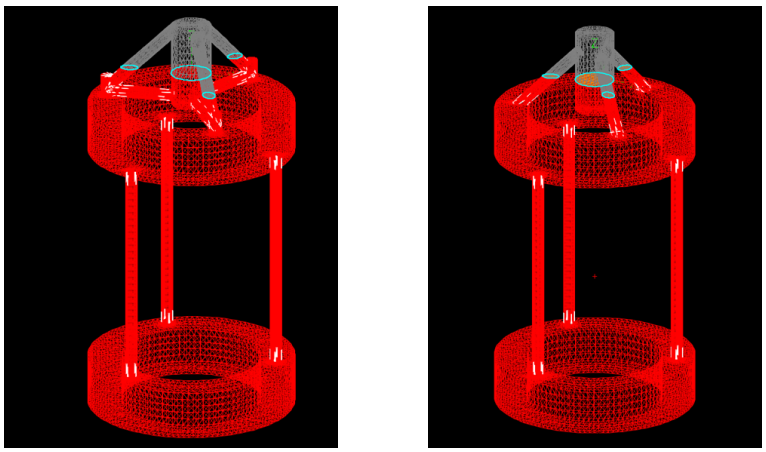

(a) Full Elevator in OrcaWave **(b)** Elevator in OrcaWave

Figure 4.4: Comparison between the full Elevator reference geometry and the diffraction-body representation used in OrcaWave. The representation retains the main wetted components and omits the horizontal tripod members and end-can connectors.

4.3.4. Mooring geometry and HMPE line properties

The mooring system consists of three inclined taut HMPE lines spaced at 120° in plan view, see Figure 4.2 and is based on the design by Belis et al. [1]. In this thesis, the mooring system is re-implemented in OrcaFlex using the $800\ \mathrm{m}$ water depth, the specified fairlead positions, and an unstretched line length calibrated to recover the pretension.

The line properties are based on the HMPE load-strain data from Belis et al. [1] and TEHO Ropes [21] and the tension level used to define the secant axial stiffness. Because the model omits some geometric components and uses adjusted global properties, the pretension level $T_{\mathrm{work}} = 0.900\ \mathrm{MN}$ is not treated as a re-optimised mooring equilibrium of the reduced-body model. Its sensitivity to unstretched line length is assessed separately in Chapter 6.1.

The same axial stiffness, fairlead positions, anchor positions, and unstretched line length are used for both mooring-line representations. The difference between the two models is the line formulation: the QS model uses instantaneous static line equilibrium, while the DYN model uses a finite-element dynamic line model. Table 4.8 lists the shared mooring geometry and HMPE line properties. Table 4.9 lists the additional hydrodynamic inputs used only in the DYN mooring-line representation.

Table 4.8: Mooring geometry and HMPE line properties used in both mooring-line representations.

Quantity	Symbol	Value	Unit
Number of lines	N	3	–
Water depth	h	800	m
Fairlead radius	r_f	26.0	m
Fairlead depth below SWL	d_f	14.0	m
Line azimuth spacing	$\Delta\psi$	120	°
Target pretension	T_{work}	0.900	MN
Unstretched line length	L_0	944.97	m
Minimum breaking load	MBL	4.040	MN
Effective axial stiffness	EA_{eff}	63.66	MN
Nominal diameter	D	0.080	m
Mass per unit length	m'	4.4	kg/m

Table 4.9: Hydrodynamic coefficients used in the DYN mooring-line representation.

Coefficient	Value
Normal drag C_d	1.2
Axial drag $C_{d,\mathrm{axial}}$	0.008
Normal added-mass C_a	1.0

The OrcaFlex line-length input is the unstretched line length L_0. Elastic elongation is estimated from the effective tension and the axial stiffness, using $\epsilon \approx T/EA$. The value $L_0 = 944.97\ \mathrm{m}$ is obtained from static OrcaFlex tuning to recover the target pretension of approximately $0.900\ \mathrm{MN}$ per line in still water. The resulting static equilibrium is verified in Section 4.5.1.

The mooring models use one uniform HMPE line type over the full mooring length. The nominal diameter, minimum breaking load and effective axial stiffness are therefore constant along each line. In the DYN model, the structural mass per unit length and hydrodynamic coefficients are also kept constant along the line. This follows the reference design input and gives one consistent rope specification for the mooring comparison [1, 21]. A tapered or segmented rope would introduce position-dependent $EA(s)$, structural mass per unit length $m'(s)$, line diameter $D(s)$, and hydrodynamic loading. This would affect line stretch and vibration characteristics and would require a separate mooring design study.

As a strength-level plausibility check, the MBL is compared with the generic HMPE strength scaling used by Hall et al. [2]:

$$\mathrm{MBL} = 580 \times 10^6 d^2 + 651 \times 10^6 d^3, \tag{4.6}$$

where d is the rope diameter in metres. For $d = 0.080\ \mathrm{m}$, this gives $\mathrm{MBL} \approx 4.05\ \mathrm{MN}$, which is close to the used value of $4.040\ \mathrm{MN}$. This comparison checks the adopted strength level. The axial stiffness remains based on the HMPE load-elongation data used for the mooring-line model.

The axial stiffness remains based on the load-elongation data from Belis et al. [1] and TEHO Ropes [21]. This is appropriate because synthetic-rope stiffness is a rope-level input that depends on load level, load rate and load history, so QS and DYN rope stiffness may differ [32]. Hall et al. [2] follows the same principle by treating synthetic-rope stiffness through different assumptions for QS and DYN

loading. Older vendor data for Dyneema ropes also show different first-load and cycled load-elongation behaviour [33].

Figure 4.5 shows the Elevator mooring geometry and the fairlead region used in the OrcaFlex model.

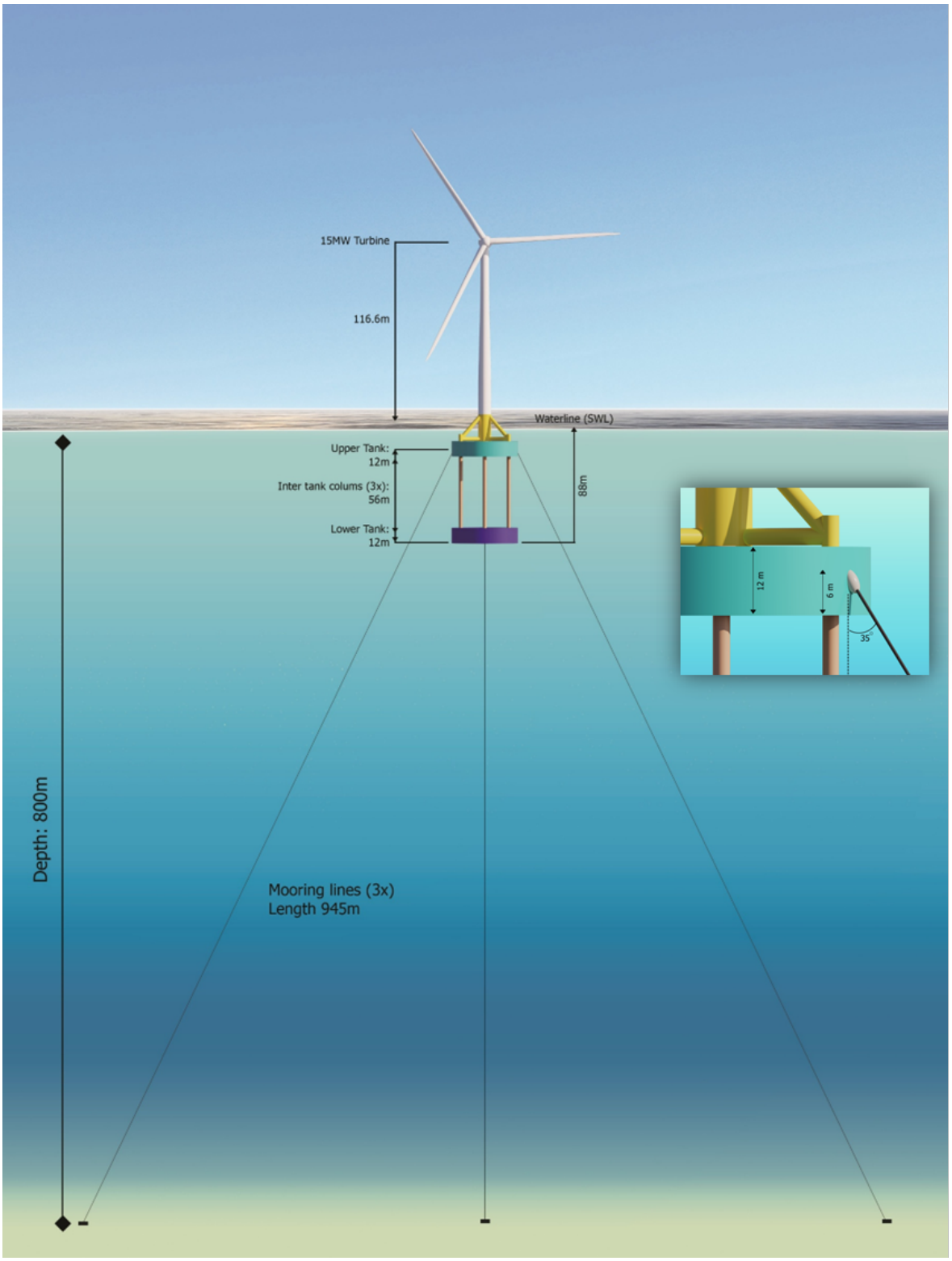

Figure 4.5: Overview of the Elevator mooring geometry and close-up of the fairlead region.

4.4. OrcaWave hydrodynamic database

This section reports the OrcaWave hydrodynamic database used in the OrcaFlex simulations. The database is based on the diffraction-body representation defined in Section 4.3. This representation retains the upper and lower annular tanks, the inter-tank columns, the tripod main column, and the tripod angled members. The horizontal tripod members and end-can connectors are not included in the OrcaWave panel body.

This section checks whether the OrcaWave body gives internally consistent hydrostatic quantities and physically plausible first-order hydrodynamic trends. These checks are not presented as a full mesh-convergence study or as validation of the complete Elevator concept. They are used to assess whether the diffraction-body representation is suitable as the common hydrodynamic basis for both mooring-line representations.

4.4.1. Mass and inertia input

The dry mass and inertia inputs are defined for the retained components of the floater model. Table 4.10 lists the mass build-up used in OrcaWave. The horizontal tripod members and end-can connectors are omitted from both the OrcaWave panel geometry and the mass build-up. The tower and RNA are included in the dry mass and inertia input, but not in the wetted panel geometry.

Table 4.10: Dry-mass build-up used for the OrcaWave model

Element	Mass (kg)	Treatment in model
Upper tank concrete shell	5.599×10^6	Panel geometry and mass input
Upper tank seawater ballast	0.233×10^6	Internal ballast mass input
Lower tank concrete shell	5.599×10^6	Panel geometry and mass input
Lower tank sand ballast	15.893×10^6	Internal ballast mass input
Inter-tank columns	1.129×10^6	Panel geometry and mass input
Tripod main column	0.256×10^6	Panel geometry and mass input
Tripod angled members	0.118×10^6	Panel geometry and mass input
Tower and RNA	1.877×10^6	Dry mass and inertia input
Total	30.704×10^6	–

The resulting rigid-body properties used in OrcaWave are listed in Table 4.11. These values are kept fixed for both mooring-line representations.

Table 4.11: Rigid-body input properties used for the OrcaWave model

Quantity	Symbol	Value	Unit
Total mass	M	30.704×10^6	kg
Centre of gravity	z_G	-54.72	m
Inertia about origin	$I_{xx,O}$	181.4×10^9	$\mathrm{kg \cdot m^2}$
Inertia about origin	$I_{yy,O}$	181.4×10^9	$\mathrm{kg \cdot m^2}$
Inertia about origin	$I_{zz,O}$	13.98×10^9	$\mathrm{kg \cdot m^2}$

The centre of gravity is obtained from the component mass build-up as

$$z_G = \frac{\sum_i m_i z_i}{\sum_i m_i}. \tag{4.7}$$

The inertias about the OrcaWave body origin are obtained using the parallel-axis theorem,

$$I_{xx,O} = \sum_i \left(I^{G_i}_{xx,i} + m_i (y_i^2 + z_i^2) \right), \tag{4.8}$$

The total mass of $30.704 \times 10^6\ \mathrm{kg}$ is close to the reference-design value of approximately $30.866 \times 10^6\ \mathrm{kg}$, but it is not identical. This difference follows from the component selection in Section 4.3.

4.4.2. Period and heading grid

The OrcaWave hydrodynamic database is calculated for the wave periods and headings listed in Table 4.12. The period range covers the peak periods of the selected sea states and extends to longer periods to inspect the low-frequency response trend of the body. The database includes headings at 30° intervals, but only the 0° and 30° headings are used for the load-case matrix because these represent the two symmetry cases introduced in Section 4.2.4.

Table 4.12: OrcaWave period and heading grid used for the hydrodynamic database.

Quantity	Values	Unit
Wave periods	$1, 1.5, 2, 2.5, 3, 4, 5, 6, 7, 8, 10, 12, 14, 16, 18, 20, 24, 30, 35, 40, 45, 50, 60$	s
Analysed wave headings	$0, 30, 60, 90, 120, 150, 180, 210, 240, 270, 300, 330$	$^\circ$
Comparison wave headings	$0, 30$	$^\circ$
Water depth	800	m

The period grid defines the frequency range of the OrcaWave database imported into OrcaFlex, while the irregular-wave simulations are defined by the sea-state spectra in Table 4.2. A refined period grid used only for RAO interpretation plots is provided in Appendix C.

4.4.3. Hydrostatic consistency

The hydrostatic quantities in Table 4.13 are not prescribed rigid-body inputs. They are computed by OrcaWave from the panel geometry. They are checked here to assess whether the diffraction-body representation gives plausible hydrostatic output before the hydrodynamic database is imported into OrcaFlex.

The displaced volume is the submerged volume enclosed by the panel body,

$$\nabla = V_{\mathrm{sub}}, \tag{4.9}$$

and the waterplane area is the area formed by the intersection between the panel body and the still water level,

$$A_{\mathrm{wp}} = A(z = 0). \tag{4.10}$$

For the Elevator geometry, this waterplane area is formed by the tripod main column and the three inclined tripod members crossing the still water level, as illustrated in Figure 4.6 by the red lines.

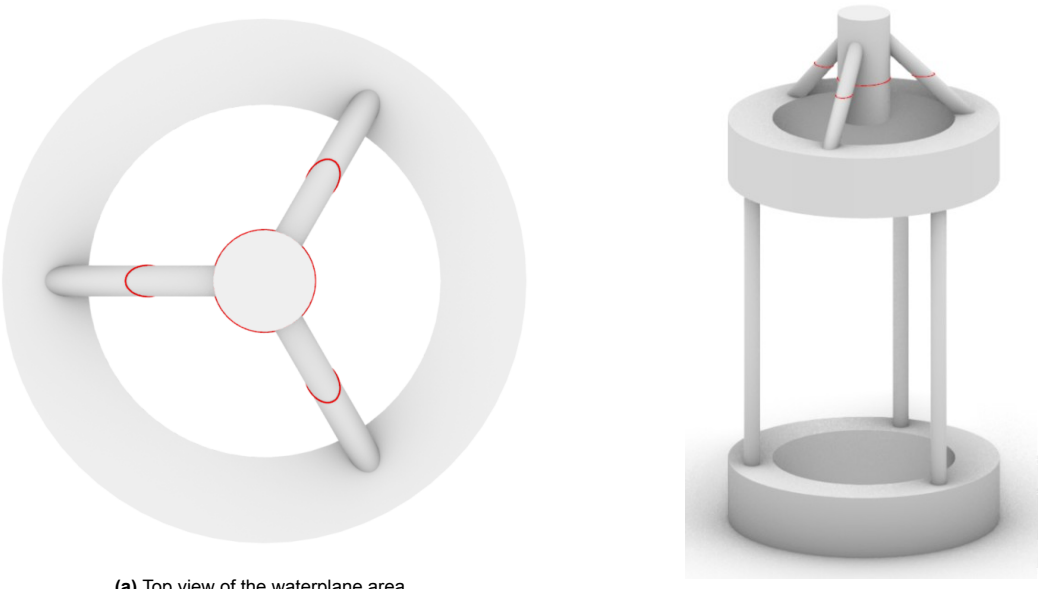

(a) Top view of the waterplane area

(b) Front view of the waterplane area

Figure 4.6: Waterplane area of the OrcaWave body used for the hydrostatic consistency check. The waterplane area is formed by the tripod main column and the three inclined tripod members crossing the still-water level.

Table 4.13: OrcaWave hydrostatic quantities for the diffraction-body representation.

Quantity	Symbol	Value	Unit
Displaced volume	∇	29.96×10^3	m^3
Centre of buoyancy	z_B	-46.70	m
Waterplane area	A_{wp}	110.43	m^2
Centre of flotation, x	x_{CF}	68.5×10^{-6}	m
Centre of flotation, y	y_{CF}	-195×10^{-6}	m
Hydrostatic heave stiffness	c_{33}^{hyd}	1.110	$\mathrm{MN/m}$

The hydrostatic heave stiffness is used as the main scalar consistency check because it can be computed directly from the waterplane area. This check is limited to the OrcaWave panel-body hydrostatics. The static equilibrium, including mooring pretension, is verified separately in Section 4.5. The heave stiffness is checked from the waterplane area:

$$c_{33}^{hyd} = \rho_w g A_{\mathrm{wp}}. \tag{4.11}$$

With $\rho_w = 1025\ \mathrm{kg/m^3}$, $g = 9.81\ \mathrm{m/s^2}$, and $A_{\mathrm{wp}} = 110.43\ \mathrm{m^2}$, this gives $c_{33}^{\mathrm{hyd}} = 1.11\ \mathrm{MN/m}$. This matches the OrcaWave value in Table 4.13 and shows that the waterplane area and hydrostatic heave restoring are internally consistent.

4.4.4. Hydrodynamic coefficient checks

The first-order added-mass and radiation-damping coefficients are inspected before the OrcaWave database is imported into OrcaFlex. This check is used to identify possible numerical irregularities in the hydrodynamic database, not to draw direct response conclusions.

The diagonal coefficient terms show physically plausible trends over the calculated period range. The largest local variations occur at short-wave periods, while the longer-period range used later for response interpretation shows smoother trends. These coefficient variations do not directly imply corresponding peaks in the displacement RAOs, because the RAOs also depend on wave excitation, restoring, total inertia, damping, and coupling between degrees of freedom.

The coefficient plots are provided in Appendix C for traceability of the hydrodynamic database. The refined frequency-domain RAO plots, including the body-only case and the case with the added linearised mooring-restoring matrix, are provided in Appendix C.3. These plots are used only to help interpret the response periods discussed in Section 5.3 and they are not used to prescribe vessel motions in the OrcaFlex time-domain simulations.

4.5. OrcaFlex import and static model verification

This section checks whether the OrcaFlex model reproduces the intended static line-tension state and local restoring behaviour of the Elevator model. The hydrodynamic database was checked separately in Section 4.4. The purpose here is to verify that the imported vessel model, adjusted mass properties, and three-line HMPE mooring layout give a stable still-water equilibrium and a local restoring level before the response comparison is performed.

All checks are carried out in still water. Wave loading, current, and steady thrust are switched off. The same floater properties and mooring geometry are used for the QS and DYN models.

Three verification steps are performed. First, the static equilibrium is checked at the intended target pretension. Second, translational restoring coefficients are obtained from small static force-displacement tests. Third, rotational restoring coefficients are obtained from small static moment-rotation tests. The resulting values are compared with the linearised reference restoring estimates from Section 3.3. These reference values are used as traceability checks, not as exact validation values.

4.5.1. Static equilibrium

After calibration of the unstretched line length, the OrcaFlex model is run to static equilibrium using the adjusted rigid-body properties from Table 4.11. The calibrated unstretched line length is listed in Table

4.8. Table 4.14 compares the resulting fairlead tensions and static vessel position for the QS and DYN models.

Table 4.14: Static equilibrium check of the QS and DYN OrcaFlex models in still water.

Quantity	QS	DYN	Unit
Fairlead tension, line 1	900.202	900.113	kN
Fairlead tension, line 2	900.176	900.086	kN
Fairlead tension, line 3	900.170	900.080	kN
Surge position, x_0	6.336×10^{-3}	6.329×10^{-3}	m
Sway position, y_0	0.603×10^{-3}	0.606×10^{-3}	m
Heave position, z_0	-1.979	-1.979	m
Roll angle, ϕ_0	1.730×10^{-3}	1.730×10^{-3}	$^\circ$
Pitch angle, θ_0	1.485×10^{-3}	1.485×10^{-3}	$^\circ$
Yaw angle, ψ_0	0.229×10^{-6}	0.229×10^{-6}	$^\circ$

The primary checks are the three fairlead tensions and the absence of a significant horizontal offset or rotation in still water. The fairlead tensions recover the target pretension of approximately $900\ \mathrm{kN}$ per line. This indicates that the mooring layout and unstretched line length reproduce the pretension target for the still-water model.

The absolute heave coordinate is not used as a direct reference design validation quantity. It depends on the OrcaFlex vessel reference origin and on the adjusted mass-buoyancy balance of the model. The heave coordinate is therefore reported for traceability. The static verification is based on the recovered line tensions, stable equilibrium, and local restoring behaviour about that equilibrium.

4.5.2. Translational stiffness

The restoring terms in surge, sway, and heave are obtained from small static force-displacement tests about the still-water equilibrium. The reported coefficients are local total restoring coefficients of the complete OrcaFlex floater-mooring model. They therefore include both vessel hydrostatic restoring and mooring restoring and should not be interpreted as mooring-only stiffness coefficients.

External forces are applied separately in each translational direction, and the resulting equilibrium displacement is recorded. The local stiffness is calculated from the applied force and resulting displacement as

$$c_{ii} = \frac{\Delta F_i}{\Delta x_i}. \tag{4.12}$$

For surge and sway, force levels of 10, 20, and $30\ \mathrm{kN}$ are used. For heave, force levels of 50, 100, and $150\ \mathrm{kN}$ are used. These applied forces are small relative to the pretension and displaced weight of the system. The stiffness values remain nearly constant over the tested load levels, which indicates approximately linear local behaviour around the static equilibrium.

Table 4.15: Translational local total restoring stiffness of the OrcaFlex model compared with the linearised reference restoring estimates.

DOF	Reference estimate	QS	DYN	Unit
Surge, c_{11}	32.17	35.83	35.58	$\mathrm{kN/m}$
Sway, c_{22}	32.17	35.82	35.57	$\mathrm{kN/m}$
Heave, c_{33}	1222.0	1246.3	1246.2	$\mathrm{kN/m}$

The QS and DYN static force-displacement tests give nearly identical translational restoring coefficients. This indicates that both mooring representations start from almost the same static restoring behaviour.

The reference values in Table 4.15 are linearised restoring estimates from the reference-design calculation. They are not OrcaFlex results and are not treated as exact validation values. The surge and sway stiffnesses from the OrcaFlex model are approximately 11% higher than the reference estimates.

This difference is plausible because OrcaFlex evaluates the explicit three-line geometry, the $800\ \mathrm{m}$ implementation, and the calibrated unstretched line length, whereas the reference calculation uses a simplified linear projection around the pretensioned equilibrium.

The heave restoring coefficient is closer to the reference estimate, with a difference of approximately 2%. This is expected because heave restoring is dominated by hydrostatic stiffness, while the mooring contribution is comparatively smaller. The translational restoring check therefore shows that the OrcaFlex model is traceable to the reference-design restoring level for the present response comparison.

4.5.3. Rotational stiffness

The rotational restoring terms are obtained from small static moment-rotation tests about the still-water equilibrium. External moments of 2, 5, and $10\ \mathrm{MNm}$ are applied separately about the roll, pitch, and yaw axes. The resulting equilibrium rotations are recorded, and the local rotational stiffness is calculated as

$$c_{ii} = \frac{\Delta M_i}{\Delta \theta_i}, \tag{4.13}$$

where ΔM_i is the applied moment and $\Delta \theta_i$ is the resulting rotation in radians.

Table 4.16: Rotational local total restoring stiffness of the OrcaFlex model compared with the linearised reference restoring estimates.

DOF	Reference estimate	QS	DYN	Unit
Roll, c_{44}	2.649	2.495	2.495	$\mathrm{GNm/rad}$
Pitch, c_{55}	2.649	2.495	2.495	$\mathrm{GNm/rad}$
Yaw, c_{66}	≈ 0	0.043	0.043	$\mathrm{GNm/rad}$

The QS and DYN moment-rotation tests give almost identical rotational restoring coefficients. Roll and pitch stiffness are about 6% lower than the linearised reference estimates. This is consistent with the difference between the explicit static OrcaFlex model and the simplified hydrostatic and mooring-restoring calculation used for the reference estimate.

The yaw stiffness remains small compared with roll and pitch, as expected for the symmetric three-line layout with 120° spacing. The rotational stiffness check is therefore used as a traceability check, not as strict validation against the reference design.

4.5.4. Summary of static model verification

The static verification consists of the equilibrium check in Table 4.14, the translational stiffness check in Table 4.15, and the rotational stiffness check in Table 4.16. Together, these checks show that the OrcaFlex model reproduces the selected target pretension and gives local total restoring coefficients of the same order as the linearised reference estimates.

The largest difference occurs in surge and sway, where the $800\ \mathrm{m}$ OrcaFlex implementation gives a slightly higher local restoring stiffness than the simplified linearised reference calculation. The difference is approximately 11%. The heave, roll, and pitch restoring terms are closer to the reference estimates, with differences of approximately 2% in heave and 6% in roll and pitch.

These checks are sufficient for the response comparison because both models have nearly identical still-water equilibrium and local restoring behaviour. The two models therefore start from the same static state, and the intended difference remains the mooring-line representation.

5

Results: QS-DYN mooring-line response comparison

This chapter presents the response comparison between the mooring-line representations for the selected first-order, wave-only cases. Section 5.1 defines the post-processing method and response metrics. Section 5.2 presents the restoring and free-vibration checks used to interpret the response. Section 5.3 relates the selected sea states to the RAO interpretation. Sections 5.4 and 5.5 compare the platform response and governing fairlead effective tension. Section 5.6 summarises the case-specific DAF values. Section 5.7 checks local mooring-line eigenfrequencies, axial line-frequency estimates, and VIV relevance. Section 5.8 discusses the interpretation and limitations of the results.

5.1. Post-processing method and response metrics

This section defines the post-processing method and response metrics used for the time-domain response comparison. For each load case, the same numerical floater model, hydrodynamic database, environmental input, wave realisation, and simulation settings are used. The only intended difference is the mooring-line representation. The resulting statistics are used as response-comparison metrics for the present model, not as certification-level extreme-value estimates.

5.1.1. Simulation window

For each irregular-wave load case, one simulation with the QS mooring-line representation and one simulation with the DYN mooring-line representation are performed using the same wave realisation. The analysed response window is kept identical for both simulations. The initial part of the simulation is excluded to avoid including transient start-up effects in the response statistics. Table 5.1 summarises the simulation and post-processing settings.

Table 5.1: Simulation and post-processing settings for the irregular-wave cases.

Quantity	Value	Unit
Total simulation duration	2460	s
Excluded transient duration	460	s
Post-processing window	460 to 2460	s
Analysed duration	2000	s
Time step	0.1	s

5.1.2. Response statistics

The response quantities are extracted from the OrcaFlex time histories within the post-processing window.

$$r(t) = \sqrt{x(t)^2 + y(t)^2}. \tag{5.1}$$

The maximum horizontal offset is then obtained from the resulting offset time series:

$$r_{\max} = \max(r(t)). \tag{5.2}$$

The standard deviation σ_r is calculated from the same $r(t)$ time series. The maximum absolute heave and pitch responses are also extracted over the post-processing window.

Fairlead effective tension is evaluated at the fairlead end of each mooring line. Both the total maximum effective tension and the tension range above the mean are used. The tension range above the mean is defined as

$$\Delta T_{\mathrm{eff}} = T_{\mathrm{eff,max}} - \bar{T}_{\mathrm{eff}}. \tag{5.3}$$

The ratio $\Delta T_{\mathrm{eff}}/\bar{T}_{\mathrm{eff}}$ is used to indicate the tension variation relative to the mean effective tension.

5.1.3. Dynamic amplification factor

The dynamic amplification factor is used as a case-specific comparison ratio between the simulations with the DYN and QS mooring-line representations. For a response quantity q, the maximum-response DAF is defined as

$$\mathrm{DAF}_{q,\max} = \frac{q_{\max,\mathrm{DYN}}}{q_{\max,\mathrm{QS}}} \tag{5.4}$$

Values above one indicate that the DYN mooring-line representation gives a larger response than the QS representation for the same load case. Values below one indicate a smaller response.

For fairlead effective tension, two DAF values are used. The first compares the total maximum effective tension:

$$\mathrm{DAF}_{T,\max} = \frac{T_{\mathrm{eff},\max,\mathrm{DYN}}}{T_{\mathrm{eff},\max,\mathrm{QS}}} \tag{5.5}$$

The second compares the tension range above the mean:

$$\mathrm{DAF}_{\Delta T} = \frac{\Delta T_{\mathrm{eff},\mathrm{DYN}}}{\Delta T_{\mathrm{eff},\mathrm{QS}}} \tag{5.6}$$

The two tension ratios have different meanings. $\mathrm{DAF}_{T,\max}$ compares the total maximum effective tension, which is relevant for ULS as the peak line load. $\mathrm{DAF}_{\Delta T}$ compares the tension range above the mean and is used as a tension-range ratio, because the total fairlead tension is strongly influenced by the mean effective tension.

5.1.4. Interpretation limits

The DAF values in this thesis are case-specific indicators. They depend on the selected sea states, wave headings, wave seed, simulation duration, response metric, and numerical model developed in this thesis. They should therefore not be interpreted as general design factors for all ULS conditions.

The wave-only comparison excludes second-order wave-drift forces, current, turbulent wind, turbine control, fatigue loading, line-failure cases, and the full design-load-case matrix required for certification-level assessment [2, 24]. These mechanisms can affect platform motion, fairlead motion, and line tension in broader design-load cases. The DAF values are therefore used only to compare the two mooring-line representations in the selected first-order irregular-wave cases.

5.2. Restoring and free-vibration checks

This section reports the restoring and free-vibration checks used to interpret the irregular-wave response results. The detailed static verification was given in Section 4.5. Here, only the additional checks needed to interpret the response of the two mooring-line representations are included.

5.2.1. Heave restoring check

A displacement-controlled heave sweep is performed around the still-water equilibrium for both mooring-line representations. Wave loading, wind loading, and current are switched off. Because the test is static, distributed line inertia, hydrodynamic drag, and added mass do not contribute. The check is therefore used only to compare the local static vertical restoring behaviour. Figure 5.1 shows the resulting mean line tension and total vertical mooring force.

The curves for the two mooring-line representations almost overlap. In the implemented model, upward displacement increases the axial extension of the inclined pretensioned lines. The mean line tension therefore increases, and the total vertical mooring force becomes more downward over the tested displacement range.

$$k_{33,\mathrm{moor}} = -\frac{\Delta F_{z,\mathrm{moor}}}{\Delta z} \approx 136\ \mathrm{kN/m}. \tag{5.7}$$

The heave sweep therefore shows that later differences between the two response calculations are not caused by different static vertical restoring levels.

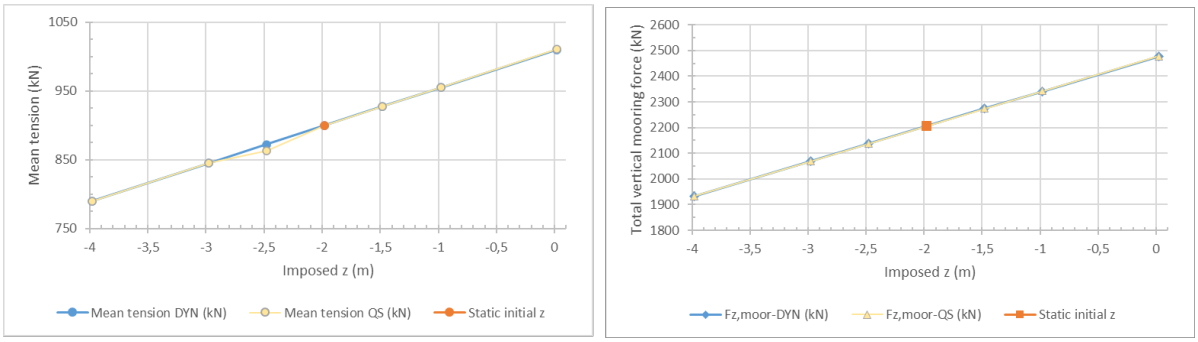

Figure 5.1: Mean line tension and total vertical mooring force during the heave sweep for the mooring-line representations.

5.2.2. Free-vibration periods

Still-water free-vibration tests are used to estimate the main rigid-body periods of the moored floater. The tests are performed for the OrcaFlex model with the QS mooring-line representation and for the same model with the DYN mooring-line representation. In each test, the body is displaced from its static equilibrium position and released. The period is extracted from successive peaks or troughs of the vessel motion relative to the static equilibrium. Table 5.2 compares the resulting period estimates with the reference values from Belis et al. [1].

Table 5.2: Comparison of moored-system free-vibration period estimates. Reference values from Belis et al. [1] are based on the linearised hydrostatic and mooring-restoring calculations. OrcaFlex values are obtained from still-water free-vibration tests at the target pretension of $900\ \mathrm{kN}$ per line.

Mode	**Reference** (s)	**OrcaFlex QS** (s)	**OrcaFlex DYN** (s)
Surge	244	253.95	253.95
Heave	39.5	43.00	43.02
Pitch	59.7	42.25	42.30

The free-vibration periods for the two mooring-line representations differ by less than $0.1\ \mathrm{s}$. This indicates that changing only the mooring-line representation does not noticeably change the still-water period estimates.

The pitch period is shorter than the reference value from Belis et al. [1]. The reference periods are used as traceability values, because they are based on linearised reference-design calculations rather than the present OrcaFlex mass, hydrodynamic, and mooring implementation. The difference is therefore treated as a model-specific outcome and is not used as a direct validation target.

5.2.3. Separation from the selected first-order wave periods

The selected sea states have peak periods between $5.70\ \mathrm{s}$ and $18.07\ \mathrm{s}$. The estimated moored-system periods are about $43\ \mathrm{s}$ in heave and pitch-type motion and about $254\ \mathrm{s}$ in surge. The first-order wave excitation is therefore well separated from the main rigid-body periods of the model.

This period separation helps explain why large first-order dynamic amplification is not expected in the evaluated platform offset and governing fairlead-tension responses. However, the soft surge mode may still be sensitive to low-frequency excitation, especially second-order wave-drift loading, which is not included in the simulations.

5.3. Frequency-domain interpretation of the selected sea states

The motion RAOs of the diffraction-body representation are used to support the frequency-domain interpretation of the selected sea states. They are not a direct comparison between the QS and DYN mooring-line representations, because OrcaWave does not include the OrcaFlex mooring-line formulations used later in the time-domain simulations. The period axis represents the wave-excitation period, with $\omega = 2\pi/T$.

For a linear response quantity y, the response spectrum can be written as

$$S_y(\omega) = |H_y(\omega)|^2 \, S_\eta(\omega), \tag{5.8}$$

where $S_\eta(\omega)$ is the wave spectrum and $H_y(\omega)$ is the corresponding response amplitude operator. A large response is therefore expected when energetic wave components overlap with a frequency range in which the system response is amplified.

Figure 5.2 shows the surge, heave, and pitch motion RAOs for two frequency-domain cases: the floater-only case and the floater with the added linearised mooring-restoring matrix from Section 3.3. The vertical dashed lines indicate the spectral peak periods of the selected first-order sea states. The refined OrcaWave period grid is used only to resolve the RAO features and does not change the irregular-wave load cases in OrcaFlex.

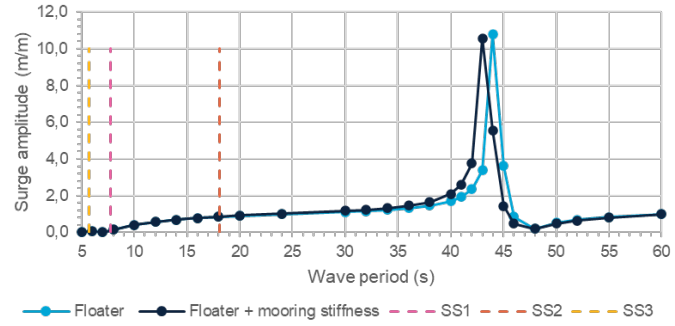

(a) Surge RAO

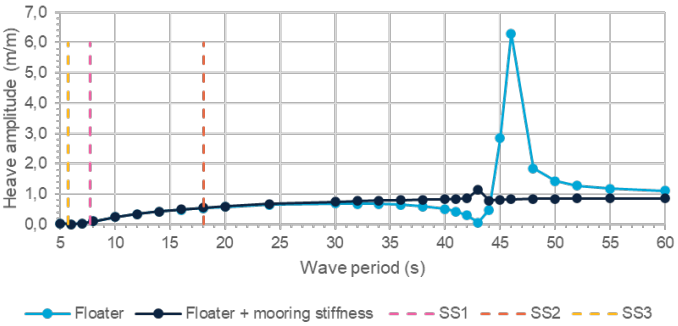

(b) Heave RAO

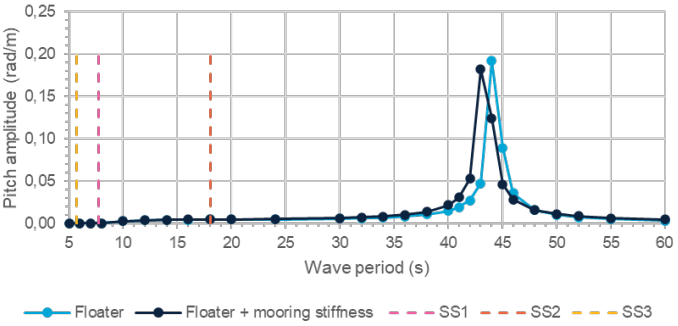

(c) Pitch RAO

Figure 5.2: Motion RAOs of the diffraction-body representation for the floater-only case and for the floater with the added linearised mooring-restoring matrix. Vertical dashed lines indicate the spectral peak periods of the selected first-order sea states.

The RAOs show long-period response features around 40 to 45 s. In the floater-only frequency-domain case, the heave RAO has a noticeable peak in this range. After adding the linearised mooring-restoring matrix, this heave peak is strongly reduced, while surge and pitch still show response features in the same period range. These trends show that the frequency-domain response is affected by the added linearised mooring restoring.

The selected sea-state peak periods are shorter than these long-period response features. The peak energy range of the first-order wave spectra therefore does not strongly excite the identified response range. This supports the interpretation of DAF values close to unity in the time-domain comparison between the two mooring-line representations, but it does not prove the result. The interpretation remains limited to the selected first-order, wave-only cases.

5.4. Irregular-wave platform response

This section compares the platform response obtained with the QS and DYN mooring-line representations for the selected irregular-wave cases defined in Section 4.2.5. The comparison focuses on horizontal offset and selected platform motions. Mooring-line tensions are treated in Section 5.5.

The three sea states represent different wave conditions. SS1 is the largest wave-height case, SS2 is the long-period swell case, and SS3 is the short and steep sea state. For each sea state, both the $0°$ and $30°$ wave headings are analysed with the same wave seed for the two mooring-line representations.

The platform-response statistics in Table 5.3 show that the two mooring-line representations give very similar horizontal offset and selected platform motions. The largest horizontal offset ($r_{\max}$) difference occurs in the long-period swell case LC2b and is about $0.003\ \mathrm{m}$. The maximum offset is approximately $1.15\ \mathrm{m}$ for both headings, while SS1 gives offsets of about $0.31\ \mathrm{m}$ and SS3 gives offsets of about $0.06\ \mathrm{m}$.

The wave heading mainly changes the distribution between surge and sway. For the 0° heading, the horizontal response is almost entirely in surge. For the 30° heading, part of the horizontal response appears in sway, as shown by the component values in Appendix D. The resultant horizontal offset remains similar between the two headings for each sea state.

Changing from the QS to the DYN mooring-line representation does not produce a systematic increase in platform response. The differences in $r_{\max}$ and σ_r are small for all cases. For these selected first-order cases, this is consistent with the same floater hydrodynamics and similar static restoring levels used in both response calculations. The added line inertia, drag, and added mass in the DYN mooring-line representation therefore do not lead to a noticeable change in platform response.

Table 5.3: Platform-response statistics for the selected irregular-wave cases. The horizontal offset r is calculated from the surge and sway time histories as defined in Eq. 5.1.

Load case	Heading $(^\circ)$	Line model	$\mathbf{r}_{\max}\ (\mathbf{m})$	$\boldsymbol{\sigma_r}\ (\mathbf{m})$	$\lvert\mathbf{z}\rvert_{\max}\ (\mathbf{m})$	$\lvert\boldsymbol{\theta}\rvert_{\max}\ (^\circ)$
LC1a	0	QS	0.308	0.059	0.202	0.133
LC1a	0	DYN	0.307	0.059	0.202	0.133
LC1b	30	QS	0.306	0.059	0.203	0.115
LC1b	30	DYN	0.306	0.059	0.203	0.115
LC2a	0	QS	1.149	0.177	0.840	0.437
LC2a	0	DYN	1.151	0.177	0.839	0.438
LC2b	30	QS	1.148	0.177	0.840	0.378
LC2b	30	DYN	1.151	0.177	0.839	0.379
LC3a	0	QS	0.057	0.009	0.039	0.038
LC3a	0	DYN	0.057	0.009	0.039	0.039
LC3b	30	QS	0.059	0.010	0.038	0.034
LC3b	30	DYN	0.059	0.010	0.038	0.034

5.5. Line-tension response

Fairlead effective tension is evaluated for all three mooring lines. To keep the main comparison compact, Table 5.4 reports only the governing line for each load case. The governing line is defined as the line with the largest maximum effective tension in that load case. The full line-by-line tension statistics are provided in Appendix D.

Table 5.4: Governing-line effective-tension statistics for the selected irregular-wave cases. The governing line is the line with the largest maximum effective tension for that load case. See Figure 4.2 for the wave headings and mooring-line definition.

Load case	Heading $(^\circ)$	Line model	Line	$\mathbf{T}_{\mathrm{eff,max}}\ (\mathbf{kN})$	$\bar{\mathbf{T}}_{\mathrm{eff}}\ (\mathbf{kN})$	$\boldsymbol{\Delta}\mathbf{T}_{\mathrm{eff}}\ (\mathbf{kN})$	$\boldsymbol{\Delta}\mathbf{T}_{\mathrm{eff}}/\bar{\mathbf{T}}_{\mathrm{eff}}\ (\%)$
LC1a	0	QS	1	917.325	900.368	16.958	1.88
LC1a	0	DYN	1	916.974	900.277	16.697	1.85
LC1b	30	QS	1	916.091	900.347	15.744	1.75
LC1b	30	DYN	1	915.770	900.256	15.514	1.72
LC2a	0	QS	1	963.492	900.711	62.781	6.97
LC2a	0	DYN	1	963.174	900.611	62.563	6.95
LC2b	30	QS	3	962.331	899.673	62.658	6.96
LC2b	30	DYN	3	961.880	899.584	62.296	6.92
LC3a	0	QS	1	903.748	900.207	3.541	0.39
LC3a	0	DYN	1	903.570	900.117	3.453	0.38
LC3b	30	QS	1	903.443	900.206	3.237	0.36
LC3b	30	DYN	1	903.276	900.116	3.159	0.35

The governing-line tension statistics in Table 5.4 show that the mean effective tension, $\bar{T}_{\mathrm{eff}}$, remains close to $900\ \mathrm{kN}$. The largest total maximum effective tension occurs in LC2a, with $T_{\mathrm{eff,max}} = 963.5\ \mathrm{kN}$ for the QS mooring-line model and $963.2\ \mathrm{kN}$ in the DYN mooring-line model. This occurs in the long-period swell case SS2, which also gives the largest horizontal offset in Section 5.4.

The governing-line maximum effective tensions ($T_{\mathrm{eff,max}}$) differ by less than $0.5\ \mathrm{kN}$ in all six cases. The DYN mooring-line representation therefore does not produce a systematic increase in maximum fairlead effective tension.

Because the total maximum effective tension is dominated by the mean effective tension, the tension range above the mean is used to interpret the time-varying part of the response. The largest tension range occurs in SS2, where ΔT_{eff} is about $63\ \mathrm{kN}$, corresponding to approximately 7% of the mean effective tension. For SS1, the tension range is about 16 to $17\ \mathrm{kN}$, or less than 2% of the mean value. For SS3, the tension range is about 3 to $4\ \mathrm{kN}$, or less than 0.4% of the mean value.

These results indicate that the tension variation remains small relative to the mean effective tension for the selected first-order cases. For these cases, the additional line inertia, hydrodynamic drag, and added mass in the DYN mooring-line representation do not lead to a noticeable change in governing fairlead effective tension.

5.6. Dynamic amplification factors

The dynamic amplification factors are summarised in Table 5.5. The values are calculated from the platform offset and governing line tension results in Sections 5.4 and 5.5.

Table 5.5: Dynamic amplification factors for the selected irregular-wave cases. $\mathrm{DAF}_{\Delta T}$ is based on the governing-line tension range above the mean effective tension.

Load case	Heading ($^\circ$)	$\mathbf{DAF}_{\mathbf{r},\max}$ ($-$)	$\mathbf{DAF}_{\mathbf{T},\max}$ ($-$)	$\mathbf{DAF}_{\mathbf{\Delta T}}$ ($-$)
LC1a	0	0.997	1.000	0.985
LC1b	30	0.997	1.000	0.985
LC2a	0	1.002	1.000	0.997
LC2b	30	1.002	1.000	0.994
LC3a	0	1.000	1.000	0.975
LC3b	30	1.000	1.000	0.976

The offset amplification factors remain close to unity for all selected cases, with values between 0.997 and 1.002. The largest values occur in the SS2 cases, but the increase is only about 0.2%. This is consistent with the platform-response statistics in Section 5.4, where the QS and DYN offsets differ only slightly.

The total tension amplification factor rounds to 1.000 in all cases. This does not mean that the QS and DYN tensions are exactly equal. It follows from the fact that $T_{\mathrm{eff,max}}$ is dominated by the mean level of approximately $900\ \mathrm{kN}$, so the small absolute differences between the two models are hidden when the total maximum tension is used.

The tension-range ratio $\mathrm{DAF}_{\Delta T}$ ranges from 0.975 to 0.997. These values show that the DYN model gives a slightly smaller tension range above the mean than the QS model for all selected cases. The results do not indicate measurable dynamic amplification of fairlead effective tension under the selected first-order, wave-only conditions.

5.7. Mooring-line frequency checks

The free-vibration results in Section 5.2.2 describe the global response periods of the moored floater. The DYN mooring-line representation also contains distributed line degrees of freedom. The natural frequencies of the dynamic HMPE lines are therefore checked separately. This check assesses whether local line frequencies overlap with the selected wave-frequency range. It also provides a first indication of whether current-induced vortex-induced vibration (VIV) should be considered in future current-loaded analyses.

5.7.1. Line eigenfrequencies

The line eigenfrequencies were obtained from OrcaFlex modal analysis about the still-water static equilibrium of the DYN mooring-line representation [34, 35]. Wave, wind and current excitation were switched off. The static fairlead effective tension was approximately $900\ \mathrm{kN}$ in each line. The modal analysis was first performed for each mooring line separately, without coupling to the vessel degrees of freedom. An additional coupled modal check was performed for Line 1 with the floater included. The coupled analysis also contained lower-frequency floater-line modes between 0.005 and $0.032\ \mathrm{Hz}$. The local line-mode groups considered in this section remained visible at approximately $0.162\ \mathrm{Hz}$ and $0.323\ \mathrm{Hz}$.

The first line modes occur in nearly equal frequency pairs. This is consistent with a tensioned three-dimensional line, where each transverse line-vibration shape can occur in two approximately orthogonal transverse directions. The first transverse line-mode pair occurs at approximately $0.1615\ \mathrm{Hz}$, corresponding to a period of approximately $6.19\ \mathrm{s}$. The three mooring lines give almost identical frequencies, which is consistent with the symmetric three-line layout. Table 5.6 lists the first four transverse line-mode pairs. The table gives the line-mode label, OrcaFlex mode numbers, frequency and period.

Table 5.6: First transverse mooring-line eigenfrequencies from the single-line OrcaFlex modal analysis.

Line-mode label	**Mode numbers**	**Period** (s)	**Frequency** (Hz)
f_1	1 to 2	6.19	0.162
f_2	3 to 4	3.10	0.323
f_3	5 to 6	2.06	0.484
f_4	7 to 8	1.55	0.646

The line-mode labels in Table 5.6 are used in the following frequency comparisons.

5.7.2. Comparison with wave spectra

The first transverse line-mode frequency is compared with the peak frequencies of the selected wave spectra in Table 5.7. The table lists the peak period and peak frequency of each sea state and includes f_1 from Table 5.6 as the relevant first line-mode frequency. The relevance for the ULS response is assessed from the DYN fairlead-tension spectra in Section 5.7.3.

Table 5.7: Comparison between selected wave peak frequencies and the first transverse line-mode frequency.

Quantity	**Period** (s)	**Frequency** (Hz)
SS1 peak	7.76	0.129
SS2 peak	18.07	0.055
SS3 peak	5.70	0.175
First transverse line mode, f_1	6.19	0.162

The comparison in Table 5.7 shows that f_1 lies between the SS1 and SS3 peak frequencies. It is closest to the SS3 peak, lies on the high-frequency side of SS1, and is clearly separated from the SS2 peak. A response near the first transverse line-mode frequency is therefore most likely to be visible in the short-period sea states, especially SS3.

Figure 5.3 shows the same comparison using the full wave spectra and the first two mooring-line eigenfrequencies. The figure shows that f_1 lies near the energetic range of SS3. The second line-mode frequency, $f_2 = 0.323\ \mathrm{Hz}$, lies in a range where the wave spectral density is much lower for all selected sea states. The following assessment therefore focuses mainly on whether the first line-mode frequency is visible in the fairlead-tension response.

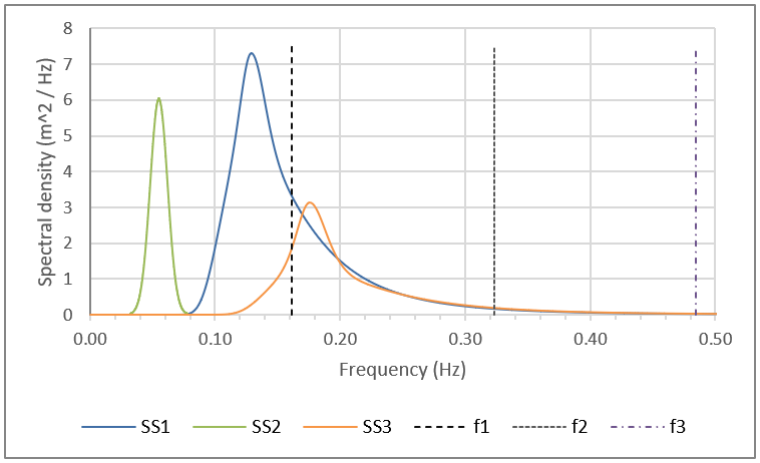

Figure 5.3: Comparison of the selected wave spectra with the mooring-line eigenfrequencies.

5.7.3. Excitation in the fairlead tension response

The wave-spectrum comparison indicates that the first transverse line-mode frequency is closest to SS3. To check whether this frequency is also visible in the dynamic line response, Figure 5.4 shows the DYN fairlead effective-tension spectra for Line 1 in the three 0° heading cases. The same analysed time window as in the time-domain response statistics is used.

In LC1a, the fairlead-tension response is concentrated around the SS1 wave-frequency range. No dominant peak occurs at the first line-mode frequency. In LC2a, the response is concentrated at lower frequencies around the SS2 peak and remains clearly separated from the first line-mode frequency. In LC3a, a response peak occurs close to $f_1 = 0.162$ Hz, which is consistent with the frequency overlap between SS3 and the first line mode shown in Figure 5.3. No clear response peak occurs near the second line-mode frequency, $f_2 = 0.323$ Hz, in the selected cases.

The LC3a peak shows that the first line mode is visible in the DYN fairlead-tension response. This peak is wave-induced and should not be interpreted as VIV, because no current is included in these simulations. Its effect on the evaluated ULS quantities remains small. In LC3a, the DYN tension range above the mean is only about 3.45 kN, compared with a mean effective tension of approximately 900 kN. The maximum effective tension and the tension range are also slightly lower with the DYN mooring-line model than with the QS model. The frequency check therefore shows a small local line response near f_1 in the short-period wave case. In the wave-only simulations, this local transverse response does not increase the governing fairlead effective tension.

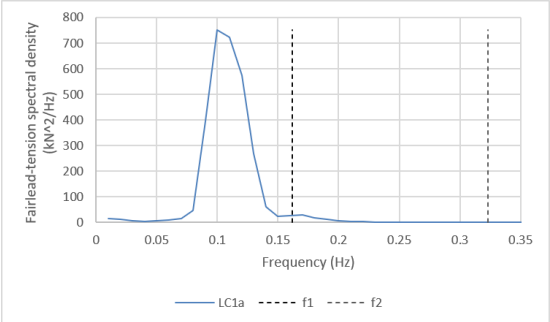

(a) LC1a

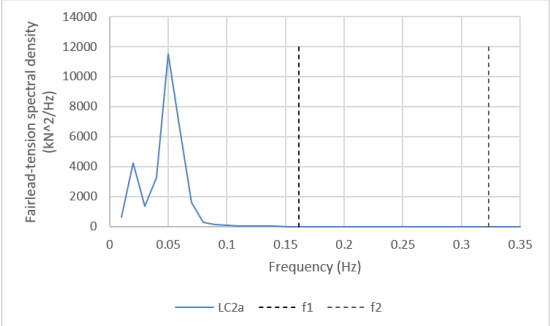

(b) LC2a

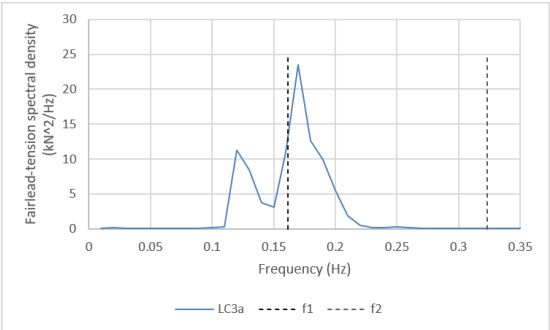

(c) LC3a

Figure 5.4: Line 1 DYN fairlead effective-tension spectra for the 0° heading cases. Dashed lines mark $f_1 = 0.162$ Hz and $f_2 = 0.323$ Hz.

5.7.4. Axial line-frequency check for tension amplification

The modal analysis above identifies transverse-line mode pairs. These modes are relevant for lateral line motion and possible current-induced VIV. Large dynamic amplification of the effective tension is more directly associated with longitudinal, or extensional, line vibration. A first axial line frequency estimate is therefore made to check whether axial frequency-coincidence is expected in the selected first-order wave-only cases.

The estimate is based on the longitudinal vibration theory for a uniform elastic bar [36]. The free longitudinal vibration equation is given as

$$\frac{\partial^2 u}{\partial t^2} = c^2 \frac{\partial^2 u}{\partial z^2} \tag{5.9}$$

where $u(z,t)$ is the axial displacement and $c = \sqrt{E/\rho}$ is the axial wave speed. For the present mooring-line estimate, this relation is rewritten using the OrcaFlex line inputs EA and $m' = \rho A$:

$$c_a = \sqrt{\frac{EA}{m'}} \tag{5.10}$$

The actual fairlead boundary condition is coupled to the moving floater, while the anchor is fixed to the seabed. The analytical bar solution is therefore used only as a first frequency bound. For a fixed-free bar the natural frequency can be written as shown in Equation 5.11 [36].

$$\omega_n = \frac{(2n+1)\pi c}{2L}, \qquad n = 0, 1, 2, \ldots \tag{5.11}$$

For the first axial mode this gives

$$f_{a,1}^{\text{fixed}-\text{free}} = \frac{c_a}{4L}. \tag{5.12}$$

For a fixed-fixed bar $\omega_n = n\pi c/L$, with $n = 1, 2, \ldots$ [36]. The corresponding first-frequency estimate is

$$f_{a,1}^{\text{fixed}-\text{fixed}} = \frac{c_a}{2L}. \tag{5.13}$$

For the adopted HMPE line used in the model, the OrcaFlex input uses $EA = 63.66$ MN and $m' = 4.4$ kg/m. This gives

$$c_a = \sqrt{\frac{63.66 \times 10^6}{4.4}} \approx 3804 \text{ m/s}. \tag{5.14}$$

Using the unstretched line length $L_0 = 945$ m gives

$$f_{a,1}^{\text{fixed}-\text{free}} \approx 1.01 \text{ Hz}, \qquad f_{a,1}^{\text{fixed}-\text{fixed}} \approx 2.01 \text{ Hz}. \tag{5.15}$$

As a sensitivity check, an estimated static elastic elongation can be calculated from the static tension and axial stiffness. With $\bar{T} \approx 900$ kN and $EA = 63.66$ MN, $\Delta L_{\text{static}} \approx \bar{T} L_0 / EA \approx 13.4$ m. Using $L_0 + \Delta L_{\text{static}}$ would reduce the fixed-free estimate from about 1.01 to 0.99 Hz.

The lowest axial-frequency estimate is the fixed-free value including the static-stretch sensitivity, approximately 0.99 Hz. This is about 5.7 times higher than the highest selected wave peak frequency, 0.175 Hz for SS3. The SS1 and SS2 peak frequencies are lower, at 0.129 Hz and 0.055 Hz. Direct axial frequency-coincidence of the mooring line is therefore not expected for the selected first-order wave-only cases.

The estimate is only a first check. It does not replace the OrcaFlex finite-element line model, and it does not include nonlinear coupling between axial and transverse line motion. It is used here only to distinguish transverse line vibration from axial tension amplification. The transverse line modes identified earlier remain relevant for local line motion and current-induced VIV, which are treated as current- and fatigue-related limitations rather than as evidence of large axial tension amplification in the selected wave-only cases.

5.7.5. First VIV screening

The mooring-line eigenfrequencies were also used for a first VIV screening. This screening checks whether current-induced vortex shedding could approach the line eigenfrequencies.

Vortex shedding from a slender circular cylinder can be described by the shedding frequency [4]

$$f_s = St\frac{U_n}{D}, \tag{5.16}$$

where f_s is the vortex-shedding frequency, St is the Strouhal number, U_n is the relative-flow component normal to the line and D is the hydrodynamic diameter. The Reynolds number is estimated as

$$Re = \frac{U_n D}{\nu}, \tag{5.17}$$

where ν is the kinematic viscosity of seawater.

The frequency-coincidence condition can also be expressed using the reduced velocity,

$$V_r = \frac{U_n}{f_n D}, \tag{5.18}$$

where V_r is the reduced velocity and f_n is the line natural frequency. VIV is a nonlinear synchronisation phenomenon in which the vortex-shedding process and the structural vibration can lock in near a natural frequency of the structure [37]. The first screening step is therefore to check whether the stationary-cylinder shedding frequency approaches a line natural frequency. This gives the frequency-coincidence condition $f_s \approx f_n$.

Using the frequency-coincidence condition $f_s \approx f_n$, Equations 5.16 and 5.18 give

$$V_r \approx \frac{1}{St}. \tag{5.19}$$

For $St = 0.2$, this corresponds to $V_r \approx 5$. The corresponding normal flow speed is obtained by rearranging Equation 5.16:

$$U_n \approx \frac{f_n D}{St}. \tag{5.20}$$

For this analysis, $D = 0.080\ \mathrm{m}$, $St = 0.2$ and $\nu = 1.35 \cdot 10^{-6}\ \mathrm{m^2/s}$ are used. The value $St = 0.2$ is an order-of-magnitude circular-cylinder screening value. Nielsen [4] reports this value for a smooth circular cylinder in the subcritical Reynolds-number range, approximately $300 < Re < 3 \cdot 10^5$. The same source also notes that the Strouhal number depends on Reynolds number and surface roughness.

Table 5.8: First VIV screening based on reduced velocity and line eigenfrequencies.

Line-mode label	Mode numbers	f_n (Hz)	U_n (m/s)	Re $(-)$
f_1	1 to 2	0.162	0.065	3.9×10^3
f_2	3 to 4	0.323	0.129	7.7×10^3
f_3	5 to 6	0.484	0.194	1.1×10^4
f_4	7 to 8	0.646	0.258	1.5×10^4

The U_n column in Table 5.8 gives the normal-flow velocity corresponding to $V_r \approx 5$ for each transverse line-mode frequency. For the first transverse line-mode pair, f_1, this condition is reached at a normal flow component of approximately $0.065\ \mathrm{m/s}$.

For a larger representative normal current component of $0.5\ \mathrm{m/s}$, the reduced velocities for f_1 to f_4 are approximately 38.6, 19.3, 12.9 and 9.7, respectively. This illustrates that increasing current speed shifts the possible VIV relevance towards higher transverse line modes. The values should not be interpreted as a lock-in prediction, but only as a first indication of which line-mode range may require further current-loaded assessment.

The Reynolds-number column is used to check whether the adopted Strouhal value is applied in the intended Reynolds-number regime. The resulting Reynolds numbers fall within the subcritical Reynolds-number range for which $St = 0.2$ is used as a circular-cylinder screening value [4].

The normal-flow velocities required to reach $V_r \approx 5$ are small for the first transverse mode pairs. This indicates that current-induced VIV cannot be excluded for current-loaded conditions. No site-specific current profile is included in the present wave-only model. This analysis is therefore not used to predict VIV amplitudes or fatigue damage. It only indicates that current-induced line vibrations require a separate assessment before extending the QS-DYN conclusion to wind-wave-current design cases. This remains a first screening result. Rope-specific roughness, marine growth, damping, spatially varying current, mode competition and fatigue damage are not modelled.

5.7.6. Implication for the response comparison

The line-frequency check does not change the QS-DYN conclusion for the selected first-order, wave-only cases. The first transverse line-mode frequency lies closest to the SS3 peak frequency and is visible in the LC3a fairlead-tension spectrum. However, the associated tension response remains small compared with the mean effective tension, and the DYN mooring-line model does not increase $T_{\mathrm{eff,max}}$ or ΔT_{eff} relative to the QS model. The axial-frequency estimate also indicates that direct axial frequency-coincidence is not expected in the selected wave-frequency range. The identified line frequencies therefore do not lead to dynamic amplification of the evaluated platform-offset and fairlead-tension responses in the present wave-only comparison.

This conclusion should not be extended to current-loaded or fatigue cases. The VIV screening indicates that current-induced excitation of transverse line modes cannot be excluded. VIV, current-induced line response, axial-transverse coupling and fatigue are therefore outside the present wave-only scope, but they are not assumed negligible.

5.8. Interpretation and limits of the response comparison

The restoring checks, free-vibration periods, RAO trends, and irregular-wave response statistics give a consistent interpretation of the response comparison. The estimated moored-system periods are approximately $254\,\mathrm{s}$ in surge, $43\,\mathrm{s}$ in heave, and $42\,\mathrm{s}$ in pitch (Table 5.2). These periods are longer than the spectral peak periods of the selected sea states, which range from $T_p = 5.7$ to $18.1\,\mathrm{s}$. The peak first-order wave excitation is therefore separated from the evaluated moored-system response periods.

The response statistics support this interpretation. The maximum horizontal offset remains below approximately $1.2\,\mathrm{m}$, and the largest governing-line tension range is about $63\,\mathrm{kN}$, corresponding to approximately 7% of the mean effective tension. A simple geometric check is added to assess whether this offset noticeably changes the fairlead-force direction. Table 5.9 estimates the line-inclination change for the maximum SS2 offset, using a still-water horizontal span of $551.18\,\mathrm{m}$ for Line 1 and a vertical fairlead-to-anchor distance of $786\,\mathrm{m}$. The offset is treated as a horizontal displacement in the x-y plane along the Line 1 axis.

The maximum inclination change is only about $0.06°$ for the line aligned with the offset direction and about $0.03°$ for the two opposite lines. The fairlead-force direction therefore changes only slightly in the selected wave-only cases. The force-component change is mainly associated with the effective-tension variation rather than with the inclination change.

Line condition	Horizontal span (m)	Inclination from vertical $(°)$	Angle change $(°)$
Still water	551.18	35.04	0.00
Stretched by 1.15 m offset	552.33	35.10	$+0.06$
Shortened by 1.15 m offset	550.03	34.98	-0.06
Opposite lines, same offset axis	≈ 550.6 to 551.7	35.01 to 35.07	≈ 0.03

Table 5.9: Geometric estimate of mooring-line inclination change for the maximum SS2 horizontal offset.

Nielsen [4] shows that dynamic line effects can become relevant when fairlead motion changes the line shape with time, because hydrodynamic drag, line inertia, and added mass may affect the top-

end tension. The present simulations do not show a noticeable effect of these mechanisms, but this conclusion is specific to the model, the selected sea states, and the first-order wave-only loading scope.

Two omitted effects or modelling choices could change this conclusion. First, the soft surge mode, with an estimated period of approximately $254\ \mathrm{s}$, may be sensitive to low-frequency second-order wave-drift excitation, which is not included in the simulations. If such excitation overlaps with the low-frequency surge response range, larger horizontal excursions and higher line-tension variations could occur [4, 38]. Second, a different pretension level or line-length calibration could change the local restoring behaviour and the relation between platform motion and line tension. This may change the difference between the two mooring-line representations, especially if the system experiences larger fairlead motions or lower restoring stiffness.

Within the present first-order, wave-only comparison setup, the DYN mooring-line representation does not noticeably change the predicted maximum horizontal platform offset or governing fairlead effective tension relative to the QS representation. This conclusion applies to the selected target pretension and the evaluated load cases only.

It should not be extended to mooring-line strength design, fatigue assessment, transient loading, line-failure cases, or certification-level design load cases. This limitation is consistent with Masciola et al. [6], who found that mooring-line dynamics can have limited influence on platform surge and heave motion in some cases, while still being important for peak mooring-line loads under more severe loading conditions.

As a strength-context check, the largest governing-line maximum effective tension in the selected cases is $963.5\ \mathrm{kN}$. Compared with the line MBL of $4040\ \mathrm{kN}$, this corresponds to approximately 23.8% of MBL. This value is included only as plausibility and utilisation context for the selected cases. It is not a certification-level strength assessment.

The VIV screening does not directly change the selected wave-only response-comparison results, but it identifies current-induced line dynamics and fatigue as important next-step analyses before extending the conclusion to wind-wave-current design cases.

6
Sensitivity analysis

This chapter examines how selected modelling assumptions affect the interpretation of the response comparison from Chapter 5. The sensitivities test whether the main conclusion changes when the mooring pretension state or the mean horizontal loading is varied.

Section 6.1 examines how the unstretched line length affects the static line-tension state. Section 6.1.1 repeats one irregular-wave case at two pretension levels. Section 6.2 evaluates a simplified steady-thrust load. Section 6.3 then discusses what these sensitivities mean for using the QS mooring-line representation as an early-stage screening approximation.

6.1. Effect of unstretched line length

This section examines how the still-water line-tension state changes when the unstretched line length is varied. The purpose is not to redefine the target pretension used in Chapter 5, but to assess how strongly the selected pretension level depends on the line-length calibration. The section first presents static line-length sensitivity and the associated strain and elastic-elongation estimates. It then checks the effect on the still-water free-vibration period estimates. Section 6.1.1 uses two of these pretension levels in one irregular-wave sensitivity case.

In Chapter 3, the reference-design tension level of $0.9\ \mathrm{MN}$ per line was used as the target pretension for the OrcaFlex mooring calibration. In OrcaFlex, this pretension is obtained through the mooring geometry and the unstretched line length. The resulting $900\ \mathrm{kN}$ state is therefore the selected pretension state for the response comparison, not a re-optimised mooring design.

Table 6.1 shows the static sensitivity to unstretched line length. Increasing L_0 from 944.97 to $947.97\ \mathrm{m}$ reduces the mean line tension from approximately 900 to $718\ \mathrm{kN}$. A further increase to $950.97\ \mathrm{m}$ reduces the mean tension to about $537\ \mathrm{kN}$. The total vertical mooring force decreases from approximately -2.21 to -1.76 and $-1.31\ \mathrm{MN}$, where the negative sign indicates a downward force on the floater. The mean tension is the mean of the three static fairlead effective tensions.

Table 6.1: Static sensitivity of mean line tension, vertical mooring force, estimated strain, and estimated elastic elongation to unstretched line length.

Case	**Unstretched length** (m)	**Mean tension** (kN)	**Total vertical mooring force** (kN)	**Strain** $\varepsilon\ (\%)$	**Elastic elongation** $\Delta \mathrm{L_{el}}\ (\mathrm{m})$
Target	944.97	900.183	-2205.576	1.414	13.363
$+3\ \mathrm{m}$	947.97	717.978	-1758.793	1.128	10.692
$+6\ \mathrm{m}$	950.97	536.841	-1314.479	0.843	8.020
$+10\ \mathrm{m}$	954.97	297.197	-726.299	0.467	4.459

Figure 6.1 shows the same static sensitivity graphically and highlights the strong dependence of mean line tension on the unstretched line length.

The strain and elastic elongation in Table 6.1 are estimated from the mean static effective tension and the axial stiffness. The strain is calculated as $\epsilon \approx \bar{T}/EA$, and the elastic elongation as $\Delta L_{\mathrm{el}} \approx \epsilon L_0$. For the target line length, the mean static tension is approximately $900\ \mathrm{kN}$. This gives a strain of 1.41% and an estimated elastic elongation of about $13.4\ \mathrm{m}$.

The sensitivity results show that small changes in unstretched line length strongly change the static line-tension state. Increasing L_0 from 944.97 to $954.97\ \mathrm{m}$ reduces the mean line tension from approximately 900 to $297\ \mathrm{kN}$. The corresponding estimated elastic elongation decreases from about 13.4 to $4.5\ \mathrm{m}$. The target case is therefore a taut, pretension-dominated mooring state.

A simple vertical-equilibrium estimate gives the same order of magnitude for the reference design. With the line inclination measured from the vertical, the per-line pretension required to balance a buoyancy

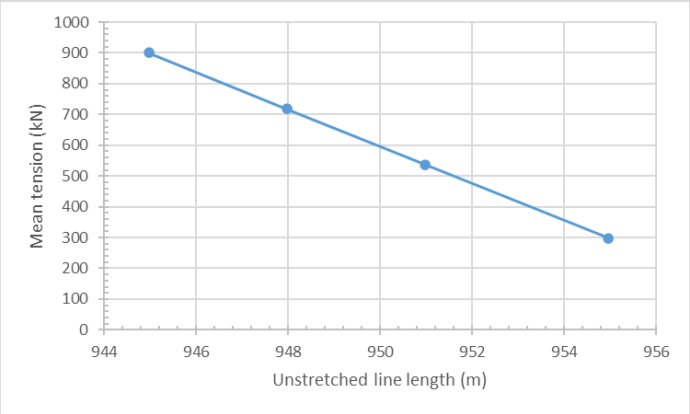

Figure 6.1: Static sensitivity of mean line tension to unstretched line length.

surplus can be estimated as

$$T_{\mathrm{pre,eq}} = \frac{B - W}{n \cos \beta}, \tag{6.1}$$

where B is the buoyancy, W is the weight, n is the number of mooring lines, and β is the line inclination from the vertical. Using the reference design values $B = 305.12$ MN, $W = 302.79$ MN, $n = 3$, and $\beta = 35°$ gives $T_{\mathrm{pre,eq}} \approx 0.95$ MN per line. This is consistent with the reference-design equilibrium tension. This estimate shows that the reference pretension is primarily a global vertical-equilibrium quantity for the reference design. The rope diameter and axial stiffness determine the strain and elastic elongation associated with this tension, while the unstretched length calibration determines how this tension is recovered in the OrcaFlex model.

For the reduced-body model, the recalculated mass and buoyancy are not identical to the full reference-design values. Therefore, the 900 kN pretension is not interpreted as a newly optimised equilibrium of the reduced geometry. It is used as the selected pretension level for the response comparison, while maintaining traceability to the reference design. An improved design model would require a separate mooring optimisation with all mass parts, buoyancy, geometry, and load cases.

Applying the same vertical-equilibrium estimate directly to the reduced-body mass and buoyancy gives a much lower per-line tension than 900 kN. In the present OrcaFlex model, increasing the unstretched line length towards this lower-tension range moved the line representation away from the intended taut-line regime. The lowest retained case is therefore used only as a sensitivity case in Section 6.1.1, not as a replacement for the target-pretension state in the main response comparison.

The effect on the free-vibration period estimates is summarised in Table 6.2.

Table 6.2: Moored-system free-vibration period estimates for the high- and low-pretension cases.

Mode	**Reference**	**Pretension** 900 kN		**Pretension** 298 kN	
	(s)	**QS** (s)	**DYN** (s)	**QS** (s)	**DYN** (s)
Surge	244	253.95	253.95	258.025	258.05
Heave	39.5	43.00	43.017	43.05	43.07
Pitch	59.7	42.25	42.30	42.58	42.58

Increasing the unstretched line length by 10 m changes the still-water mean line tension strongly, from approximately 900 kN to 298 kN. The estimated moored-system periods change much less. The surge period increases from about 254 s to 258 s, while the heave and pitch periods remain close to the high-pretension values.

This does not mean that unstretched line length or pretension is generally unimportant. It only shows that, for these two tested line-length cases, the estimated still-water periods remain far from the selected first-order wave peak periods.

6.1.1. Pretension sensitivity in a selected irregular-wave case

The static line-length sensitivity in Section 6.1 shows that the still-water pretension is strongly affected by the unstretched line length. To check whether this also affects the difference between the two mooring-line representations in waves, one irregular-wave case is repeated for the high- and low-pretension cases. The selected case is SS1 at 30° wave heading.

The high-pretension case uses an unstretched length of $944.97\ \mathrm{m}$. The low-pretension case uses $954.97\ \mathrm{m}$, corresponding to the lowest still-water tension level retained for the sensitivity comparison in Table 6.1. The same floater model, hydrodynamic database, sea state, wave heading, wave seed, simulation duration, and post-processing window are used for the two mooring-line models. The steady-thrust load is not included. Table 6.3 summarises the response statistics.

Table 6.3: Pretension sensitivity results for SS1 at 30° wave heading. The governing line is the line with the largest maximum effective tension in each run.

Pretension	Line model	$\mathbf{L_0}$ (m)	$\mathbf{r}_{\max}$ (m)	Line	$\mathbf{T}_{\mathrm{eff,max}}$ (kN)	$\bar{\mathbf{T}}_{\mathrm{eff}}$ (kN)	$\boldsymbol{\Delta}\mathbf{T}_{\mathrm{eff}}$ (kN)	$\boldsymbol{\Delta}\mathbf{T}_{\mathrm{eff}}/\bar{\mathbf{T}}_{\mathrm{eff}}$ (%)
High	QS	944.97	0.306	1	916.049	900.348	15.701	1.74
High	DYN	944.97	0.305	1	915.729	900.257	15.472	1.72
Low	QS	954.97	0.302	1	312.750	297.339	15.411	5.18
Low	DYN	954.97	0.301	1	312.551	297.318	15.233	5.12

Line 1 is the governing line in all four simulations. Reducing the pretension strongly changes the absolute fairlead tension level: $T_{\mathrm{eff,max}}$ decreases from approximately $916\ \mathrm{kN}$ in the high-pretension case to approximately $313\ \mathrm{kN}$ in the low-pretension case. The platform response changes only slightly, with $r_{\max}$ remaining close to $0.30\ \mathrm{m}$ in all four simulations.

The tension range above the mean remains approximately $15\ \mathrm{kN}$ for both pretension levels. However, the same tension range represents a larger percentage of the mean effective tension when the pretension is reduced. In the high-pretension case, the tension range is about 1.7% of the mean value. In the low-pretension case, it increases to about 5.1% of the mean value. The main change is therefore not the absolute tension range itself, but its size relative to the mean effective tension.

The difference between the two mooring-line models remains small at both pretension levels. In the high-pretension case, the values of $\mathrm{DAF}_{r,\max}$, $\mathrm{DAF}_{T,\max}$, and $\mathrm{DAF}_{\Delta T}$ are 0.997, 1.000, and 0.985, respectively. In the low-pretension case, the corresponding values are approximately 0.996, 0.999, and 0.988. The DYN mooring-line model therefore gives slightly smaller maximum tensions and tension ranges than the QS model in this selected case.

These results indicate that the tested pretension reduction changes the absolute tension level and the relative importance of the wave-induced tension range, but does not lead to noticeable dynamic amplification of platform offset or fairlead effective tension. This conclusion is limited to this selected first-order, wave-only sensitivity case. It should not be generalised to second-order drift excitation, current loading, transient loading, or other pretension levels outside the tested range.

6.2. Steady-thrust sensitivity

The comparison in Chapter 5 is limited to wave-only loading. This section examines how a simplified steady rotor-thrust load affects the static mooring state and the difference between the mooring-line representations. The purpose is to assess whether a mean horizontal load changes the platform equilibrium and the mooring-line tension distribution.

The thrust sensitivity is applied to SS1 at $30°$ wave heading. SS1 is selected because it represents the maximum-H_s wind-sea case in the load-case matrix. The case is used only as a sensitivity case. Current, turbulent wind, turbine control, and second-order wave-drift loading are not included.

The SS1 ERA5 wind speed at $10\ \mathrm{m}$ height is $13.50\ \mathrm{m/s}$. When extrapolated to hub height, this exceeds the rated wind speed of the IEA $15\ \mathrm{MW}$ reference turbine. The thrust is therefore not extrapolated with a constant C_T at the SS1 wind speed. Instead, a rated-thrust-level load is used as a simplified steady load. This gives a horizontal thrust force of $2.483\ \mathrm{MN}$ and an equivalent pitch moment of $0.450\ \mathrm{GNm}$.

Because the tower, nacelle, and rotor are not included as aerodynamic objects in the OrcaFlex model, the thrust is not applied through the OrcaFlex wind-load model. It is applied as a constant vessel-applied load at the vessel reference point, using an equivalent force-moment pair. For the time-domain thrust case, the platform offset is calculated from the total OrcaFlex vessel position outputs X and Y. The Dynamic x and Dynamic y outputs are not used because they describe motion relative to the static equilibrium and would exclude the thrust-induced mean offset [39].

Figure 6.2 shows the thrust implementation schematically. The left figure shows the physical interpretation of the rotor thrust acting at hub height. The right figure shows the equivalent OrcaFlex implementation at the vessel reference point.

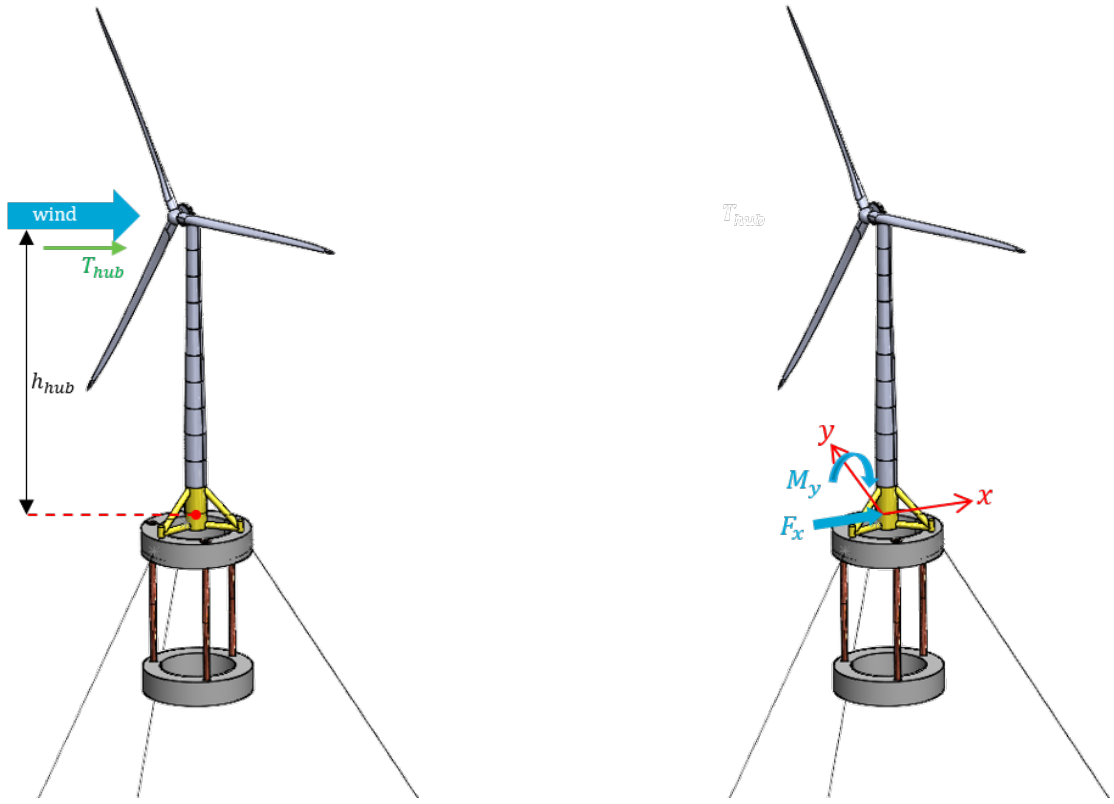

(a) Physical thrust at hub height.

(b) Equivalent OrcaFlex force-moment pair.

Figure 6.2: Schematic implementation of the steady-thrust sensitivity. The left figure shows the physical rotor thrust at hub height. The right figure shows the equivalent OrcaFlex implementation as a global x-force, F_X, and pitch moment, $M_Y = T_{\mathrm{hub}} h_{\mathrm{hub}}$, applied at the vessel reference point.

A static ramp is first carried out using 0%, 25%, 50%, 75%, and 100% of the rated-thrust-level load. The force and moment are scaled with the same factor. The results are shown in Table 6.4. The QS and

DYN static results are nearly identical. This indicates that the static equilibrium shift is governed by the applied thrust and the common static restoring behaviour of the two mooring-line representations.

Table 6.4: Static thrust-ramp results for SS1 at 30° wave heading. The thrust is applied as a constant global x-force and equivalent pitch moment at the vessel reference point.

Line model	Thrust (%)	$\mathbf{F_X}$ (kN)	$\mathbf{M_Y}$ (kN · m)	Surge x (m)	Pitch θ (°)	$\mathbf{T_1}$ (kN)	$\mathbf{T_2/T_3}$ (kN)
QS	0	0	0	0.006	0.001	900.202	900.176/900.170
QS	25	621	112469	16.437	2.306	234.772	1244.730/1244.724
QS	50	1242	224938	47.147	4.665	4.075	1879.612/1879.605
QS	75	1862	337406	79.253	7.063	2.136	2591.939/2591.929
QS	100	2483	449875	106.445	9.472	1.559	3244.598/3244.586
DYN	0	0	0	0.006	0.001	900.120	900.086/900.080
DYN	25	621	112469	16.449	2.305	234.282	1244.707/1244.701
DYN	50	1242	224938	47.210	4.664	3.994	1880.319/1880.120
DYN	75	1862	337406	79.270	7.063	2.120	2592.157/2592.147
DYN	100	2483	449875	106.458	9.472	1.546	3244.764/3244.753

The full rated-thrust-level load causes a large static equilibrium shift. At 100% thrust, the floater moves more than $100\ \mathrm{m}$ in the positive global x-direction, and line 1 is almost fully unloaded. From 50% thrust onwards, line 1 carries only a few kilonewtons of static effective tension. These cases are therefore not used as direct irregular-wave QS-DYN sensitivity cases, because they no longer represent the three-taut-line working regime used in the wave-only comparison.

The 25% rated-thrust case is retained as a reduced time-domain sensitivity after the static ramp showed that higher thrust levels strongly unload one mooring line. It introduces a substantial mean offset and line-tension redistribution, while all three lines remain in tension in the static check. The corresponding force $\mathrm{F_X}$ is $621\ \mathrm{kN}$ and the pitch moment $\mathrm{M_Y}$ is $112.469\ \mathrm{MN \cdot m}$. This case is then repeated in time-domain irregular waves for both mooring-line representations, using the same SS1 sea state, wave heading, wave seed, simulation duration, and post-processing window as in the wave-only comparison. Table 6.5 summarises the resulting response statistics.

Table 6.5: Dynamic response for the 25% rated-thrust sensitivity case in SS1 at 30° wave heading. The governing line is the line with the largest maximum effective tension.

Line model	$\bar{\mathbf{r}}$ (m)	$\mathbf{r}_{\max}$ (m)	$\boldsymbol{\sigma_r}$ (m)	$\bar{\theta}$ (°)	$\lvert\theta\rvert_{\max}$ (°)	Governing line	$\mathbf{T}_{\mathrm{eff,max}}$ (kN)	$\bar{\mathbf{T}}_{\mathrm{eff}}$ (kN)	$\boldsymbol{\Delta}\mathbf{T}_{\mathrm{eff}}$ (kN)
QS	16.434	16.675	0.086	2.306	2.404	3	1259.139	1244.607	14.531
DYN	16.446	16.687	0.086	2.306	2.404	3	1258.971	1244.585	14.386

The 25% thrust case shifts the mean equilibrium much more than the wave-only SS1 case. The mean horizontal offset, $\bar{\mathbf{r}}$, is approximately $16.4\ \mathrm{m}$, and the mean pitch angle, $\bar{\theta}$, is approximately 2.3°. The thrust also redistributes the mooring-line tensions. Line 1 is unloaded to a mean effective tension $\bar{\mathrm{T}}_{\mathrm{eff}}$ of about $235\ \mathrm{kN}$, while lines 2 and 3 increase to approximately $1245\ \mathrm{kN}$. This shows that the reduced steady-thrust load changes the static mooring-equilibrium state.

The difference between the two mooring-line models remains small despite this shifted static equilibrium. The maximum horizontal offset is $16.675\ \mathrm{m}$ for the QS model and $16.687\ \mathrm{m}$ in the DYN model. The governing line is line 3 in both simulations, with maximum effective tensions of $1259.139\ \mathrm{kN}$ and $1258.971\ \mathrm{kN}$, respectively. The corresponding amplification factors are $\mathrm{DAF}_{r,\max} = 1.001$, $\mathrm{DAF}_{T,\max} = 1.000$, and $\mathrm{DAF}_{\Delta T} = 0.990$.

These results indicate that the reduced steady-thrust case changes the mean platform position and the distribution of mean line tensions, but does not lead to noticeable dynamic amplification of platform offset or fairlead effective tension between the two mooring-line representations. The result is specific to

the selected 25% rated-thrust sensitivity case. The full rated-thrust static ramp shows that an operating-thrust case cannot be assessed with the present mooring input parameters alone, because one mooring line becomes almost fully unloaded. A design-level thrust assessment would require revised mooring input parameters or a coupled operating-turbine load case.

6.3. Implications for the mooring-line model comparison

The sensitivity analyses clarify how the Chapter 5 results should be interpreted. The wave-only comparison showed small differences between the two mooring-line representations for the selected first-order cases. The sensitivity checks show that this result is linked to the target pretension level, mooring geometry, and the limited set of loads included in the comparison.

The unstretched-line-length sensitivity shows that the static line-tension state is strongly affected by the line-length calibration. Increasing the unstretched length from $944.97\ \mathrm{m}$ to $954.97\ \mathrm{m}$ reduces the still-water mean tension from approximately $900\ \mathrm{kN}$ to about $298\ \mathrm{kN}$. This shows that the $900\ \mathrm{kN}$ pretension is not a general optimum, but a selected target pretension that retains traceability to the reference design and keeps the model in the intended taut-line regime.

The tested pretension reduction does not shift the evaluated free-vibration periods into the selected first-order wave-period range. The surge period remains around 254 to $258\ \mathrm{s}$, while the heave and pitch estimates remain close to $43\ \mathrm{s}$. The pretension sensitivity run also does not introduce a measurable QS-DYN difference. In that case, reducing the pretension changes the absolute tension level and increases the tension range as a percentage of the mean value, but the DAF values remain close to unity.

The steady-thrust sensitivity shows a different limitation. A full rated-thrust-level static load causes a large equilibrium shift and almost complete unloading of one mooring line. The mooring input parameters or layout must be reconsidered before design-level thrust conclusions can be drawn. The reduced 25% rated-thrust case is therefore used only as a time-domain sensitivity case. It shifts the mean offset to approximately $16.4\ \mathrm{m}$ and redistributes the mean line tensions, but it still does not introduce noticeable dynamic amplification between the two mooring-line representations in the selected first-order case.

Together, these results support the main interpretation of Chapter 5: for the selected first-order screening cases, the QS and DYN mooring-line representations give very similar predictions of maximum horizontal platform offset and governing fairlead effective tension. However, this conclusion is case-specific. It applies to the floater model, selected sea states, wave seeds, first-order loading scope, and tested pretension levels.

The sensitivity analyses also show where this conclusion should not be generalised. Larger differences between the two mooring-line representations may occur when the mooring system enters a different static tension state, when one line becomes strongly unloaded, or when low-frequency excitation generates larger fairlead motions. Second-order wave-drift loading, current, turbulent wind, turbine-control interaction, fatigue, transient loading, line-failure cases, and certification-level design load cases remain outside the present comparison. The steady-thrust sensitivity also shows that wind-wave design conclusions would require revised mooring input parameters or a coupled operating-turbine load case. These mechanisms should be addressed before the QS model is used for design-level mooring conclusions.

7
Conclusions and recommendations

This chapter answers the research questions and summarises the two main outcomes of the thesis. The thesis developed and verified a numerical Rhino-OrcaWave-OrcaFlex model of the Elevator floating wind concept. This model was then used to assess whether a dynamic (DYN) mooring-line representation changes the predicted maximum horizontal platform offset and governing fairlead effective tension compared with a quasi-static (QS) mooring-line representation.

The comparison used the same floater representation, hydrodynamic database, mooring geometry, target pretension, unstretched line length, sea states, wave headings, wave seed, simulation settings, and post-processing method. The only intended difference was the mooring-line representation. Section 7.1 answers the research questions directly. Section 7.2 gives the overall conclusion on the use of the QS mooring-line representation for the Elevator case. Section 7.3 gives the recommended next steps for extending the comparison to a broader wind-wave-current load basis.

7.1. Conclusions

RQ1: What response quantities, load mechanisms, and modelling assumptions are relevant for comparing quasi-static and dynamic mooring line models of a taut synthetic mooring system in deep water?

The most relevant response quantities are the resultant horizontal platform offset, the governing fairlead effective tension, and selected platform motions. The horizontal offset is important because it changes the mooring geometry and redistributes the line loads. The governing fairlead effective tension is the main mooring load quantity for ULS screening. Platform pitch is treated as a supporting quantity because it affects the global force and moment equilibrium of the floater and can influence the fairlead positions.

For the taut HMPE mooring system, the pretension and unstretched line length define the static line-tension state of the mooring system. The total fairlead tension is dominated by the mean effective tension, which remains close to the tension level of approximately $900\ \mathrm{kN}$ per line in the selected wave-only cases. The line-tension response is therefore interpreted using both the total maximum effective tension, $T_{\mathrm{eff,max}}$, and the tension range above the mean, ΔT_{eff}. The tension range above the mean is especially useful for interpreting the QS-DYN difference, because the total maximum effective tension is dominated by the mean pretension level.

The dominant load mechanism in the main comparison is first-order irregular-wave excitation. Second-order wave-drift loading, current, and wind thrust from an operating turbine are not included in the main comparison because the scope is deliberately limited to isolating the effect of the mooring-line representation. These effects are not assumed to be negligible. They are outside the selected comparison setup and require a broader wind-wave-current load basis. A steady rated-thrust-level load is therefore considered only as a separate sensitivity case to examine how a simplified mean aerodynamic load affects the mean offset and line-tension distribution.

Both the mooring-line representations use the same mooring geometry, target pretension, unstretched line length, and effective axial stiffness. The difference is in how the line force is computed in time. In the QS model, the line force follows from the instantaneous static line equilibrium at the current fairlead position. In the DYN mooring-line model, the mooring lines are represented as dynamic line elements, so distributed line inertia, hydrodynamic drag, added mass, and time-dependent line motion are included. Material effects of the HMPE rope, such as creep, fatigue degradation, and nonlinear load-history effects, are outside the scope of the comparison.

RQ2: How can a numerical Rhino-OrcaWave-OrcaFlex model of the Elevator concept be developed and verified for the QS-DYN mooring-line comparison?

A numerical Elevator model was developed and verified for the QS-DYN mooring-line comparison. The model was built through a Rhino-OrcaWave-OrcaFlex workflow using the Elevator reference design as

input basis. The reference design provided the initial geometry, target mooring tension, mass properties, hydrostatic quantities, and linearised restoring estimates used to define and check the numerical model.

The verification was performed at three levels. First, the OrcaWave diffraction body was verified for hydrostatic consistency. The displaced volume, centre of buoyancy, waterplane area, and hydrostatic heave stiffness were reviewed. The heave stiffness was also checked against the analytical relation based on the waterplane area. This confirmed that the panel body gives an internally consistent hydrostatic representation.

Second, the OrcaFlex mooring implementation was calibrated and then verified at the still-water equilibrium. The unstretched line length was adjusted to recover the target fairlead tension of approximately $900\ \mathrm{kN}$ per line. This calibration defines the target pretension state used in the model. After this calibration, the still-water equilibrium was checked by comparing the three fairlead tensions, the vessel position, and the vessel rotations in the QS and DYN mooring-line models. Both models recovered nearly identical fairlead tensions and a stable, almost symmetric equilibrium, which shows that they start from the same static mooring state before the response comparison is made.

Third, the local restoring behaviour was verified through small static force-displacement and moment-rotation tests about the equilibrium. These tests showed that the mooring-line representations have nearly identical local translational and rotational restoring behaviour. The resulting restoring coefficients were compared with the linearised reference estimates as consistency checks.

The developed numerical model is therefore a consistent comparison model for isolating the effect of the mooring-line representation.

RQ3: How do quasi-static and dynamic mooring line representations compare under the selected first-order irregular-wave ULS screening cases in terms of horizontal platform offset, fairlead effective tension, and selected platform motions?
For the selected first-order, wave-only screening cases, the mooring-line representations give nearly identical platform responses. The largest horizontal offset occurs in SS2, the long-period swell case. The maximum offset is approximately $1.15\ \mathrm{m}$ for both wave headings, and the largest QS-DYN difference in $r_{\max}$ is about $0.003\ \mathrm{m}$. SS1 gives a maximum offset of about $0.31\ \mathrm{m}$, while SS3 gives a maximum offset of about $0.06\ \mathrm{m}$. The selected heave and pitch responses also remain almost unchanged when switching from the QS to the DYN mooring-line representation. The DYN mooring-line model therefore does not produce a systematic increase in platform response for the selected cases.

The line-tension response shows the same trend. The largest governing-line maximum effective tension occurs in LC2a, with $963.5\ \mathrm{kN}$ for the QS model and $963.2\ \mathrm{kN}$ for the DYN mooring-line model. The corresponding tension range above the mean is approximately $63\ \mathrm{kN}$, or about 7% of the mean effective tension. For SS1, the tension range is about 16 to $17\ \mathrm{kN}$, while for SS3 it is about 3 to $4\ \mathrm{kN}$.

These results show that the tension range above the mean remains small relative to the mean effective tension, which stays close to the $900\ \mathrm{kN}$ pretension level. Under the selected wave-only cases, the additional line inertia, hydrodynamic drag, and added mass included in the DYN mooring-line model do not lead to a noticeable increase in maximum horizontal platform offset, selected platform motions, or governing fairlead effective tension.

RQ4: How can the differences between the quasi-static and dynamic mooring-line predictions be quantified using dynamic amplification factors for the selected response quantities?
The QS-DYN differences were quantified using case-specific dynamic amplification factors. For horizontal offset, $\mathrm{DAF}_{r,\max}$ ranges from 0.997 to 1.002. This means that the maximum offset predicted by the DYN mooring-line model differs from the QS prediction by less than approximately 0.3% in the selected cases.

For total maximum effective tension, $\mathrm{DAF}_{T,\max}$ rounds to 1.000 in all selected load cases. This does not mean that the QS and DYN tensions are exactly equal. It follows from the fact that the total maximum effective tension is dominated by the mean effective tension, which remains close to the $900\ \mathrm{kN}$ pretension level.

The tension-range ratio $\mathrm{DAF}_{\Delta T}$ ranges from 0.975 to 0.997. These values indicate that the DYN mooring-line model gives a slightly smaller tension range above the mean than the QS model for all

selected first-order screening cases. The results therefore do not indicate measurable dynamic amplification of fairlead effective tension in the tested wave-only matrix.

The DAF values are useful as comparison indicators. They are specific to the model, selected sea states, wave headings and response definitions used in this thesis.

RQ5: How do pretension, unstretched line length, and simplified steady-thrust loading affect the QS-DYN comparison and the interpretation of the dynamic amplification factors?
The sensitivity analyses show that the near-unity DAF values are linked to the selected pretension, mooring geometry, and load types included in the comparison. The static line-tension state is strongly affected by the unstretched line length. Increasing the unstretched length from $944.97\ \mathrm{m}$ to $954.97\ \mathrm{m}$ reduces the still-water mean line tension from approximately $900\ \mathrm{kN}$ to about $298\ \mathrm{kN}$. The $900\ \mathrm{kN}$ tension level should therefore be interpreted as a selected, reference-traceable target pretension for the mooring-line comparison, not as a re-optimised final mooring equilibrium of the reduced-body model.

The tested pretension reduction changes the absolute tension level and the relative size of the wave-induced tension range, but it does not introduce a measurable QS-DYN difference in the selected SS1 sensitivity case. In SS1 at 30° wave heading, the maximum effective tension decreases from about $916\ \mathrm{kN}$ in the high-pretension case to about $313\ \mathrm{kN}$ in the low-pretension case. The tension range above the mean remains about $15\ \mathrm{kN}$ in both cases. However, this corresponds to about 1.7% of the mean effective tension in the high-pretension case and about 5.1% in the low-pretension case. The DAF values remain close to unity.

The tested pretension reduction also has only a small effect on the evaluated free-vibration periods. The surge period remains around 254 to $258\ \mathrm{s}$, while the heave and pitch estimates remain close to $43\ \mathrm{s}$. These periods remain well separated from the selected first-order wave peak periods, which range from 5.70 to $18.07\ \mathrm{s}$. The pretension sensitivity therefore does not shift the tested system into a wave-frequency resonance range.

The steady-thrust sensitivity shows that the mean mooring state is also sensitive to mean horizontal loading. A full rated-thrust-level static load causes a large equilibrium shift and almost complete unloading of one mooring line. A reduced 25% rated-thrust case is therefore used as a time-domain sensitivity case. This case shifts the mean horizontal offset to approximately $16.4\ \mathrm{m}$ and redistributes the mean line tensions, while the QS-DYN difference remains small. The corresponding DAF values are $\mathrm{DAF}_{r,\max} = 1.001$, $\mathrm{DAF}_{T,\max} \approx 1.000$, and $\mathrm{DAF}_{\Delta T} = 0.990$.

The sensitivity analyses therefore support the main interpretation of Chapter 5: for the selected first-order screening cases and tested pretension levels, the QS and DYN mooring-line representations give very similar predictions. At the same time, the sensitivities show that the conclusion depends on the selected pretension, mooring geometry, and load types. Future work should therefore assess cases with stronger low-frequency fairlead motion and changed mean mooring states, including second-order wave-drift loading, current, and operating turbine loads.

7.2. Overall conclusion

For the Elevator model, the QS mooring-line model gives equivalent predictions of maximum horizontal platform offset and governing fairlead effective tension to the dynamic mooring-line model in the selected first-order, wave-only screening cases. The offset DAF remains between 0.997 and 1.002, while the total tension DAF rounds to 1.000 in all selected cases. When only the tension range above the mean is compared, the DYN mooring-line model gives slightly smaller values than the QS model, with $\mathrm{DAF}_{\Delta T}$ ranging from 0.975 to 0.997.

This result can be explained by the response characteristics of the developed model. The selected first-order wave peak periods do not coincide with the estimated moored-system response periods. The platform motions remain small, with the largest horizontal offset below approximately $1.2\ \mathrm{m}$. The tension variations also remain limited relative to the mean effective tension, which stays close to the $900\ \mathrm{kN}$ pretension level. As a result, the additional line inertia, hydrodynamic drag, and added mass included in the DYN mooring-line model are only weakly excited in the tested cases.

Current, second-order wave drift, VIV, and time-dependent turbine loading were not included in the main comparison. This does not mean that these effects are negligible. They may change the mean

mooring state, excite low-frequency fairlead motion, or introduce current-induced line response and fatigue. These effects therefore define the next modelling step before the QS-DYN conclusion can be extended to a broader wind-wave-current design-load basis.

The conclusion is therefore specific to the comparison setup. It applies to the developed numerical Elevator model, the selected first-order wave-only screening cases, and the tested pretension levels. It should not be generalised to cases with stronger low-frequency fairlead motion, including second-order wave-drift loading, current, or wind thrust from an operating turbine. The main contribution of this thesis is therefore twofold. First, the Elevator concept was translated into a numerical Rhino-OrcaWave-OrcaFlex model and checked through hydrostatic, static-equilibrium, restoring, and free-vibration verification steps. Second, this developed model is used for a same-input QS-DYN mooring-line comparison, which explains why dynamic mooring-line effects are small under the selected first-order wave-only conditions.

7.3. Recommendations

The recommendations focus on the next modelling steps that are most likely to change the interpretation of the mooring-line comparison. Priority is given to load effects that may increase fairlead motion, modelling choices that may change the static mooring state, and model improvements needed before design-level conclusions can be drawn.

7.3.1. Include low-frequency and combined environmental loading

The first recommended next step is to extend the load types beyond the selected first-order, wave-only screening cases. The moored model has a soft surge response, with an estimated surge period of approximately $254\ \mathrm{s}$. This range is not strongly excited by the selected first-order wave spectra, but it may be affected by second-order wave-drift loading and current.

Future work should therefore assess second-order wave-drift loading, current, combined wind-wave-current loading, additional environmental directions, and multiple wave seeds. This is needed to determine whether larger low-frequency excursions, changed mean mooring states, and current-induced line response make dynamic mooring-line effects more important than in the present comparison. Because the line-frequency check indicates possible current-induced excitation of transverse line modes, future current-loaded analyses should also include VIV and fatigue assessment.

7.3.2. Develop a coupled aerodynamic load model

The steady-thrust sensitivity shows that mean aerodynamic loading can shift the platform equilibrium and redistribute the line tensions. With the present mooring input parameters, a full rated-thrust-level static load also causes strong unloading of one mooring line.

Future work should therefore include a coupled aerodynamic load model with turbine-control representation. This is needed to assess realistic wind-wave response, thrust variation, aerodynamic damping, and the interaction between platform motion and turbine thrust.

7.3.3. Re-optimise the mooring layout and assess line behaviour

The mooring system used in this thesis is based on Belis et al. [1] and calibrated to a target pretension of $900\ \mathrm{kN}$ per line. A design study should re-optimise the mooring layout using the full floater geometry, mass properties, buoyancy distribution, and design-load types. The optimisation should include pretension, unstretched line length, anchor radius, line inclination, and line material. For the HMPE mooring lines, long-term effects such as creep, fatigue degradation, and nonlinear load-history effects should also be assessed before extended design conclusions are drawn.

7.3.4. Improve and validate the hydrodynamic model

The hydrodynamic model is a reduced diffraction-body representation. It is suitable as a common hydrodynamic basis for the QS-DYN mooring-line comparison, but it is not a validated hydrodynamic model of the complete Elevator concept.

Future work should improve the geometric representation, assess the effect of the omitted members, and perform mesh-convergence and sensitivity checks before using the hydrodynamic model for design-level load assessment.

References

[1] I. A. Belis et al., “A Floating Wind Farm for Curaçao,” Delft University of Technology, Tech. Rep., Oct. 2025.

[2] M. Hall et al., “The IEA Wind Task 49 Reference Floating Wind Array Design Basis (NREL/TP-5000-89709),” International Energy Agency Wind Technology Collaboration Programme (IEA Wind), Tech. Rep., Jun. 2024.

[3] Z. Jiang, “Mooring design for floating wind turbines: A review,” *Renewable and Sustainable Energy Reviews*, vol. 212, Jan. 2025. DOI: 10.1016/J.RSER.2024.115231.

[4] F. G. Nielsen, *Offshore Wind Energy: Environmental Conditions and Dynamics of Fixed and Floating Turbines*. Cambridge University Press, 2024. DOI: 10.1017/9781009341455.

[5] Z. Lin, X. Liu, and S. Lotfian, “Impacts of water depth increase on offshore floating wind turbine dynamics,” *Ocean Engineering*, vol. 224, Feb. 2021. DOI: 10.1016/j.oceaneng.2021.108697.

[6] M. Masciola, A. Robertson, J. Jonkman, A. Coulling, and A. Goupee, “Assessment of the Importance of Mooring Dynamics on the Global Response of the DeepCwind Floating Semisubmersible Offshore Wind Turbine,” in *Proceedings of the Twenty-Third International Offshore and Polar Engineering Conference*, Anchorage, Alaska, USA: International Society of Offshore and Polar Engineers, 2013.

[7] A. Cooperman et al., “Investigation of the Challenges of Offshore Wind in Ultradeep Water (NREL/TP-5000-90849),” National Renewable Energy Laboratory, Tech. Rep., Dec. 2024. [Online]. Available: https://www.nrel.gov/docs/fy25osti/90849.pdf.

[8] E. C. Edwards, A. Holcombe, S. Brown, E. Ransley, M. Hann, and D. Greaves, “Evolution of floating offshore wind platforms: A review of at-sea devices,” *Renewable and Sustainable Energy Reviews*, vol. 183, 2023. DOI: 10.1016/J.RSER.2023.113416.

[9] K.-t. Ma, Y. Wu, S. F. Stolen, L. Bello, M. van der Horst, and Y. Luo, “Mooring designs for floating offshore wind turbines leveraging experience from the oil & gas industry,” in *Proceedings of the ASME 2021 40th International Conference on Ocean, Offshore and Arctic Engineering*, American Society of Mechanical Engineers, 2021. DOI: 10.1115/OMAE2021-60739.

[10] J. M. Jonkman, “Dynamics of offshore floating wind turbines-model development and verification,” *Wind Energy*, vol. 12, no. 5, pp. 459–492, 2009. DOI: 10.1002/we.347.

[11] J. Jonkman and D. Matha, “A Quantitative Comparison of the Responses of Three Floating Platforms (NREL/CP-500-46726),” in *European Offshore Wind 2009 Conference and Exhibition*, Stockholm, Sweden: National Renewable Energy Laboratory, Mar. 2010.

[12] M. Hall, M. Biglu, S. Housner, K. Coughlan, M. Y. Mahfouz, and E. Lozon, “Floating Wind Farm Layout Optimization Considering Moorings and Seabed Variations,” *Journal of Physics: Conference Series*, vol. 2767, no. 6, 2024. DOI: 10.1088/1742-6596/2767/6/062038.

[13] E. Gaertner et al., “Definition of the IEA 15-Megawatt Offshore Reference Wind Turbine (NREL/TP-5000-75698),” National Renewable Energy Laboratory, Tech. Rep., Mar. 2020. DOI: 10.2172/1603478.

[14] T. T. Tran and D. H. Kim, “The platform pitching motion of floating offshore wind turbine: A preliminary unsteady aerodynamic analysis,” *Journal of Wind Engineering and Industrial Aerodynamics*, vol. 142, pp. 65–81, Jul. 2015. DOI: 10.1016/J.JWEIA.2015.03.009.

[15] L. Cottura, R. Caradonna, R. Novo, A. Ghigo, G. Bracco, and G. Mattiazzo, “Effect of pitching motion on production in a OFWT,” *Journal of Ocean Engineering and Marine Energy*, vol. 8, no. 3, pp. 319–330, 2022. DOI: 10.1007/s40722-022-00227-0.

[16] DNV GL, “DNVGL-RP-C205: Environmental conditions and environmental loads,” DNV GL AS, Tech. Rep., Aug. 2017.

[17] J. M. J. Journée and W. W. Massie, “Offshore hydromechanics,” TU Delft, Delft, Tech. Rep., Jun. 2008.

[18] DNV, “DNV-RP-H103: Modelling and analysis of marine operations,” Tech. Rep., 2011.

[19] A. Campanile, V. Piscopo, and A. Scamardella, “Mooring design and selection for floating offshore wind turbines on intermediate and deep water depths,” *Ocean Engineering*, vol. 148, pp. 349–360, Jan. 2018. DOI: 10.1016/j.oceaneng.2017.11.043.

[20] S. D. Weller, L. Johanning, P. Davies, and S. J. Banfield, “Synthetic mooring ropes for marine renewable energy applications,” *Renewable Energy*, vol. 83, pp. 1268–1278, Nov. 2015. DOI: 10.1016/J.RENENE.2015.03.058.

[21] TEHO Ropes, *Magnaro HMPE Plus ropes*. [Online]. Available: https://tehoropes.nl/product/magnaro-hmpe-plus-ropes/.

[22] H. Liu, W. Huang, Y. Lian, and L. Li, “An experimental investigation on nonlinear behaviors of synthetic fiber ropes for deepwater moorings under cyclic loading,” *Applied Ocean Research*, vol. 45, pp. 22–32, Mar. 2014, ISSN: 01411187. DOI: 10.1016/j.apor.2013.12.003.

[23] D. Kim, Y. H. Bae, and S. Park, “Design strategy for resonance avoidance to improve the performance of tension leg platform-type floating offshore wind turbines,” *Ocean Engineering*, vol. 306, Aug. 2024. DOI: 10.1016/J.OCEANENG.2024.118080.

[24] DNV, “DNV-ST-0119: Floating wind turbine structures,” DNV AS, Tech. Rep., Jun. 2021.

[25] American Bureau of Shipping, “Guide for Building and Classing Floating Offshore Wind Turbines,” American Bureau of Shipping, Tech. Rep., Jul. 2020.

[26] M. Ikhennicheu et al., “Review of the state of the art of mooring and anchoring designs, technical challenges and identification of relevant DLCs,” COREWIND D2.1, Tech. Rep., Mar. 2020.

[27] G. Benassai, A. Campanile, V. Piscopo, and A. Scamardella, “Ultimate and accidental limit state design for mooring systems of floating offshore wind turbines,” *Ocean Engineering*, vol. 92, pp. 64–74, Dec. 2014. DOI: 10.1016/J.OCEANENG.2014.09.036.

[28] Orcina Ltd., *Line theory: Calculation stage 1 tension forces*. [Online]. Available: https://www.orcina.com/webhelp/OrcaFlex/Content/html/Linetheory,Calculationstage1tensionforces.htm.

[29] Orcina Ltd., *Vessel types: RAOs*. [Online]. Available: https://www.orcina.com/webhelp/OrcaFlex/Content/html/Vesseltypes%2CRAOs.htm.

[30] Copernicus Climate Change Service, *ERA5 hourly data on single levels from 1940 to present*, 2018. DOI: 10.24381/cds.adbb2d47.

[31] Orcina Ltd., *Vessel data: Applied loads*. [Online]. Available: https://www.orcina.com/webhelp/OrcaFlex/Content/html/Vesseldata%2CAppliedloads.htm.

[32] S. H. Sørum, N. Fonseca, M. Kent, and R. P. Faria, “Assessment of nylon versus polyester ropes for mooring of floating wind turbines,” *Ocean Engineering*, vol. 278, Jun. 2023. DOI: 10.1016/j.oceaneng.2023.114339.

[33] The Vryhof Companies, “Polyester & Dyneema mooring ropes manual,” Bexco N.V.; Le Lis N.V.; Vryhof Anchors B.V., Krimpen aan den IJssel, The Netherlands, Tech. Rep., 2004.

[34] Orcina Ltd., *Modal analysis: Theory*. [Online]. Available: https://www.orcina.com/webhelp/OrcaFlex/Content/html/Modalanalysis,Theory.htm.

[35] Orcina Ltd., *Modal analysis: Data and results*. [Online]. Available: https://www.orcina.com/webhelp/OrcaFlex/Content/html/Modalanalysis,Dataandresults.htm.

[36] S. S. Rao, *Mechanical vibrations*. Prentice Hall, 2011, p. 1084, ISBN: 9780132128193.

[37] C. H. Williamson and R. Govardhan, “Vortex-induced vibrations,” *Annual Review of Fluid Mechanics*, vol. 36, 2004. DOI: 10.1146/annurev.fluid.36.050802.122128.

[38] A. N. Simos, F. Ruggeri, R. A. Watai, A. Souto-Iglesias, and C. Lopez-Pavon, “Slow-drift of a floating wind turbine: An assessment of frequency-domain methods based on model tests,” *Renewable Energy*, vol. 116, pp. 133–154, Feb. 2018. DOI: 10.1016/J.RENENE.2017.09.059.

[39] Orcina Ltd., *Vessel results*. [Online]. Available: https://www.orcina.com/webhelp/OrcaFlex/Content/html/Vesselresults.htm.

A

Reference design values

This appendix summarises the reference-design values from Belis et al. [1] that are used to define and interpret the Elevator model. The values are included for traceability. They are not all used directly as final OrcaWave or OrcaFlex input values. Quantities that are re-derived or transformed for the thesis model are collected separately in Appendix B.

Table A.1: Total weight of the structure. Source: Belis et al. [1], Table 4.1.

Substructure	**Material**	**Volume** (m^3)	**Density** ($\frac{\mathrm{kg}}{\mathrm{m}^3}$)	**Mass** (te)	**Weight** (MN)
Tripod	Steel	68.80	7800	536.66	5.26
Columns	Steel	144.78	7800	1129.31	11.08
Upper Tank	Concrete	2332.76	2400	5598.62	54.92
	Seawater Ballast	227.04	1025	232.71	2.29
Lower Tank	Concrete	2332.76	2400	5598.71	54.92
	Sand Ballast	11352.02	1400	15892.82	155.91
NREL 15 MW Turbine	-	-	-	1877	18.41
Total Structure				30865.83	302.79

Table A.2: Buoyancy of the submerged structure. Source: Belis et al. [1], Table 4.2.

Sub-Structure	**Displaced Water Volume** (m^3)	**Buoyancy** (MN)
Tripod (part below SWL)	1266.44	12.73
Columns	1708.24	17.18
Upper Tank	13684.78	137.6
Lower Tank	13684.78	137.6
Total Submerged Structure	30344.24	305.12

Table A.3: Results of vertical equilibrium. Source: Belis et al. [1], Table 4.3.

Quantity	**value**	**unit**
Total structure weight	302.79	MN
Total structure buoyancy	305.12	MN
Inclination angle mooring w.r.t. vertical	35	○
Reported equilibrium mooring line tension (T_0)	0.95	MN

In this study, T_0 denotes the static equilibrium line tension of one line at the operating mean position. When the reference design uses a static working tension as input for the HMPE secant stiffness, this value is reported separately as T_{work}.

Table A.4: List of Hydrostatic Parameters. Source: Belis et al. [1], Table 4.4.

Quantity	Symbol	Value	Unit
Displaced volume of water at equilibrium	V	$30\,344.24$	m^3
Waterplane area at the free surface	A_{wp}	111.09	m^2
Second moment of the waterplane area about x -axis	$I_{wp,x}$	4987.15	m^4
Second moment of the waterplane area about y -axis	$I_{wp,y}$	4987.15	m^4
Vertical distance from the keel to the center of buoyancy	KB	41.81	m
Vertical distance from the keel to the centre of gravity	KG	33.35	m
Transverse metacentric height (rolling ϕ)	GM_T	8.63	m
Longitudinal metacentric height (pitching θ)	GM_L	8.63	m
Eccentric static trimming moment	$M_{trim}^{(e)}$	-85.5	MNm
Wind thrust heel moment	$M_{heel}^{(w)}$	0	MNm
Aerodynamic thrust force acting at the turbine hub	T_{hub}	1.42	MN
Wind thrust trimming moment ($\theta = 0$)	$M_{trim,max}^{(w)}$	257.05	MNm

Table A.5: Additional waterplane-geometry inputs to construct A_{wp} and I_{wp}. Source: Belis et al. [1], Appendix D Sheet 1.

Quantity	Symbol	Value	Unit
Main column radius at WL	r_c	5.025	m
Ellipse semi-axis (from $\varnothing 3.05$)	a	1.525	m
Ellipse semi-axis (from $\varnothing 4.31$)	b	2.155	m
Radius to ellipse centroid (plan view)	r_e	15.5	m
Number of ellipses at WL	N_e	3	–

Table A.6: Hydrostatic results. Source: Belis et al. [1], Table 4.5.

Quantity	Symbol	Value	unit
Waterplane area	A_{wp}	1.103×10^2	m^2
Waterplane second moment	I_{wp}	4.987×10^3	m^4
Displacement	Δ	3.051×10^8	N
Metacentric radius	B_M	1.643×10^{-1}	m
Transverse metacentric height	GM_T	8.624	m
Hydrostatic heave	$c_{33}^{(hyd)}$	1.091×10^6	$\mathrm{N/m}$
Hydrostatic roll	$c_{44}^{(hyd)}$	2.631×10^9	$\mathrm{N \cdot m/rad}$
Hydrostatic pitch	$c_{55}^{(hyd)}$	2.631×10^9	$\mathrm{N \cdot m/rad}$
Total mass	m	3.086×10^7	kg
Vertical centre of gravity (origin at SWL)	z_G	-54.49	m

Note: Small inconsistencies exist between the hydrostatic summary values and the Appendix D calculation outputs in Belis et al. [1]. These values are therefore used as reference and consistency-check quantities only. The implemented numerical model is verified separately in Chapter 4.

Table A.7: Rigid-body inertia properties about O' at SWL. Source: Belis et al. [1], Appendix D Sheet 2.

Quantity	Symbol	Value	Unit
Inertia about O' (SWL)	$I_{xx}^{(O)}$	180.862×10^9	$\mathrm{kg \cdot m^2}$
	$I_{yy}^{(O)}$	180.862×10^9	$\mathrm{kg \cdot m^2}$
	$I_{zz}^{(O)}$	14.069×10^9	$\mathrm{kg \cdot m^2}$
Products of inertia	$I_{xy}^{(O)}$	0	$\mathrm{kg \cdot m^2}$
	$I_{xz}^{(O)}$	0	$\mathrm{kg \cdot m^2}$
	$I_{yz}^{(O)}$	0	$\mathrm{kg \cdot m^2}$

Table A.8: Mooring system results. Source: Belis et al. [1], Table 4.6.

Quantity	Symbol	Value	Unit
Per-line axial stiffness	k_i	65.18×10^3	$\mathrm{N/m}$
Sum of line stiffness	$\sum k_i$	195.5×10^3	$\mathrm{N/m}$
Surge and sway	$c_{11} = c_{22}$	32.17×10^3	$\mathrm{N/m}$
Heave	c_{33}^{tendon}	131.2×10^3	$\mathrm{N/m}$
Roll	c_{44}^{tendon}	17.21×10^6	$\mathrm{N \cdot m/rad}$
Pitch	c_{55}^{tendon}	17.21×10^6	$\mathrm{N \cdot m/rad}$
Total heave	c_{33}^{total}	1.222×10^6	$\mathrm{N/m}$
Ratio	$c_{33}^{\text{tendon}} / c_{33}^{\text{hyd}}$	≈ 0.12	-
Working fraction	$f = T_{\frac{\text{work,line}}{MBL}}$	0.223	–
Secant strain at f (interpolated)	$\varepsilon(f)$	14.139×10^{-3}	–
Rope axial stiffness, secant at T_{work}	EA_{rope}	63.655×10^6	N
Effective axial stiffness (secant)	EA_{eff}	63.655×10^6	N
Yaw restoring (tendons)	$c_{66}^{(tendon)}$	≈ 0	$\mathrm{N \cdot m/rad}$

Table A.9: Added mass totals at $T_w = 12\ \mathrm{s}$. Source: Belis et al. [1], Table 4.7.

Quantity	Symbol	Value	Unit
Total added mass (surge/heave)	$a_{11} = a_{33}$	17.46×10^6	kg
Total added inertia (roll/pitch)	$a_{44} = a_{55}$	57.05×10^9	$\mathrm{kg \cdot m^2}$

Table A.10 gives the component-level calculation output from the reference-design report. It is included only to document how the reported total mass and buoyancy were reconstructed.

Table A.10: Component-level reference calculation outputs used to reconstruct the reported mass and buoyancy build-up of the Elevator concept.

Part	Length (m)	Diameter (m)	Thickness (m)	Amount (no.)	Volume (m^3)	Submerged (m^3)	Mass (kg)	Buoyancy (MN)
1	21	10.1	0.05	1	33.2	640.9	2.586×10^5	6.44
2	16.95	3	0.025	3	11.9	359.4	9.268×10^4	3.61
3	5.5	3.05	0.025	3	3.9	120.6	3.058×10^4	1.21
4	21.46	3.05	0.025	3	15.3	149.9	1.193×10^5	1.51
5	0.05	10.1	0	1	4.0	4.0	3.125×10^4	0.04
6	0.025	3.05	0	3	0.5	0.5	4.274×10^3	0.01
Total tripod					68.8	1275.4	5.367×10^5	12.8
7	80	3	0.06	3	133	640.9	1.037×10^6	17.1
8	0.1	5	0	6	11.8	359.4	9.189×10^4	0.1
Total column					144.8		1.129×10^6	17.2
9	12	52 (outer) 35 (inner)	0.4	1	2332.8	13 684.8	5.599×10^6	137.6
10	-	-	-	2% full	227	-	2.327×10^5	-
Total upper tank					144.8	13 684.8	5.831×10^6	137.6
11	12	52 (outer) 35 (inner)	0.4	1	2332.8	13 684.8	5.599×10^6	137.6
12	-	-	-	100% full	11 352	-	1.589×10^7	-
Total lower tank					13 684.8	13 684.8	2.149×10^6	137.6
Total structure (with FOWT)							3.087×10^7	305.2

Tripod:

1. Main column
2. Horizontal member
3. End-cans
4. Angled member
5. Main column bottom plate
6. End-can top plate

Columns:

7. Column
8. Column plates

Upper tank:

9. Concrete
10. Ballast (water)

Lower tank:

11. Concrete
12. Ballast (sand)

B

Derived reference quantities used for model setup

This appendix lists derived reference quantities used to support the numerical model setup and verification. The values are based on the reference-design report and its appendices. They are used as reference targets and consistency checks, not as a complete list of final OrcaFlex input values. The developed OrcaWave-OrcaFlex model is defined and verified in Chapter 4.

Table B.1: Location where the derived reference quantities are used in the main report.

Appendix table	Content	Used in main text
Table B.2-B.3	Hydrostatic and inertia reference values	Sections 3.2 and 4.4
Table B.4	Turbine mass properties	Sections 3.3 and 4.4
Table B.5-B.6	mooring input parameters and restoring values	Sections 3.3 and 4.5
Table B.7-B.9	Selected hydrodynamic quantities and natural periods	Sections 3.4 and 5.2

Table B.2: Reference hydrostatic values. Source: Belis et al. [1, Appendix D].

Quantity	Symbol	Value	Unit
Total mass	m	30.861×10^6	kg
Total weight	W	302.8×10^6	N
Total buoyancy	B	305.119×10^6	N
Draft	T	88	m
Centre of gravity	KG	33.35	m
Center of buoyancy	KB	41.81	m
Metacentric radius	BM	0.164	m
Transverse metacentric height	GM	8.63	m

Note: The mass value follows the Appendix D calculation output. Small differences with the summary-table mass in Appendix A are treated as reference-report rounding/source differences.

Table B.3: Reference inertia values. Source: Belis et al. [1, Appendix D].

Inertia about O' at SWL	$I_{xx}^{(O')}$	180.862×10^9	$\mathrm{kg \cdot m^2}$
Inertia about O' at SWL	$I_{yy}^{(O')}$	180.862×10^9	$\mathrm{kg \cdot m^2}$
Inertia about O' at SWL	$I_{zz}^{(O')}$	14.069×10^9	$\mathrm{kg \cdot m^2}$

Table B.4: 15 MW reference wind turbine characteristics. Source: Belis et al. [1, Appendix C], citing Gaertner et al. [13].

Parameter	Value	Unit
Rotor–Nacelle Assembly (RNA) mass	1.017×10^6	kg
Tower mass	8.60×10^5	kg
Total turbine mass	1.877×10^6	kg
Turbine centre of gravity height	1.036×10^2	m

Note: The turbine centre-of-gravity height is reported as a reference turbine value and should not be confused with the global Elevator KG.

Table B.5: Mooring geometry and line-tension quantities used for the model setup. Source: Belis et al. [1, Appendix D, Sheet 3].

Quantity	Symbol	Value	Unit
Number of mooring lines	N	3	–
Line diameter	D	80×10^{-3}	m
Line inclination to vertical	β	35	$^\circ$
Reference straight-line length	L	976.62	m
Anchor radius	r_a	586.2	m
Working tension for secant stiffness	T_{work}	0.900×10^{6}	N
Reported equilibrium tension	T_0	0.950×10^{6}	N
Minimum breaking load per line	MBL	4.040×10^{6}	N
Working fraction	f	2.228×10^{-1}	–
Rope strain at working fraction	$\epsilon(f)$	14.14×10^{-3}	–
Secant axial stiffness at T_{work}	EA_{sec}	63.66×10^{6}	N
Linear axial stiffness per line	k_i	65.18×10^{3}	$\mathrm{N/m}$

Table B.6: Mooring and hydrostatic restoring coefficients. Source: Belis et al. [1, Appendix D, Sheets 1, 3 and 4].

Quantity	Symbol	Value	Unit
Mooring restoring in surge	c_{11}^{tendon}	32.17×10^{3}	$\mathrm{N/m}$
Mooring restoring in sway	c_{22}^{tendon}	32.17×10^{3}	$\mathrm{N/m}$
Mooring restoring in heave	c_{33}^{tendon}	131.2×10^{3}	$\mathrm{N/m}$
Mooring restoring in roll	c_{44}^{tendon}	17.21×10^{6}	$\mathrm{N \cdot m/rad}$
Mooring restoring in pitch	c_{55}^{tendon}	17.21×10^{6}	$\mathrm{N \cdot m/rad}$
Mooring restoring in yaw	c_{66}^{tendon}	0	$\mathrm{N \cdot m/rad}$
Hydrostatic restoring in heave	c_{33}^{hyd}	1.091×10^{6}	$\mathrm{N/m}$
Hydrostatic restoring in roll	c_{44}^{hyd}	2.631×10^{9}	$\mathrm{N \cdot m/rad}$
Hydrostatic restoring in pitch	c_{55}^{hyd}	2.631×10^{9}	$\mathrm{N \cdot m/rad}$
Total restoring in surge	c_{11}^{total}	32.17×10^{3}	$\mathrm{N/m}$
Total restoring in heave	c_{33}^{total}	1.222×10^{6}	$\mathrm{N/m}$
Total restoring in roll	c_{44}^{total}	2.649×10^{9}	$\mathrm{N \cdot m/rad}$
Total restoring in pitch	c_{55}^{total}	2.649×10^{9}	$\mathrm{N \cdot m/rad}$

Table B.7: Selected hydrodynamics inputs. Source: Belis et al. [1, Appendix D, Sheet 4].

Quantity	Symbol	Value	Unit
Evaluation wave period	T_w	12	s
Angular frequency	ω	0.524	$\mathrm{rad/s}$
Water depth	h	800	m
Wave number	k	27.95×10^{-3}	$\mathrm{m^{-1}}$
Relative depth	kh	22.36	–
Added-mass kernel mode	–	fit	–

Table B.8: Selected hydrodynamics outputs. Source: Belis et al. [1, Appendix D, sheet 4].

Quantity	Symbol	Value	Unit
Effective surge mass	$M_1 = m_{11} + a_{11}$	48.32×10^6	kg
Effective heave mass	$M_3 = m_{33} + a_{33}$	48.32×10^6	kg
Effective roll inertia	$M_4 = I_{xx}^{(O')} + a_{44}$	237.9×10^9	$\mathrm{kg \cdot m^2}$
Effective pitch inertia	$M_5 = I_{yy}^{(O')} + a_{55}$	237.9×10^9	$\mathrm{kg \cdot m^2}$
Modal damping ratio used	ζ_r	0.030	–
Surge linear damping	b_{11}	74.80×10^3	$\mathrm{N \cdot s/m}$
Heave linear damping	b_{33}	461.1×10^3	$\mathrm{N \cdot s/m}$
Roll linear damping	b_{44}	1.506×10^9	$\mathrm{N \cdot m \cdot s/rad}$
Pitch linear damping	b_{55}	1.506×10^9	$\mathrm{N \cdot m \cdot s/rad}$

Table B.9: Natural periods from the linear screening model. Source: Belis et al. [1, Table 4.8].

DOF	Natural Period (T_n)	Notes
Surge ($r = 1$)	$244\ \mathrm{s}$	Very soft horizontal restoring
Heave ($r = 3$)	$39.5\ \mathrm{s}$	Hydrostatics dominated
Roll ($r = 4$)	$59.7\ \mathrm{s}$	Large (ΔGM_T), large inertia
Pitch ($r = 5$)	$59.7\ \mathrm{s}$	Symmetry with roll

C
Hydrodynamic assessment

This appendix provides frequency-domain interpretation checks of the OrcaWave database. Figures C.1 and C.2 show the diagonal added-mass and radiation-damping terms used to inspect the hydrodynamic database before import into OrcaFlex. Figure C.3 shows the six-degree-of-freedom motion RAOs computed on an additional refined OrcaWave period grid.

C.1. Added-mass terms

Figure C.1 shows the diagonal added-mass terms of the OrcaWave database. The translational terms A_{11}, A_{22} and A_{33} are expressed in t, while the rotational terms A_{44}, A_{55} and A_{66} are expressed in $\mathrm{t\,m^2}$. The curves are used to inspect the smoothness and plausibility of the hydrodynamic database.

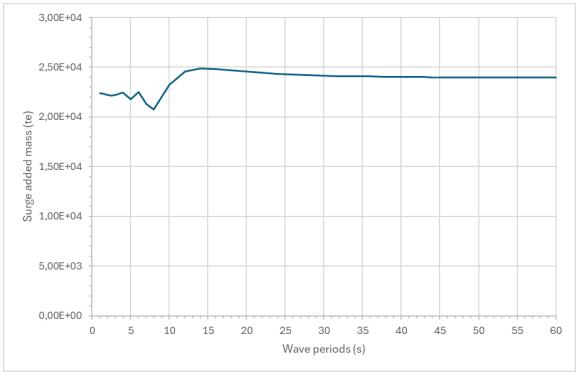

(a) Surge added mass

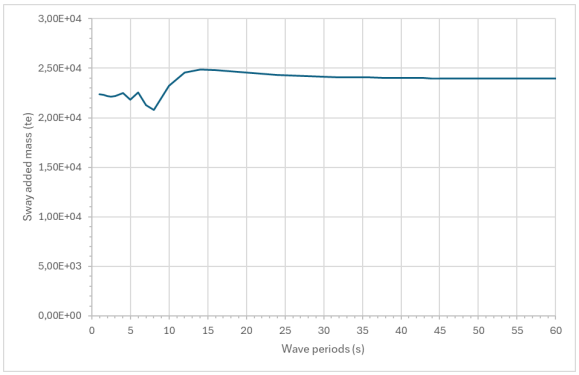

(b) Sway added mass

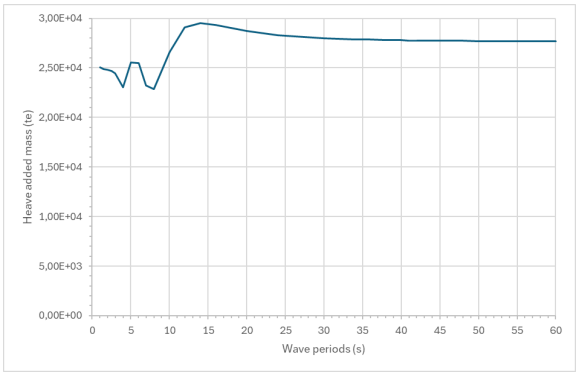

(c) Heave added mass

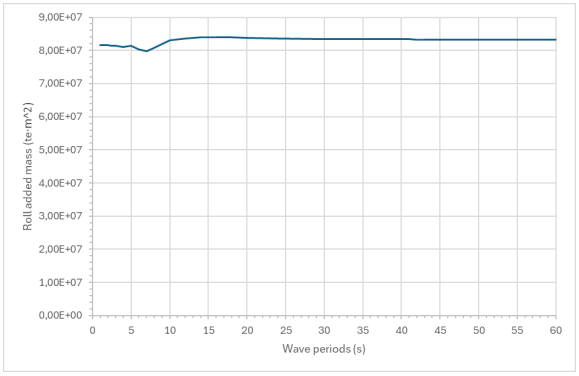

(d) Roll added mass

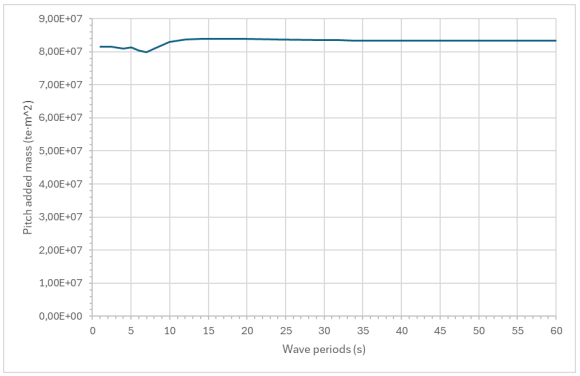

(e) Pitch added mass

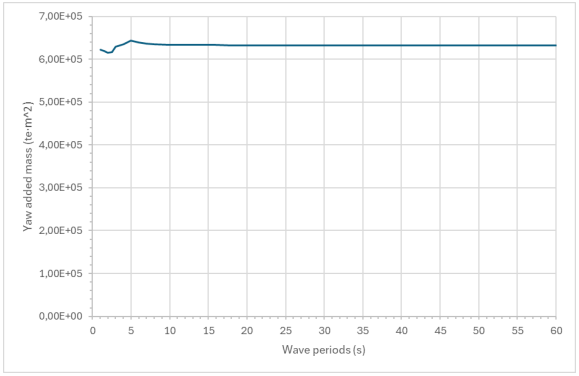

(f) Yaw added mass

Figure C.1: Diagonal added-mass terms from the OrcaWave database.

C.2. Damping terms

Figure C.2 shows the diagonal radiation-damping terms. The damping coefficients show clear frequency dependence, with local peaks at short to intermediate wave periods and low values at longer periods. These trends are used only as supporting checks of numerical smoothness and plausibility. They are not interpreted as direct response results, because the displacement response also depends on wave excitation, restoring, total inertia, damping, and coupling between degrees of freedom.

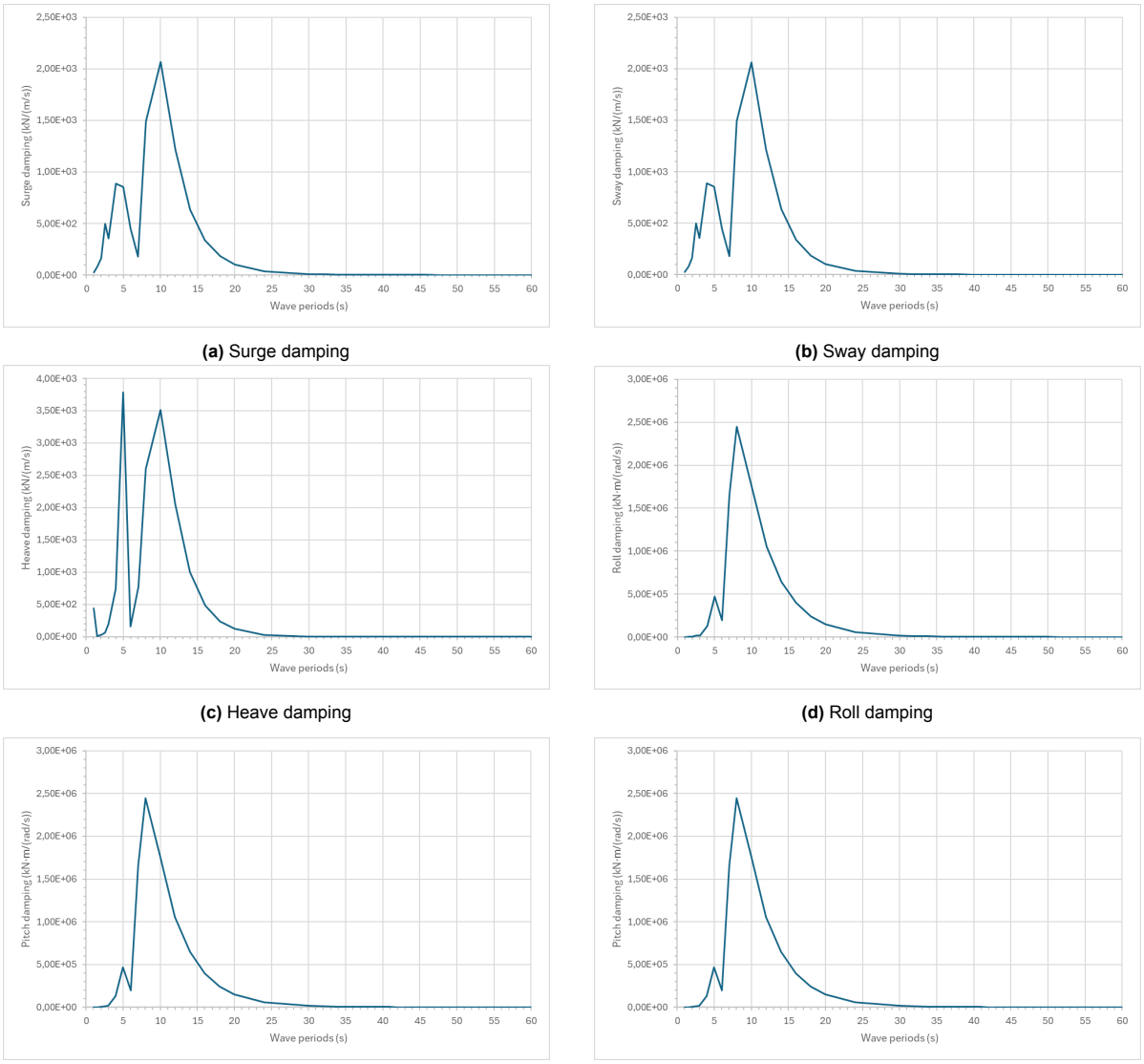

(a) Surge damping **(b)** Sway damping

(c) Heave damping **(d)** Roll damping

(e) Pitch damping **(f)** Yaw damping

Figure C.2: Diagonal radiation-damping terms from the OrcaWave database. The translational terms B_{11}, B_{22} and B_{33} are expressed in $\mathrm{kN/(m/s)}$, while the rotational terms B_{44}, B_{55} and B_{66} are expressed in $\mathrm{kN\,m/(rad/s)}$. The plots are used as supporting checks of the frequency-dependent hydrodynamic database and are not interpreted as direct response results.

C.3. 6DOF motion RAOs

The RAO plots are based on an additional refined OrcaWave period grid. This grid was used only for the frequency-domain interpretation, to give more resolution around the long-period response range. The wave-excitation periods are 1, 1.5, 2, 2.5, 3, 4, 5, 6, 7, 8, 10, 12, 14, 16, 18, 20, 24, 30, 32, 34, 36, 38, 40, 41, 42, 43, 44, 45, 46, 48, 50, 52, 55, and 60 s. The selected irregular-wave cases in OrcaFlex are still defined by the sea-state parameters in Section 4.2.3 and the load-case matrix in Section 4.2.5.

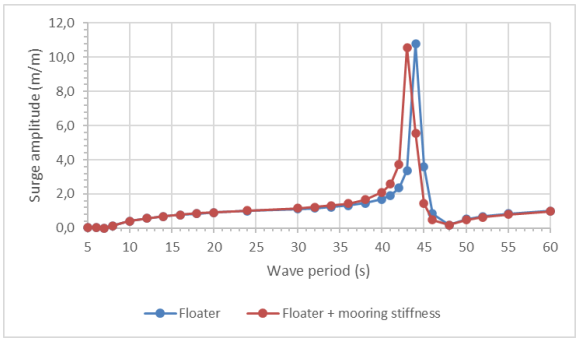

(a) Surge RAO

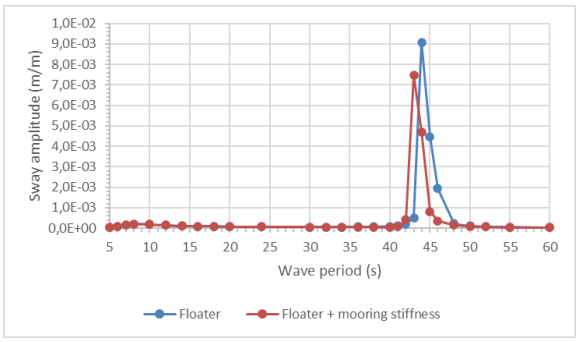

(b) Sway RAO

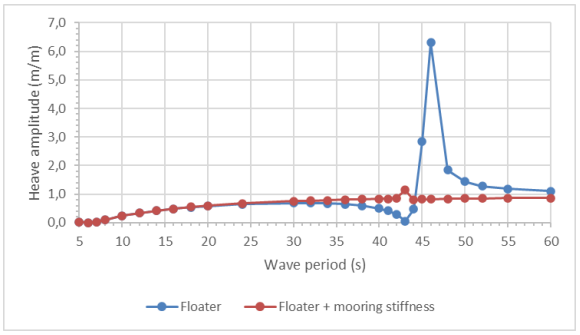

(c) Heave RAO

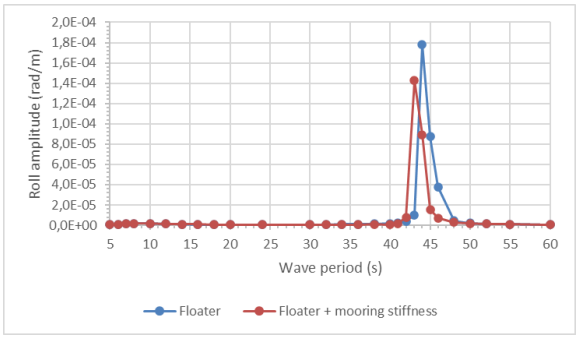

(d) Roll RAO

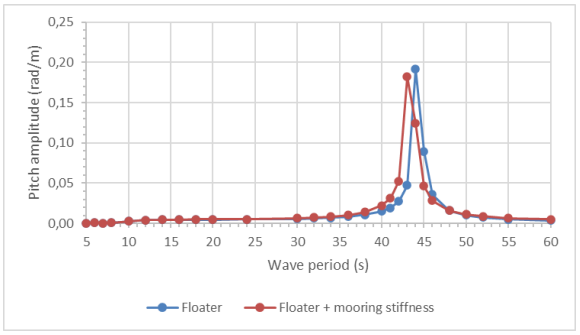

(e) Pitch RAO

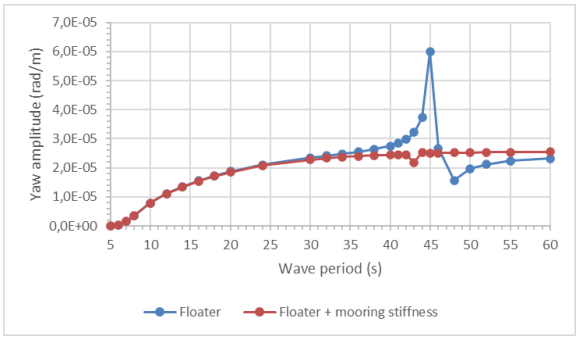

(f) Yaw RAO

Figure C.3: Six-DOF motion RAOs computed on the refined period grid for frequency-domain interpretation. The floater-only response is compared with the response obtained after adding the linearised mooring-restoring matrix.

Two frequency-domain cases are shown: the floater-only diffraction-body response and the same body with the added linearised mooring-restoring matrix. The plots are used to inspect frequency-domain response trends. They are not used as prescribed vessel motions in the OrcaFlex time-domain simulations.

D

Additional response statistics

This appendix gives the additional response statistics used to support the compact results in Chapter 5. The same post-processing window as defined in Section 5.1 is used. The horizontal offset is calculated from the surge and sway time histories, while the line-tension statistics are evaluated at the fairlead end of each mooring line.

The component maxima $|x|_{\max}$ and $|y|_{\max}$ are reported in Table D.1 only to show the directional distribution of the response. They are not combined to calculate $r_{\max}$. The resultant offset $r_{\max}$ is obtained from the time series $r(t)$, as defined in Section 5.1.

Table D.1: Directional platform-motion components for the selected irregular-wave cases.

Load case	**Heading** $(^\circ)$	**Model**	$\|\mathbf{x}\|_{\max}$ (m)	$\|\mathbf{y}\|_{\max}$ (m)	$\mathbf{r}_{\max}$ (m)
LC1a	0	QS	0.308	0.000	0.308
LC1a	0	DYN	0.307	0.000	0.307
LC1b	30	QS	0.265	0.154	0.306
LC1b	30	DYN	0.264	0.153	0.306
LC2a	0	QS	1.149	0.001	1.149
LC2a	0	DYN	1.151	0.001	1.151
LC2b	30	QS	0.995	0.574	1.148
LC2b	30	DYN	0.996	0.575	1.151
LC3a	0	QS	0.057	0.000	0.057
LC3a	0	DYN	0.057	0.000	0.057
LC3b	30	QS	0.050	0.031	0.059
LC3b	30	DYN	0.050	0.031	0.059

Table D.2: Effective-tension statistics for all mooring lines in the selected irregular-wave cases.

Load case	Heading (°)	Model	Line	$\mathbf{T}_{\mathrm{eff,max}}$ (kN)	$\bar{\mathbf{T}}_{\mathrm{eff}}$ (kN)	$\mathbf{\Delta T}_{\mathrm{eff}}$ (kN)	$\mathbf{\Delta T}_{\mathrm{eff}}/\bar{\mathbf{T}}_{\mathrm{eff}}$ (%)
LC1a	0	QS	1	917.325	900.368	16.958	1.88
LC1a	0	QS	2	911.811	900.113	11.698	1.30
LC1a	0	QS	3	911.811	900.107	11.704	1.30
LC1a	0	DYN	1	916.974	900.277	16.697	1.85
LC1a	0	DYN	2	911.619	900.023	11.596	1.29
LC1a	0	DYN	3	911.619	900.016	11.602	1.29
LC1b	30	QS	1	916.091	900.347	15.744	1.75
LC1b	30	QS	2	911.018	900.189	10.829	1.20
LC1b	30	QS	3	914.376	900.052	14.325	1.59
LC1b	30	DYN	1	915.770	900.256	15.514	1.72
LC1b	30	DYN	2	910.837	900.099	10.738	1.19
LC1b	30	DYN	3	914.142	899.961	14.181	1.58
LC2a	0	QS	1	963.492	900.711	62.781	6.97
LC2a	0	QS	2	951.113	899.875	51.238	5.69
LC2a	0	QS	3	951.090	899.858	51.231	5.69
LC2a	0	DYN	1	963.174	900.611	62.563	6.95
LC2a	0	DYN	2	950.740	899.784	50.956	5.66
LC2a	0	DYN	3	950.728	899.778	50.950	5.66
LC2b	30	QS	1	958.758	900.637	58.120	6.45
LC2b	30	QS	2	943.012	900.143	42.868	4.76
LC2b	30	QS	3	962.331	899.673	62.658	6.96
LC2b	30	DYN	1	958.445	900.539	57.906	6.43
LC2b	30	DYN	2	942.718	900.050	42.668	4.74
LC2b	30	DYN	3	961.880	899.584	62.296	6.92
LC3a	0	QS	1	903.748	900.207	3.541	0.39
LC3a	0	QS	2	902.524	900.173	2.351	0.26
LC3a	0	QS	3	902.520	900.167	2.352	0.26
LC3a	0	DYN	1	903.570	900.117	3.453	0.38
LC3a	0	DYN	2	902.393	900.084	2.309	0.26
LC3a	0	DYN	3	902.388	900.078	2.310	0.26
LC3b	30	QS	1	903.443	900.206	3.237	0.36
LC3b	30	QS	2	902.273	900.175	2.098	0.23
LC3b	30	QS	3	902.754	900.166	2.588	0.29
LC3b	30	DYN	1	903.276	900.116	3.159	0.35
LC3b	30	DYN	2	902.144	900.085	2.059	0.23
LC3b	30	DYN	3	902.614	900.077	2.538	0.28

Table D.3: Line-by-line effective-tension statistics for the 25% rated-thrust sensitivity case in SS1 at 30° wave heading.

Model	Line	$\mathbf{T}_{\mathrm{eff,max}}$ (kN)	$\bar{\mathbf{T}}_{\mathrm{eff}}$ (kN)	$\mathbf{\Delta T}_{\mathrm{eff}}$ (kN)	$\mathbf{\Delta T}_{\mathrm{eff}}/\bar{\mathbf{T}}_{\mathrm{eff}}$ (%)
QS	1	250.766	234.909	15.857	6.75
QS	2	1255.386	1244.738	10.648	0.86
QS	3	1259.139	1244.607	14.531	1.17
DYN	1	250.198	234.417	15.781	6.73
DYN	2	1255.308	1244.717	10.591	0.85
DYN	3	1258.971	1244.585	14.386	1.16